ANTICIPATING TATHREEINE

Searching for Stable Planetary Orbits Around a Compact Hierarchical Triple

by

FRANCO BUSETTI

submitted in partial fulfillment of the

requirement for the degree of

MASTER OF SCIENCE IN ASTRONOMY

at the

FACULTY OF SCIENCES, UNIVERSITY OF SOUTHERN QUEENSLAND

and

SCHOOL OF ENGINEERING, JAMES COOK UNIVERSITY

Supervisor: PROF. BRAD CARTER

2013

Abstract

Around a third of the stars in our Galaxy are binary or multiple systems, with triples possibly accounting for up to a tenth. While planets have been found in S-type orbits around the single or binary components of triples, only two P-type orbits have been found, both being circumbinary. A planet in a circumtriple orbit has not yet been found. The anticipated discovery of such exoplanet orbits motivated this study.

Hierarchical triple systems that are compact enough to possibly harbour exoplanets in P-type orbits form a small minority of hierarchical triples, with only 7 of the catalogued 724 systems being suitable. From these we selected and analysed the recently-discovered HD 181068 or Trinity system, using *N*-body simulations to analyse the stability of the stellar system and possible planetary orbits around it.

Mercury6 was selected as the orbital integration package; it was tested on simple systems and used to replicate a previously published study on HW Virginis, where it performed well. We then generated a stability map for the stellar system, which showed a stability zone for the outer body which differed from the published orbital parameters, suggesting an eccentricity much higher than zero.

Using this geometry we then calculated the limits of the habitability zone and extracted the probable parameters for planetary systems from various exoplanet databases. A comprehensive search using 33 810 test particles failed to find any stable orbits. Simplifying the model by consolidating the central binary into a single body resulted in stable but highly eccentric orbits.

We concluded that Mercury6, which was originally designed for configurations comprising one central dominant body, probably became inappropriate when adding more bodies to a compact triple system of stars of almost equal mass, possibly in the coordinate system used for its test particlesparticles, i.e. in the splitting of the Hamiltonian.

Key words: methods: planets and satellites: dynamical evolution and stability – *N*-body simulations – celestial mechanics – triples: close – planetary systems.

Contents

For there is a single general space, a single vast immensity which we may freely call Void; in it are innumerable globes like this one on which we live and grow... In it are an infinity of worlds of the same kind as our own.

Giordano Bruno, *On the Infinite Universe and Worlds* (1584)

1. Introduction

1.1 Stellar multiplicity

It has been variously estimated that 12% - 40% of the stars in our Galaxy are binary or multiple systems, that multiplicities of three and higher can occur in 2% - 25% of all stellar systems and that many, if not most, close binaries have distant tertiary components (Alexander 2012; Kane & Hinkel 2012; Tokovinin 2004). Binary frequency appears to correlate well with stellar ages, with low-mass pre-main sequence stars having very high binary frequencies of 80% - 100%.

Similarly, a study that considered stellar systems with multiplicities ranging from one to seven in the set of stars with combined magnitude brighter than 6.00 on the Hipparcos scale (which was effectively limited to systems with mass above about $1M_s$, since very few systems of lower mass are included among the bright stars) identified 4 558 such bright systems, of which 60% were single stars, 32% binaries and 6% triples, with an observed average multiplicity of 1.53 (Eggleton & Tokovinin 2008). Although reasonably representative of stars more massive than the Sun, the Eggleton study is unlikely to be representative of the Galaxy as a whole because of its magnitude constraint.

Multiplicity data is also obtainable from the Multiple Star Catalogue (MSC), available at vizier.cfa.harvard.edu/viz-bin/VizieR?-source=J/A+AS/124/75 (Tokovinin 1997-1999), which is complete to a distance of around 10 pc.

1.2 Exoplanet multiplicity

A recent study (Roell et al. 2012) of 477 stellar systems identified 57 multiple systems (47 double and 10 triple systems) with at least one exoplanet. Some data from this study is shown in Table 1. The resulting multiplicity rate of about 12% is lower than

previously published values. A suggested reason is the increasing number of transiting exoplanets in recent years, which were excluded by previous studies.

Solar-like stars				
46%	54%	34%	9%	1
44%	56%	38%	4%	2
Exoplanet host stars				
22.90%	77.10%	19.80%	3.10%	3
17.20%	82.80%	14.80%	2.40%	4
11.95%	88.05%	9.85%	2.10%	5

1: Raghavan et al. (2010), 2: Duquennoy & Mayor (1991)
3: Raghavan et al. (2006), 4: Mugrauer & Neuhauser (2009)
5: Roell et al. (2012)

Table 1. Multiplicities of solar-like and exoplanet host stars.

The multiplicity for exoplanet host stars of 12% is also approximately a quarter of the multiplicity of solar-like stars. *To date, no S-type (see following section) planet has been found in a binary with a (projected) separation of under 10 AU and (S-type) multi-planet systems have only been found in stellar systems with (projected) separations larger than 100 AU.*

Combining the Eggleton and Roell data results in the average frequencies shown in Table 2. These are approximate because of the different binnings of the data.

Ref.	Multiplicity			
	1	2	3+	4+
1	54	34	9	
2	56	38	4	
3	77.1	19.8	3.1	
4	82.8	14.8	2.4	
5	88.05	9.85	2.10	
Eggleton[1]	59.61	31.53	6.30	2.60
Average	69.59	24.66	4.48	2.60

[1] Excluding the Sun

Table 2. Frequencies of multiplicities. (References are those in Table 1).

Eggleton found that the frequencies of various multiplicities follow a power law up to septuple multiplicity.

Turning to extrasolar planets, at October 2013 the total number of extrasolar planets had grown to 954 confirmed exoplanets with 162 multiple planet systems. Putting together all the results of planet frequency studies, it appears that, on average, every star should harbour at least one planet. Our Galaxy has at least 100 billion stars, implying approximately the same number of planets.

From 2009 to June 2013, NASA's Kepler spacecraft continuously monitored over 160 000 stars for transiting exoplanets. By June 2013, 3 216 planet candidates had been found (nearly quadrupling the sample of previously known planets) of which 132 planets in 69 stellar systems have been confirmed. Of the planet candidates, only 5% - 10% are likely to be false positive detections. In addition, Kepler identified 2 165 eclipsing binary stars.

1.3 Exoplanet orbit types

Initial discoveries were of planets orbiting single stars. Later, stellar companions were discovered around several dozen exoplanet host stars formerly believed to be single. The existence of circumbinary planets had been suspected and Kepler provided the first confirmed identification of transiting circumbinary planets. Most of these exoplanet candidates are orbiting one stellar component of a binary. This is denoted an S-type orbit configuration, while the circumbinary orbit of a planet around both binary stars of a binary or multiple star system is called a P-type orbit.

A summary of exoplanet nomenclature, which is particularly important regarding circumbinary planets, is provided in Appendix A.

Kepler recently discovered planets in P-type circumbinary orbits around both wide binaries (e.g. NN Ser (AB) c, d, DP Leo b, HU Aqr (AB) c and UZ For (ab) d) and close binaries (e.g. HWVir (AB) b, Kepler-16 (AB) b, dubbed the first "Tatooine" planet, Kepler-34 (AB) b, Kepler-35 (AB) b Kepler-38 (AB) b, and Kepler-47 (AB) b, c, which are all Neptune or Jupiter-like planets) and it began to find planets in triple star systems (e.g. 16 Cygni B b). The Kepler team estimates that about 1% of binary stars of close separations have giant planets in a nearly coplanar P-type orbit.

A planet (Kepler-64b) has already been discovered in a quadruple star system, orbiting outside a 20-day period eclipsing binary, with another visual binary orbiting ~1 000 AU away (Schwamb, Orosz et al, 2012).

Many possible combinations of planets orbiting triples can be listed (Verrier & Evans 2007). The current number of discovered planets by configuration of star system and hence orbit type, as compiled from various sources, is shown in Table 3.

Stellar multiplicity	Name	Stellar frequency (%)	Orbit code	type	name	number	frequency (%)	Exoplanet number	frequency (%)	Relative frequency[1]
1	Singles	69.6	1,1	P	Circumstellar	834	92.1	1456	91.6	0.8
2	Binaries	24.7				65	7.2	127	8.0	3.1
			2,1	S	Circumbinary	51	5.6	107	6.7	
			2,2	P		14	1.5	20	1.3	
3	Triples	4.5				7	0.8	7	0.4	10.2
			3,1	S	Circumtrinary/	6	0.7	6	0.4	
			3,2	P	circumtriple	1	0.1	1	0.1	
			3,3	P		-	-			
4+	Higher	2.6	4,2	P		1	0.1	1	0.1	41.3
Total		101				906	100	1590	100	

[1] Stellar frequency to exoplanet frequency. Note some rounding has occurred.

Table 3. Frequency of exoplanets by type of orbit.

The exoplanet data was extracted from the Open Exoplanet Catalogue (OEC) (Rein 2012) and the NASA Exoplanet Archive database (Akeson et al. 2013); the procedure used for the latter is presented in Appendix B. The planet orbit code we created in Table

3 represents [(number of stars in system),(number of stars orbited)].

Note that exoplanet host star multiplicity suffers from strong observational bias and selection effects produced by the original planet search programmes. For example, the Kepler input catalog was selected for certain stellar spectral types and radii.

Comparing the stellar multiplicity frequencies with those for the exoplanets is interesting. While approximately 70% of stellar systems are single, over 90% of exoplanet discoveries have been of this type. Conversely, while triple systems comprise over 5% of stellar systems, the frequency of exoplanet discoveries in these has been only 0.4%. The ratios of these frequencies suggest that, on the assumption that the true occurrence of exoplanets is not skewed as acutely as this, a huge potential exists for future discoveries in binary and higher multiple systems, with this potential increasing with multiplicity.

To support this assumption, comparing the exoplanet orbit type frequencies with the planet number frequencies shows that they are quite similar for single and binary stars. It has been found that the frequency of planets in binaries is not statistically different from planets orbiting single stars and that it cannot be lower by more than a factor of three compared to planets orbiting single stars. For moderately wide binaries, the frequency of planets is independent of separation and the wide companion plays only a marginal role in the formation and evolution of giant planets (Bonavita & Desidera 2007). It has also been reported that the presence of distant companions (separation >300 AU – 500 AU) does not significantly affect the process of planet formation, as the mass and period distribution of planets in such wide binaries are similar to those of planets orbiting single stars (Desidera & Barbieri 2007).

However, comparing the frequency of S-type orbits with P-type orbits in binaries shows that the former are almost four times more common. (A further type of

orbit, the L-type, where the planet co-orbits with one of the stars, i.e. librates about the triangular Lagrangian points like the Trojan asteroids in the Solar System, is ignored in this study.)

The exoplanet frequencies for triples and higher (hidden by rounding) are approximately half those for the orbit frequencies, implying that there are fewer planets in these systems. However, one must once again be beware of the small sample size and selection effects.

Most binary and multiple stellar systems found to be harbouring planets are wide, with separations larger than 100 AU (Eggenberger, Udry & Mayor 2004), and nearly half of the exoplanets found are in very wide binaries with average stellar separations greater than 1 000 AU (Roell et al. 2012). However, several systems with separations as low as ∼20 AU, such as HD 196885, have been shown to contain giant planets. Close binaries have a tendency to be found in higher-multiplicity systems, showing that close and wide binarity is statistically related (Tokovinin 2001).

Most multiple star systems are triple (also called trinary or ternary), with systems of four or more components less likely to occur. Some researchers expect that there will be more cases discovered of planets orbiting outside compact binaries than inside wide binaries, and this may also hold for triples. It appears that most triples are hierarchical, consisting of a close binary with the third star in a wide orbit, e.g. 16 Cyg Bb, which orbits a single star of its triple system.

Systems with multiplicities of three or higher containing planets are shown in Table 4, extracted from the OEC.

Planet name	Discovery year	Mass [MJup]	Radius [RJup]	Semimajor axis [AU]	Eccentricity	Number of stars in system	Orbit type	Number of planets in system	Distance [pc]
PH-1 (AaAb) b	2012	-	0.563	0.634	0.0539	4	P	1	1500
HW Vir (AB) b	2008	14.3	-	4.69	0.4	3	P	1	181
16 Cygni B b	1996	1.68	-	1.68	0.689	3	S	1	21.4
91 Aquarii A b	2003	3.2	-	0.7	0.03±0.03	3	S	1	45.9±0.6
HD 178911 B b	2001	6.29	-	0.32	0.1243	3	S	1	46.7
HD 196050 A b	2002	2.83	-	2.47	0.21	3	S	1	46.9
HD 40979 A b	2002	3.28	-	0.83	0.25	3	S	1	33.3
HD 41004 A b	2004	2.54	-	1.7	0.74	3	S	1	43

Table 4. Exoplanets discovered in stellar systems of multiplicity three and higher.

Only two P-type orbits have been found to date, and both are circumbinary.

PH-1 is a multiple star system of at least four stellar components, which hosts at least one planet, PH-1 (AaAb) b, which was found by amateurs at www.planethunters.org. It is in a circumbinary orbit around a binary that in turn is being orbited by a second binary approximately 1 000 AU away.

HW Virginis is a multiple star system of at least three stellar components, which hosts at least one planet, HW Vir (AB) b, detected by eclipse timing variations. An additional object orbits the binary every 16 yr - 55 yr. At around 20 - 65 Jupiter masses it is classified a brown dwarf.

A planet in a circumtriple orbit of a triple system has not yet been found. However, it appears inevitable that this configuration will eventually be discovered.

The object of this study was to identify a compact triple that is also likely to harbour planets, establish the orbital stability landscape around the system and see where this lies relative to the habitable zone.

1.4 Computational approaches

A computational approach was used. Numerical stability studies are a powerful tool to guide the search for new exoplanets, or additional exoplanets in known planetary

systems.

For example, over the last decade a number of studies have shown that, for systems that contain more than one planetary body, the orbits proposed initially are simply not dynamically feasible, "illustrating the critical importance of performing dynamical analyses as a part of the discovery process for multiple-planet exoplanetary systems." (Horner et al. 2012).

Also in recent years, numerous numerical investigations have estimated stability zones in known systems that might harbour undiscovered planets. *However, none of these were compact triple systems.*

As an example of this type of approach, Verrier and Evans investigated the stability zones for planets and asteroids in the γ Cephei system using the Bulirsch-Stoer algorithm in John Chambers's Mercury6 program. This is a binary system with a stable giant planet orbiting the larger star at about a tenth of the binary's separation (Verrier & Evans 2006).

They subsequently examined orbits around each of the stars in hierarchical triple systems (Verrier & Evans 2007). They extended Chambers's symplectic integrator algorithm (Quintana et al. 2002) to this triple system by defining a coordinate system where the positions of the stars are followed in hierarchical Jacobi coordinates while the planets are referenced only to their primary, then deriving the split Hamiltonian required in each hierarchical case. They applied only one case, to a circumbinary situation, to determine the extent of the stable zone that can support long-lived planetary orbits, and provided fits to the inner and the outer edges. An important finding was that the addition of a stable third star does not distort the original binary stability boundaries and that the binary stability criteria can be used to quite accurately predict the stability zones in any hierarchical stellar system, irrespective of the number of stars. They also

concluded that circumbinary planets are unlikely to exist in at least 50% of observable systems. However, they did not apply their analysis to P-type circumtriple orbits.

They also found that in the dynamics of planetesimals in the quadruple star system HD 98800, there were significant numbers of stable particles in circumbinary polar orbits about the inner binary pair, which are apparently able to evade the Kozai instability[1](Verrier & Evans 2009). In 2009 they analysed and confirmed this situation, concluding that high mutual planet-star inclinations are very likely, and that if there are regions of stability, then the outlook for planetary systems in these environments is more promising than previously thought.

The numerical results of Verrier and Evans were later explained purely analytically (Farago & Laskar 2010) and other researchers in turn expanded on this work numerically, investigating the dynamics and stability of orbits in three-dimensional circumbinary phase space as a function of binary eccentricity and mass fraction. They found that these orbits are surprisingly stable. In the words of one team of researchers, "circumbinary phase space is rich and dynamic, full of remarkable and stable orbits which do not behave simply. We should not presume any given binary system to lack a circumbinary component unless otherwise demonstrated." (Doolin & Blundell 2011).

A further development has been an analytical theory to model the motion of the recently discovered circumbinary planets Kepler-16 b, Kepler-34 b and Kepler-35 b (Leung & Lee 2013). Their orbits are significantly non-Keplerian due to the large

[1] The Kozai mechanism often destabilizes high-inclination orbits. It couples changes in the eccentricity and inclination, and drives high-inclination circular orbits to low-inclination eccentric orbits.

secondary-to-primary mass ratio and orbital eccentricity of the binaries as well as the proximity of the planets to the binaries.

However, it appears that orbit stability analyses have not yet been applied to actual circumtriple systems. The anticipated discovery of exoplanets in triple systems and the fact that a meaningful proportion of stars in the Galaxy are such systems, makes this a worthwhile field of investigation.

We focused on systems that have not yet been studied in detail regarding their stable regions.

The rest of this document is organized as follows:

Section 2 deals with the preparations for the research, including a review of available integrators, the selection of the compact triple to be investigated, the choice of parameters for the planet search and an initial examination of the selected integrator by applying it to a simple binary model before using it to replicate some previous research results on HW Virginis.

Section 3 comprises the major portion of the work, in which we investigate the stability of the stellar system, calculate the bounds of the habitable zone and then search for planetary orbits around the system.

Section 4 consists of a discussion of these results and the conclusions that may be drawn from them, followed by Section 5 in which we suggest the direction of future work on this topic.

2. Method

2.1 Numerical methods

The fastest algorithms that are reliable for long-term numerical orbit integrations are

symplectic integrators[2]. In particular, mixed-variable symplectic integrators exhibit substantially faster speed than conventional *N*-body algorithms. However, they become inaccurate whenever two bodies approach one another closely. This occurs because the potential energy term for the pair undergoing the encounter becomes comparable to the terms representing the unperturbed motion in the Hamiltonian. The problem can be overcome by using a hybrid method in which the close encounter term is integrated using a conventional integrator whilst the remaining terms are solved symplectically.

One of the earliest symplectic integrators was developed by Wilson and Holman (Wisdom & Holman 1991).

In 1993 Swift was created (Levison & Duncan 1994, 2013). Swift is designed to symplectically integrate the motion of massive bodies and test particles orbiting a more massive center, and is well suited for studying the dynamics of planetary systems. A later version for orbital simulation was SyMBA (Duncan, Levison & Lee 1998), an extension of Swift that uses a multiple time step technique and can symplectically integrate a full *N*-body system including close approaches between massive bodies. However, it fails in integrating close encounters with the central star.

Hervé Beust has developed an add-on for Swift that is designed to handle the dynamics of hierarchical systems of any size and structure, provided this hierarchy is preserved (Beust 2003). It comes in the form of the HJS (Hierarchic Jacobi Symplectic) package, a set of routines that can be added to the Swift package and allow one to integrate the dynamics of multiple stellar system.

---

[2] A symplectic integrator is a numerical integration scheme for a specific group of differential (in this case, Hamiltonian) equations, using classical mechanics and symplectic geometry.

The package probably most frequently used for problems involving a dominant central mass has been Mercury6 (Chambers 1999). However, dealing with planetary orbits in a binary system is problematical since the system no longer contains just one single dominant body. Fortunately, all long-lived planetary systems of binary and triple stars are likely to be hierarchical, i.e. they orbit one star with the second binary star orbiting a considerable distance away, or the planets orbit the centre of mass of a binary pair of small separation with the remaining star orbiting at a considerably larger distance. In this case one can modify symplectic schemes while still permitting close encounters. The original Mercury6 was later expanded to do this (Chambers et al. 2002).

A suite of *N*-body algorithms has also been developed by Sverre Aarseth, as described in his book (Aarseth 2003). While focused mainly on modelling clusters and galaxies, some programs (e.g. Triple) may be applied to planetary systems and small-*N* experiments.

Another integrator, written by Piet Hut to investigate a planet bouncing between the two stars of a binary, was built on a fourth-order Hermite integrator; it is a robust and flexible integrator for small-*N* systems as it has no preferred dominant force or geometry (Moeckel & Veras 2012).

Some of the more recent integrators have been designed for parallel or multicore/GPU implementation, such as QYMSYM (Moore & Quillen 2011) and GENGA (Elser, Grimm & Stadel 2013). The GENGA code is a hybrid symplectic integrator based on the Mercury6 code. At a low number of simulations (~ 30), the GPU overhead dominates and Mercury6 is faster. At a high number of simulations, GENGA begins to benefit from the large number of GPU cores, until at around 1 000 simulations

the GPU is fully occupied and the computation time begins to increase again. At 16 000 simulations the GPU is about 40 times faster than one CPU.

In 2007 Verrier & Evans developed a stand-alone program for triple systems, Moirai, based on the Chambers et al. (2002) algorithm, and tested it on the three main orbital configurations for triples (Verrier & Evans 2007). However, the code was not made public.

Other codes include the HNBody package, for the symplectic integration of nearly-Keplerian systems.

Of these scientific-grade symplectic integrators, perhaps the most popular and well-used codes are Mercury6 and Swift, with the latter's HJS add-in being particularly appropriate for the triple star system to be investigated. This code was supplied to us by its author (Beust 2013, private communication).

Evaluating these two integrators on their suitability for our purpose, the symplectic integration scheme in Mercury6 is the algorithm from Wisdom and Holman, which only uses Jacobi coordinates for massive objects. For masses around an hierarchical triple these would in theory be the same as Beust's hierarchical Jacobi coordinates, as long as one of the binary pair from the triple was specified as the central object. (As Chambers has pointed out, the Chambers et al. (2002) technique is identical to the Breust algorithm if only one planet is present in the system.)

We use test particles to investigate the regions of orbital stability, and Wisdom and Holman used a different coordinate scheme for test particles, where they were taken as the first relative Jacobi index, and this may not work for circumtriple objects. It therefore looked as if Beust's hierarchical Jacobi coordinate scheme might be more appropriate for a triple system. Much research that looks at hierarchical systems uses

this code (Verrier 2013, private communication). However, it appeared that the use of Mercury6's robust Bulirsch-Stoer algorithm would probably circumvent this problem.

Therefore, after evaluating both Mercury6 and Swift/HJS, we elected to use Mercury6.

Although this package cannot incorporate collisions, since these cannot be modelled symplectically, it performs well on most metrics, especially for modelling relatively few bodies (where it is very accurate) and the handling of close encounters. It can therefore be used in our proposed planetary simulations, where there are no collisions and only test particles. Its simplicity of use and clarity of documentation are attractive. It is written in Fortran 77 and uses the following *N*-body algorithms:

(1) A second-order mixed-variable symplectic (mvs) algorithm incorporating simple symplectic correctors. It is very fast but cannot compute close encounters between objects.

(2) A general Bulirsch-Stoer (bs) algorithm. This is slow but accurate in most situations. It can be used when all else fails, or to test whether the other algorithms are appropriate for a specific problem.

(3) A conservative Bulirsch-Stoer algorithm (bs2). This is twice as fast as the general bs routine, but it will only work for conservative systems, in which accelerations are a function of position only, e.g. Newtonian gravity but not general relativity.

(4) Everhart's RA15 (Radau) algorithm. This scheme is 2 - 3 times faster than the general Bulirsch-Stoer. It is usually reliable, except for very close encounters or very eccentric (e.g. Sun grazing) orbits.

(5) A hybrid symplectic/Bulirsch-Stoer integrator (hyb). This is very fast, quite robust but only moderately accurate. It can compute close encounters.

The main characteristics of these algorithms are summarised in Table 5.

Description	Abbrev.	Relative speed	Close encounters?	Timestep
Bulirsh-Stoer (general)	bs	1x	Yes	Variable
Bulirsh-Stoer (conservative systems)	bs2	2x	Yes	Variable
Second order mixed-variable symplectic	mvs	"Very fast"	No	Fixed
Hybrid (symplectic/Bulirsh-Stoer)	hyb	Intermediate	Yes	Fixed and variable
Radau 15th order	rad	2-3x	No	Variable

Table 5. Main characteristics of the Mercury6 algorithms.

For a compact triple, close encounters are likely. The two Bulirsch-Stoer algorithms and the hybrid scheme are able to handle these. However, the mvs algorithm is unsuitable for this configuration, which therefore excludes the hybrid scheme. Note also that the symplectic integrators may give spurious results if some objects have highly eccentric orbits during an integration.

The Bulirsch-Stoer algorithm will work with any system, but it may, however, be slow (Chambers 2013, private communication). Since the system is conservative, ie. has no relativistic effects, the conservative Bulirsch-Stoer becomes the best choice because of its relatively higher speed.

On a more practical level, the program settings for the number of time steps between progress alerts, output notifications and data dumps, as well as the number of time steps between checks for ejections and the recomputation of Hill radii can be critically important, since the writing of output is much slower than computation. For example, frequent output can negate the intrinsic speed advantage of the mvs and hybrid algorithms because of their fixed time steps (which result in a fixed number of steps), decreasing their speed by orders of magnitude relative to Bulirsch-Stoer, which may have increased the initial time step selected (resulting in a smaller number of steps). The sensitivity of speed to these factors becomes highly apparent when running integrations.

2.2 Selecting the compact triple

Identifying candidate hierarchical compact triples

Some multiple stars, termed trapezian, are usually very young, unstable systems. The relative distances between these bodies are comparable and they are usually unstable on time-scales of a few million years or less. These are thought to form in stellar nurseries and quickly fragment into stable multiple stars, which in the process may eject components as galactic high-velocity stars. An example of such a system is the Trapezium at the centre of the Orion nebula.

However, most multiple stars are organized in a structured manner, with smaller orbits nested inside larger orbits. In these systems there is little interaction between the orbits and, as in binary stars, the orbits are stable.

A gravitational three-body system is called hierarchical if its motion is well approximated by a pair of non-crossing elliptic orbits.

In a triple star system, each star orbits the center of mass of the system. Usually, two of the stars form a close binary system and the third orbits this pair at a distance much larger than that of the binary orbit. This arrangement is therefore hierarchical. The reason for this is that if the inner and outer orbits are comparable in size, the system may become dynamically unstable, leading to one star being ejected from the system. Hierarchical triple systems are important for testing theories of star formation and of stellar evolution in the presence of nearby companions.

In 1887 Heinrich Bruns proved that only specific solutions to the generalised three-body problem were possible. The motion of three bodies is now known to be generally nonrepeating, although some specific repeating solutions have been found. However, these were sparse, consisting of just three families. Recently, though, a surprising 13 new families were discovered (Šuvakov & Dmitrašinovic 2013). It

remains to be established which of these new solutions are stable and may represent actual systems, of both stars and planets.

While triple systems are less common than binaries, as previously discussed, and compact triples are rarer still, their prevalence is not insignificant. *A very recent study of the photometric database of eclipsing Kepler binaries identified 39 candidate triple systems and estimated that at least 20% of all close binaries have tertiary companions and that at least 8% have tertiary companions with a period less than approximately 7 yr.* (Rappaport et al. 2013).

Roell et al (2012) defined the multiplicity of an exoplanet host star by its inclusion in the Catalogue of Components of Double and Multiple Stars or CCDM (Dommanget & Nys 2002), available at vizier.cfa.harvard.edu/viz-bin/VizieR?-source=I/274. We followed this approach in our search for good candidate compact triples.

The current list of discovered planets in triple systems is shown in Table 6, reproduced from Desidera (Desidera et al. 2011). The first two columns list the name and the mass of the planet's host star. The third and fourth columns list the individual masses of the two components of the close pair and their semimajor axis or projected separation. The fifth column lists the projected separation between the planet host and the distant pair and the sixth column shows the critical semimajor axis for dynamical stability of planetary companions around the planet host. The seventh, eighth and ninth columns list the main planet parameters and finally the tenth column reports the references for the individual objects.

Planet Name	Host Mass $M\odot$	Close pair Comp. Mass $M\odot$	Close pair ρ_{close} AU	Wide pair ρ_{wide} AU	Wide pair a_{crit} [a] AU	Planet M_{pl} MJ	Planet a_{pl} AU	Planet e_{pl}	Ref
30 Ari B	1.16	1.31+0.13[b]	0.02	1500	318	9.88	1.00	0.29	1,2
HD 40979	1.19	0.83+0.38	129	6400	1452	3.83	0.85	0.27	3
HD 65216	0.92	0.09+0.08	6	253	82	1.21	1.47	0.41	4,5
HD 132563B	1.01	1.08+0.56[c]	10	400	78	1.49	2.62	0.22	6
HD 178911B	1.06	1.10+0.79	3	640	120	7.35	0.35	0.14	7
16 Cyg B	0.99	1.02+0.17	70	850	183	1.68	1.68	0.68	8
HD 196050	1.15	0.29+0.19	20	511	146	2.90	2.45	0.23	5
91 Aqr[d]	1.23	0.87+0.84	18	2250	461	2.90	0.30	–	9,10,6

Table 6. Hierarchical triple systems with planets.

References: 1: Guenther et al. (2009); 2: Morbey & Brosterhus (1974); 3: Mugrauer et al. (2007a), 4: Mugrauer et al. (2007b), 5: Eggenberger et al. (2007); 6: Desidera et al. (2011); 7: Tokovinin et al. (2000); 8: Patience et al. (2002); 9: Raghavan et al. (2006); 10: Washington Double Star Catalog (WDS) (Mason et al. 2001).

Notes: [a]: The critical semimajor axis for dynamical stability was obtained from the projected separation as in Bonavita & Desidera (2007). [b]: Minimum mass from spectroscopic orbit. [c]: Value of plausible mass. [d]: Planet announced in 2003 (Mitchell et al. 2003) but never published in refereed journals, confirmed at the Conference "Planetary Systems Beyond the Main Sequence", as reported in the Extrasolar Planet Encyclopedia. Stellar mass of 91 Aqr obtained from parameter interface (Da Silva et al. 2006) using the input parameters from Hekker et al. (2007); stellar masses of the companions from magnitudes in the Washington Double Star Catalog (WDS) and mass-luminosity relation.

In all these systems the planet orbits the isolated component of the hierarchical triple, with a close stellar pair at a much larger separation.

As a first-order approximation, the dynamic effects of the distant pair can be approximated as a single star with the sum of the masses of the individual components. After deriving the critical semimajor axis for dynamical stability (Holman & Wiegert

1999) in this way, no systems have been found for which the outer pair has a strong impact on the planetary region.

One investigator summarised this as follows: “It seems that hierarchical triple systems do not represent an hostile environment for planet formation around the isolated component, regardless of the mass ratio between the planet host and the sum of the masses of the other components. …In all but one stellar triple with planets, the separation of the stellar pair is larger than the planet semimajor axis. While selection effects certainly play a role, a moderately wide pair in a triple system guarantees that the present stellar orbits are not disruptive for the planetary system around the isolated component. A wide stellar triple might also indicate a rather unperturbed dynamical history for the system.” (Desidera et al. 2011).

In comparison, the circumbinary planets around eclipsing binaries that have been found to date are all rather massive and have long periods.

Our objective was to map the stability landscape of an hierarchical compact triple. The geometry of the stability zone would indicate not only where to look for planets but how to look, i.e. whether radial velocity, transit or microlensing methods would be most suitable.

So the next step was to identify a triple amenable to this investigation and which may harbour planets in P-type circumtriple orbits. Ideally, one would like to select a triple system that:

(1) Has a known geometry

One option is to choose it from the Rappaport 2013 list of 39 triple candidates, for which orbital parameters are given. These triples were selected from the Kepler eclipsing binary data, i.e. no planets had been found. The disadvantage is that these

triples have been inferred from eclipse timing variations and are only tentative.

A better option would be to select it from the Eggleton & Tokovinin 2008 data, which was based on catalog searches. However, of the 285 triples in the Eggleton and Tokovinin catalogue, 74 have only an inferred third component. Of the remaining 211, the dozen most compact systems are shown in Table 7, ranked by the period of the outer component, which is arbitrarily truncated at 5 000 d.

No.	System name	Full record ref.	Configuration (per Eggleton 2008)	Inner period (d)	Outer period (d)	Period ratio
1	Lam Tau	34	((A4IV + B3V; 3.953d SD) + ?; 33.03d, e=0.15)	3.95	33.0	8
2	VV Ori	57	((B1V + B5-9V; 1.485d) + A7V:; 119.1d e=.29)	1.49	119.1	80
3	Bet Per	24	((6.0G8IV + 2.2B8V; 2.87d SD) + 4.72F1; 1.86y, e=0.23)	2.87	679.4	237
4	B Per	37	((A2V + ?; 1.527d e=.02) + ?; 1.921y, e=.24)	1.53	701.6	459
5	The Car	132	((B0.2Vp + ?; 2.139d e=.24) + 13.0; 2.242:y)	2.14	818.9	383
6	Phi Phe	13	((A3V + ?; 41.49d e=.32) + ?; 2.403y)	41.49	877.7	21
7	Lam Sco	208	((B1.5IV + ?; 5.953d e=.26) + B2IV; 1053d, e=.12)	5.95	1 053.0	177
8	4 Dra	143	((WD + M4V; 0.16d, SD, CV) + M3III; 1703d, e=0.30)	0.16	1 703.0	10 644
9	HR 6469	205	((F2V + F8:; 2.23d) + G8III-IV; 2019d e=.67)	2.23	2 019.0	905
10	15Eta Vir	141	((A2IV + A4V; 71.79d e=.27) + A8-F0; 4791d, e=.08)	71.79	4 791.0	67
11	1 Gem	67	(4.77(G6III + ?; 9.597d) + K0III; 13.20y e=.34)	9.60	4 821.3	502
12	64 Ori	66	((B7III + B8III; 14.57d e=.39) + B5V; 13.22y, e=0.73)	14.57	4 828.6	331

Table 7. Most compact triples from the Eggleton & Tokovinin 2008 survey.

Only two can be considered very compact triples: VV Ori with an inner binary orbital period of 1.485 d and an outer component with a period 119.09 d (and masses 10.2 M_s, 4.5 M_s and 2.3 M_s respectively), and 35 Lam Tau with periods of 3.95 d and 33.025 d (and masses 6.8 M_s, 1.8 M_s and ~1 M_s respectively). However, the geometry of these two systems remains uncertain, especially regarding VV Ori's outer star (Terrell, Munari & Siviero 2007; Van Hamme & Wilson 2007).

The same uncertainty pervades some of the subsequent less compact systems, with the possible exception of 64 Orionis. Indeed, some studies even suggest that Phi Phe (Pourbaix et al. 2013) and 4 Draconis (Wheatley, Mukai & De Martino 2003) are not triple at all.

(2) Will be searched for planets.

The difficulty lies in finding what is on the target lists of the myriad searches, including ground-based, that are being undertaken for exoplanets. For example, a forthcoming probe such as GAIA will to some extent close the gap left by the end of the Kepler programme. But unlike Kepler, which generally provided only estimates of planet radii and orbital periods, many of the GAIA planets will have their full orbits revealed. *But GAIA does not have a target list as such.* It will conduct an unbiased astrometric survey of all stars down to 20th magnitude to search for companions (either stars or planets). Although it will be sensitive to planetary companions only for fairly bright stars, it is expected to find around 2 500 new planets.

(3) Alternatively, has been searched for planets without success (but may still harbour planets that were not detected).

Options (1) and (3) are to some extent related, and preferable to option (2). We therefore pursued the third option.

Very compact hierarchical triple systems form a very small minority of hierarchical triples, with only 7 of the catalogued 724 systems having outer periods shorter than 150 days.

The first compact hierarchical triple system, discovered from Kepler photometric data, was the triple KOI 646 (Fabrycky 2010).

In 2011 eclipse timing variations in Kepler photometry discovered the compact hierarchical triple KOI 928, where a low-mass eclipsing binary orbits a more massive third star (Steffen et al. 2011). For KOI 928, the orbital period of the star orbiting the binary of 116 d is quite short compared to the known hierarchical triples (Eggleton &

Tokovinin 2008), and the mass ratio of this star to the binary of 2.5 is exceptionally large.

This was followed by the detection of the eclipsing compact hierarchical triple KOI 126 (Carter et al. 2011) and HD 181068, a red giant in a triply-eclipsing compact hierarchical triple (Derekas et al. 2011). A subsequent detailed investigation of the structure of HD 181068 indicated that the close and wide subsystems revolve in almost exactly coplanar and prograde orbits (Borkovits et al. 2013).

KOI 126 and HD 181068 are the first representatives of a new category of triply eclipsing triple systems. *These two systems are unusual even amongst the very few similarly compact triples in having reversed outer mass ratios*, i.e. the wide, single component is the more massive star, and also the largest and brightest. Before Kepler, the highest known outer mass ratio was below 1.5 and for 97% of known hierarchical triples it remained under one, i.e. in almost all the catalogued systems, the total mass of the close binary exceeded the mass of the tertiary. In contrast, the outer mass ratios of these two new systems are ∼3.0 for KOI 126, and ∼1.9 for HD 181068.

KOI 126 has an outer period of 34 d while for HD 181068 it is 45 d; there is only one system with an outer orbital period shorter than this (λ Tau, at 33 d).

Of these two systems, KOI 126 has been dynamically checked by numerical simulations but HD 181068 has not. In addition, dynamical analysis of HD 181068 is much less complex than for KOI 126, because of the much simpler and apparently constant orbital configurations.

For these reasons and because it appears to be the more interesting system, we decided to investigate the stability of, and the landscape around, HD 181068.

Analytical prediction for the stability of the triple

The most recent stellar and orbital parameters for the HD 181068 system are shown in Table 8.

Stellar parameters				
Star		Ba	Bb	A
Mass	[M_s]	0.915(34)	0.870(43)	3.0(1)
Radius	[R_s]	0.865(10)	0.800(20)	12.46(15)
	[AU]	0.00402	0.00372	0.05793
Density (calculated)	[g cm^{-3}]	1.995	2.398	2.189E-03
Orbital parameters				
Subsystem		Ba–Bb	A–B	
Period	[d]	0.9056768(2)	45.4711(2)	
a	[R_s]	4.777(39)	90.31(72)	
	[AU]	0.02221	0.41986	
e	[-]	0	0	
ω	[-]	–	–	
i	[°]	86.7(14)	87.5(2)	
$\Delta\Omega$	[°]	0.0(5)		
i_m	[°]	0.8(14)		

Table 8. Stellar and orbital parameters for HD 181068 (from Borkovits et al. 2013).

A combination of the obtained Ω parameter with the two observable inclinations results in a mutual inclination of $i_m = 0.8° \pm 1.4°$, which suggests exact coplanarity.

Generally (and unlike S-type orbits) the stability limits for P-type orbits are almost independent of the mass ratio of the primaries. The stability criterion for triples in particular is given by (Mardling & Aarseth 2001)

$$a_{trip} \gtrsim C \left(\frac{M_{trip}}{M_{bin}}\right)^{\frac{2}{5}} \frac{(1+e)^{\frac{2}{5}}}{(1-e)^{\frac{6}{5}}} a_{bin} \qquad (1)$$

where a_{trip} and e are the full semimajor axis of the triple (i.e. of the outer orbiting star) and its corresponding orbital eccentricity, a_{bin} is the orbital separation of the two stars in the binary and M_{trip} and M_{bin} are the mass of the triple and binary respectively, while C

= 2.8 is determined empirically. This relationship is shown in Figure 1, which plots the ratio of semimajor axes against the triple's eccentricity for various mass ratios.

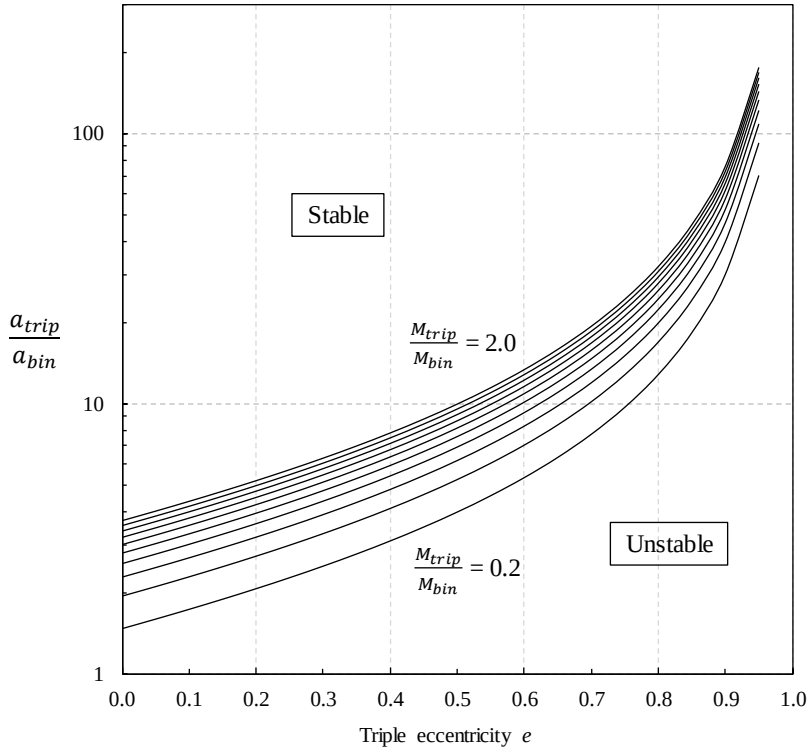

Figure 1. Stability criterion for triples - semimajor axis ratio and eccentricity.

Converting equation (1) to orbital periods,

$$P_{trip} \gtrsim 4.7 \left(\frac{M_{trip}}{M_{bin}}\right)^{\frac{1}{10}} \frac{(1+e)^{\frac{3}{5}}}{(1-e)^{\frac{9}{5}}} P_{bin} \qquad (2)$$

where P_{trip} and P_{bin} are the orbital periods of the triple and binary respectively.

Although the errors in the estimated masses of the binary and triple may be large, the small exponent on the mass ratio of means the dependence of period on masses is very weak. This can be seen in Figure 2, which plots the period ratio against the triple's eccentricity for various mass ratios.

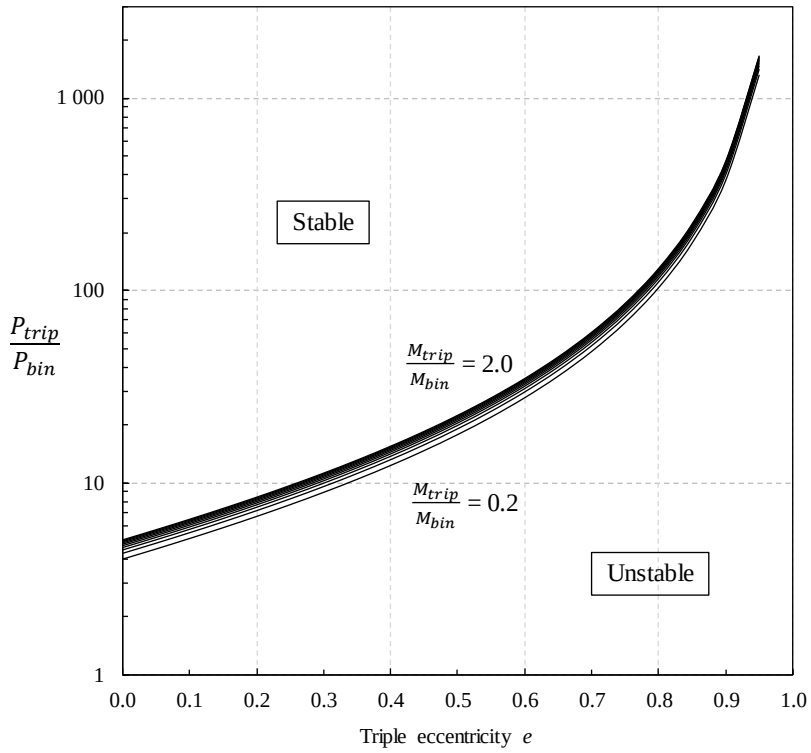

Figure 2. Stability criterion for triples - period ratio and eccentricity.

However, we usually have quite good estimates of eccentricities *e*. As shown in Table 8, the values for P_{bin} and P_{trip} are quite accurate and there is evidence from the radial velocity solution of Derekas (Derekas et al. 2011) that both orbits are circular, so one can evaluate the stability of this triple with some confidence.

For HD 181068 the eccentricity of the triple is thought to be zero, the mass ratio is 1.68 and the period ratio is 50.2. The period ratio stability criterion given by equation (2) and Figure 2 is 4.95. *This suggests that the system should be stable. For the system to become unstable, the triple's outer orbit would have to be quite eccentric, with an eccentricity of over 0.67.*

2.3 Parameters

Initial parameter selection

Numerical simulations first investigated long-term orbital stability within the coplanar,

circular, restricted three-body problem – mainly circumstellar and circumbinary orbits. With improvements in computing power, the circular constraint was relaxed to model eccentric binary systems, e.g. (Haghighipour 2008; Holman & Wiegert 1999) and there is now sufficient computational power to relax the coplanar constraint and investigate inclined orbits.

However, because of the added complexity of modelling a circumtriple four-body problem, as well as limited computational power, we reverted to the coplanar, circular case.

Databases

We used the Open Exoplanet Catalogue (OEC) as our database. The OEC was created because some exoplanet catalogues, e.g. www.exoplanets.org (Wright et al. 2011) are updated only irregularly and often lag several weeks behind important discoveries. Other websites, most importantly www.exoplanet.eu (Schneider et al. 2011), are usually updated very quickly after an announcement is made, but have had typographical errors and inconsistencies and some information such as discovery method, while available on the website, was not in the downloadable files.

The OEC also claims to be the only catalogue that can correctly represent the orbital structure of planets in arbitrary binary, triple and quadruple star systems as well as orphan planets (Rein 2012).

Note that exoplanets.org only lists exoplanets that are validated in peer-reviewed journal articles, whereas exoplanet.eu includes exoplanets that are only candidates, and the NASA Exoplanet Archive (exoplanetarchive.ipac.caltech.edu/) lists and distinguishes planets at various stages of the confirmation process. Also, the NASA Exoplanet Archive uses the Washington Double Star Catalog (WDS) catalog for its stellar multiplicities, and the WDS also contains optical systems, i.e. stars that are

not actually physically associated. Therefore, the fact that a star is listed as having multiple components in the NASA Exoplanet Archive does not necessarily mean it is a true multiple system.

Orbital distance

The mass-semimajor axis distance diagram for all the confirmed exoplanets is shown in Figure 3, created from data downloaded from the OEC database.

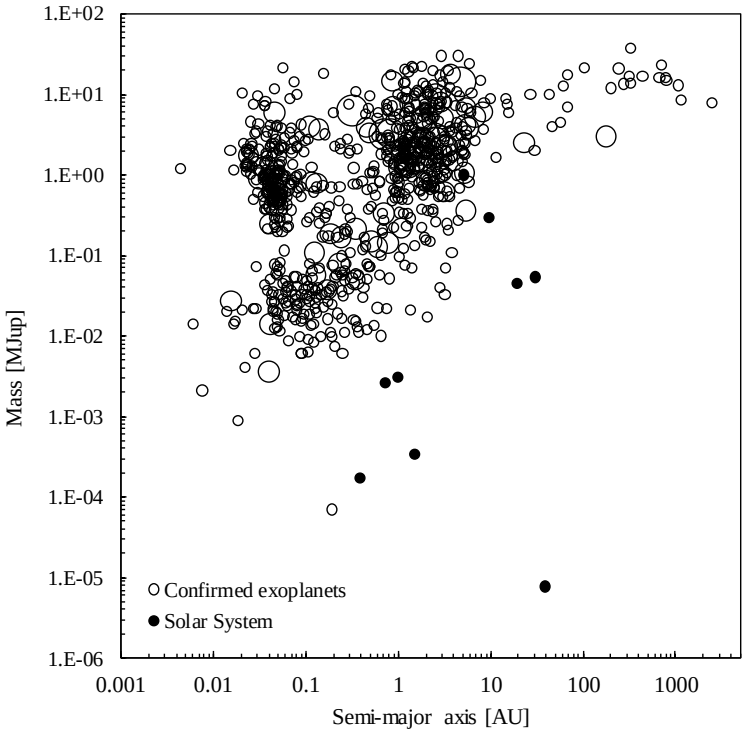

Figure 3. Exoplanets: mass – semimajor axis distance, with stellar multiplicity.

We have made the width of the circles proportional to the number of stars in the system (from 1 to 4) and the solid circles represent the planets in the Solar System for comparison.

The planets' semimajor axes span 0.004 AU to 2 500 AU, with masses ranging from 8×10^{-6} M_J to 38 M_J. The planet sample shows observational and selection biases – the sample consists of planets generally more massive than most planets in the Solar

System and they tend to have semimajor axes that are generally smaller, although there is a clear bimodal distribution, with its peaks at around 2 AU and 0.5 AU. Another noticeable characteristic of the distribution is the lack of massive planets (say > 1 M_J) with small semimajor distances (say < 0.02 AU). Small semimajor distances of course imply short-period orbits. There is also a dearth of exoplanets in the region where the Solar System planets lie. Semimajor distances larger than 10 AU imply longer orbits that can require many years of observation to confirm just a few planetary orbits. At these distances, for the more massive planets there is a small tail of observations; however, since smaller planets are more difficult to detect there are no observations in the large-orbit, small-planet region.

Although the sample size is small, there appears to be no obvious difference in distribution between the different stellar multiplicities shown in the graph. This is highlighted in Figure 4, which shows, on an identically scaled graph, the confirmed planets discovered in stellar systems of multiplicities greater than one. It also identifies those in S-type and P-type orbits, together with the Solar System planets.

These planets have semimajor distances spanning 0.02 AU to 180 AU, with masses ranging from 0.004 M_J to 18 M_J. Again, they tend to be more massive than the Solar System planets and in smaller orbits.

However, here a difference in distribution becomes more apparent – planets in P-type orbits are in larger orbits than S-type orbits. This is unsurprising, since the inner stability region will tend to be further away for binary and higher multiplicities. The masses of planets in P-type orbits are approximately twice those in S-type orbits and they move in orbits approximately three times larger.

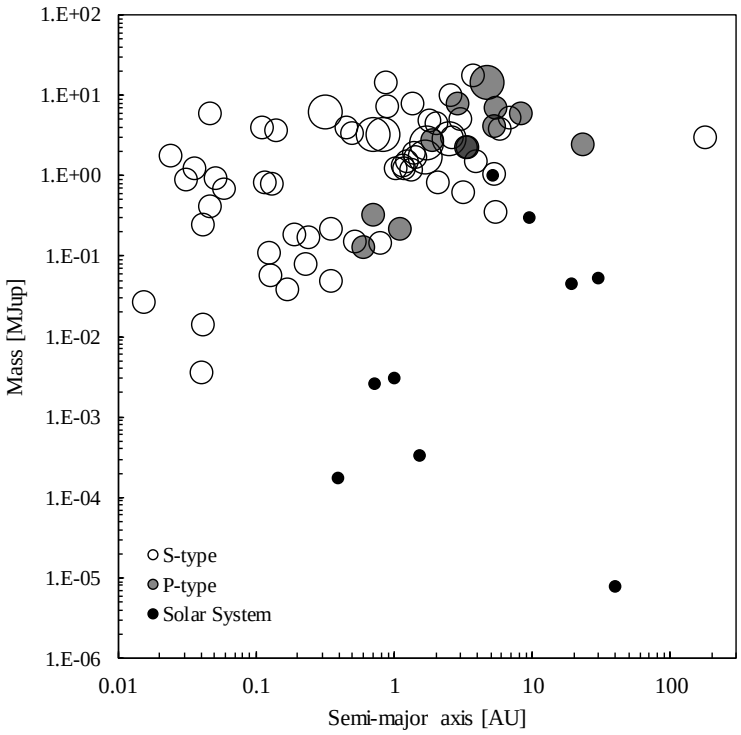

Figure 4. Exoplanets: mass – semimajor axis distance, with stellar multiplicity and orbit type.

In our searches we will sample orbit semimajor axes from a uniform distribution.

Eccentricity

Eccentric orbits are a consequence of strong gravitational interactions; eccentric planetary orbits in systems with no other detected planets suggest prior scattering events where their original siblings were ejected. Planets in multiple systems tend to have lower eccentricities, suggesting these interactions did not occur. Planets orbiting their central star very closely tend to have very low eccentricities as tidal interactions with the star circularises their orbits over long timescales.

Figure 5 shows the orbital eccentricity of all the confirmed exoplanets against their semimajor orbital distances, together with the Solar System planets for comparison.

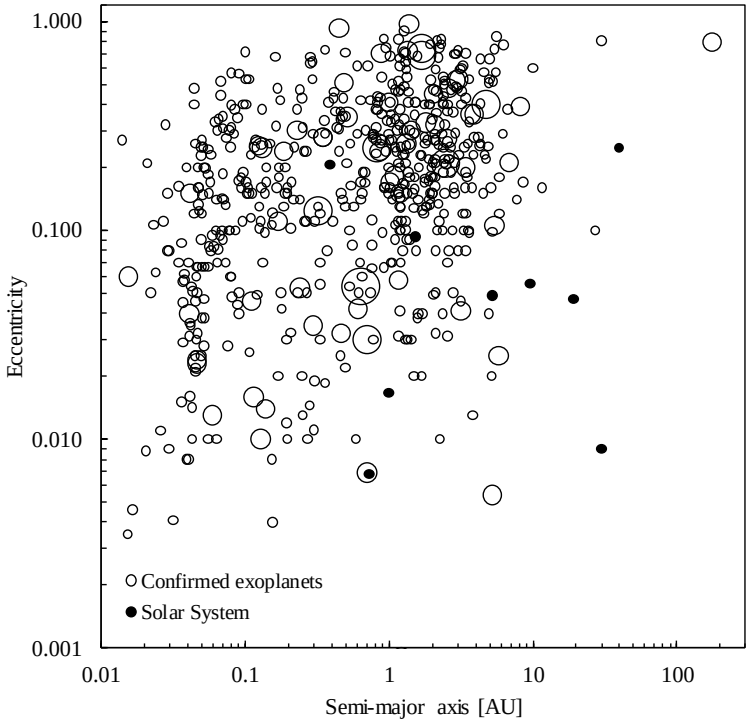

Figure 5. Exoplanets: eccentricity – semimajor axis distance, with stellar multiplicity.

The distribution of orbital distances is the same as discussed in the previous section, whereas the eccentricities display a more uniform distribution, ranging from close to zero to almost one, with their peak at around 0.20. Again, the distribution of eccentricities for planets orbiting in multistellar systems does not appear dissimilar to that for planets orbiting single stars, and is less different to that of the planets of the Solar System than it is for mass.

This is shown in more detail in identically scaled Figure 6.

The exoplanets are generally in smaller orbits than the average Solar System planet and their eccentricities are higher. The average eccentricity of S-type orbits is 0.25 and that for P-type orbits is 0.16, with both being higher than the Solar System planets' average of 0.08.

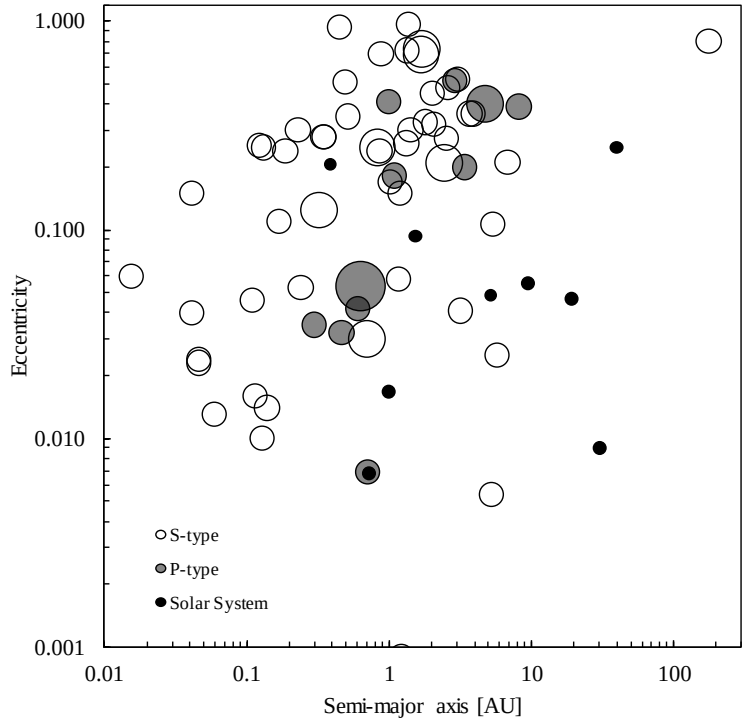

Figure 6. Exoplanets: eccentricity – semimajor axis distance, with stellar multiplicity and orbit type.

For S-type orbits the gravitational force of the secondary star (or stars) is the main source of orbital perturbation, while P-type orbits' stability is determined by the orbital geometry of the stars being orbited.

One of the proposed explanations is that when the orbit of a close-in planet is excited by an outer companion planet, the planets' gravitational interaction combined with tidal effects between the host star and the close-in planet can give rise to an increasing growth in the eccentricity of the close-in planet (Alexandre, Gwenaël & Jacques 2012).

We will select eccentricities from a uniform distribution spanning the range from zero to almost one.

Orbital inclination and coplanarity

Inclination is defined here as the angle of the orbit relative to the plane of the sky, and inclinations of over 90° represent retrograde orbits. The distribution of inclinations of the confirmed exoplanets, from the OEC database, are shown in Figure 7.

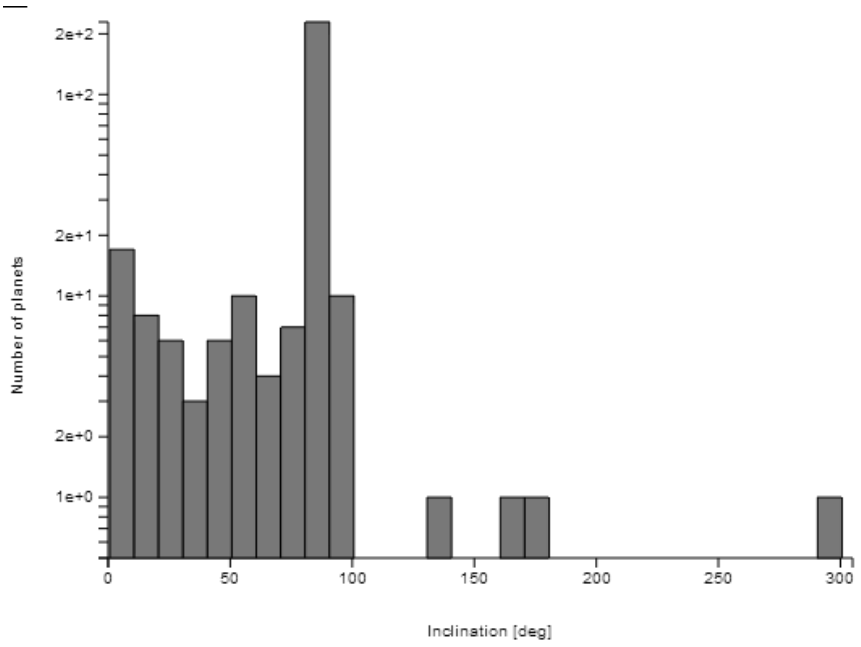

Figure 7. Exoplanets: number of discovered orbital inclinations.

The most common inclination found is 80°– 90°, by an order of magnitude. This is the natural result of the fact that most discoveries have been made by the transit method. While the above graph therefore tells one little about the actual distribution of inclinations, on the basis that future discoveries are likely to continue to be via the transit method, we will use this range of inclinations in our model. (Using a different definition, we will in fact use the equivalent 0°.)

Turning to coplanarity, one early study determined that at least one third of triple stars have non-coplanar orbits (Fekel Jr 1981).

Planetary orbits in the Solar System are close to coplanar and stable. If multiple stars form by hierarchical fragmentation of a rotating cloud (Bodenheimer 1978) or by

fragmentation of a circumbinary disk (Bonnell & Bate 1994), similarly coplanar configurations would be expected.

Close to 85% of Kepler's multi-planet systems are coplanar to within 3° as a consequence of the transit technique it used. However, several other studies from radial velocity searches reach a similar conclusion: that planets in multiple systems usually have very low mutual inclinations. This implies that these planets formed together inside a protoplanetary disc and did not experience any large gravitational perturbations, which would have increased their orbital inclinations.

The relative orientation of inner and outer orbits in a triple or higher multiplicity system can be measured by the angle $\varnothing$ between angular momenta of the orbits. One expects totally uncorrelated orbital spins ($\varnothing = 90°$) for purely dynamical processes and correlated spins ($\varnothing = 0°$) for a cascade fragmentation of a rotating protostellar cloud. A coplanar system ($\varnothing = 0°$) will stay coplanar forever. Early studies showed that the available data could only be interpreted by involving a small degree of orbital momentum alignment (Tokovinin 1993). A later study of $\varnothing$ statistics showed that both extreme hypotheses (co-aligned and random orbital spins) could be rejected. The average $\varnothing$ was around 50° (Tokovinin 2000).

Also, if a planetary system forms in a primordial binary system, the orbits of the planets and the companion star are expected to be essentially coplanar. If a planetary system forms around an initially single star, which becomes a binary later through an encounter, the orientation of the orbits of the planets is random with respect to the orbit of the companion star (Malmberg, Davies & Chambers 2007).

Linking inclination with eccentricity, the Kozai effect was discovered over fifty years ago (Kozai 1962). This mechanism causes the eccentricity of a planet to vary periodically if the orbits of the planet and the companion star are sufficiently inclined. A

planetary system can be affected strongly by the presence of a companion star, even if the semimajor axis of the companion's orbit is large. However, this is only true if the initial inclination between the orbital planes of the planet and the companion star is larger than a critical angle of 39.23°.

It has been shown that for systems which have formed this way, around 80% will have an initial inclination above 39.23° and hence be in the region where the Kozai mechanism can be important (Malmberg, Davies & Chambers 2007). The Kozai mechanism will lead to an increase in the eccentricity of the outer planet, if the binary is not too wide. The increased eccentricity of the outer planet leads to strong planet-planet interactions in the system, which can lead to the ejection of one or more planets and also result in the remaining planets being left on more eccentric orbits than before.

It has been pointed out (Perryman 2011) that, based on limited data, planets with the highest eccentricities ($e > 0.8$) tend to be accompanied by a stellar or brown dwarf companion. This suggests eccentricities are caused by the Kozai mechanism, in which hierarchical triple systems with high relative inclinations cause large-amplitude periodic oscillations of the eccentricity of the inner. The coupling of these Kozai oscillations with tidal friction (Kozai migration) may also lead to circular orbits for short-period planets. In multiple systems this may bring massive planets close to their stars and may explain why the most massive short-period planets are found in binary or multiple systems.

A simulation of planetary orbits around triples (Verrier & Evans 2007) assumed all orbits to be coplanar, justifying this assumption on the basis that higher inclinations will be subject to Kozai instability, causing large variations in the stellar orbits, which would be expected to destabilize test particles rapidly. Their simulations always kept one star in a circular orbit.

Another assumption of coplanarity between the orbital plane of the binary and the planetary system was based on the fact that this should have only a secondary effect on the results, since planetary ejections from scattering do not occur strictly in the plane of the planetary system (Moeckel & Veras 2012).

It has been predicted (Alexander 2012) that disks around close binaries with semimajor axes less than 1 AU live longer than those around single stars, but disk lifetimes decline as photoevaporation increases at larger binary semimajor axes. As a result, they predict a dearth of circumbinary planets around wide binaries with $a > 10$ AU and an abundance of circumbinary planets in stellar binaries with $a < 1$ AU. It has also been predicted that circumstellar disks around binaries with $a < 100$ AU should be coplanar to the orbit of the binary. Thus any planets formed from such a disk are expected to be aligned with the binary's orbit (Bate et al. 2000).

Also, most (85%) multi-planet systems have mutual inclinations of less than 3° (Julia & Jean-Luc 2012).

For all these reasons we will assume coplanarity in the system under investigation. It appears that triple star systems tend to be coplanar, and that it is likely that any planets are also coplanar with the triple. This assumption will also simplify the modelling.

2.4 Examining the integrators

Selecting a test system

In order to examine the capabilities of Mercury6, it was applied to two simple problems – first modelling a binary star system and then modelling an exoplanet in a P-type orbit around the binary, by approximating the system as a single star and planet.

HW Virginis, previously seen in Table 4, was selected for this test and approximation. It contained the first circumbinary planet to be detected around a host other than a pulsar (Lee et al. 2009), and is a triple system with its planet in a P-type orbit around the binary. A conceptual diagram of the geometry is shown in Figure 8.

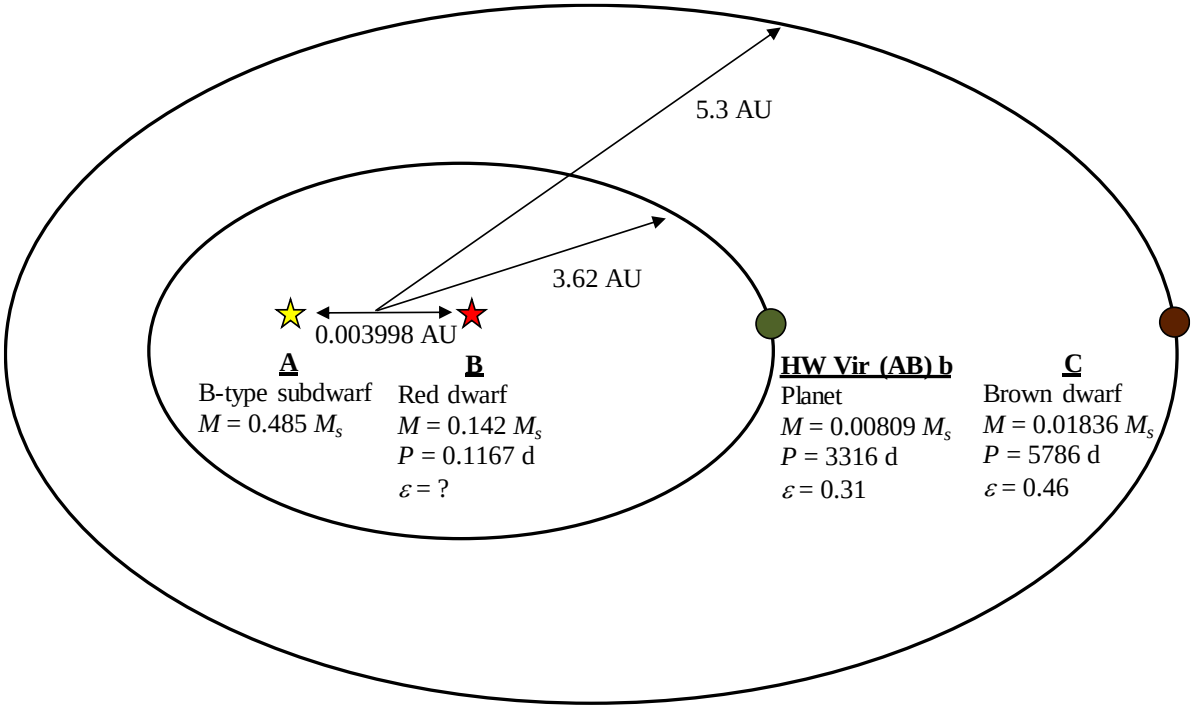

Figure 8. The HW Virginis system data, per Lee et al, 2009.

The present age of HW Vir is estimated to be at most 12 Gyr. It comprises a very close binary consisting of a B-type subdwarf of mass 0.485 M_s and a red dwarf of 0.142 M_s orbiting each other with a period of 0.1167 days or 2.8 hours, with the planet orbiting this binary in 3 316 days or just over 9 yr and the third star, a brown dwarf of 0.0184 M_s, orbiting the binary with a period of around 16 yr. The influence of the brown dwarf on the binary and planet is therefore likely to be small and it will be a good approximation to consider the system as a single star and planet.

Another reason for this choice was that two detailed orbital analyses, also using Mercury6, have been done on this system, by (Beuermann et al. 2012) and (Horner et al.

2012) and can be used as a further check on results. Interestingly, while the studies were virtually contemporaneous, Beuermann found dynamically stable orbital solutions while Horner was unable to find any feasible orbits at all. (One possible reason was that Beuermann et al assumed that the eccentricity of the outer companion's orbit was near-circular and fixed, with a period of 55 yr.) If this is the case, the sensitivity of this type of numerical study to its assumptions is a bit disconcerting. We used both their sets of assumptions for this exercise.

The parameters of the system, including the parameters proposed initially by Lee et al and later by Beuermann et al are shown in Table 9.

Name		HW Vir	HW Vir (AB) b	HW Vir (AB) C	HW Vir (AB) b	HW Vir (AB) C
RA		44:20.0				
Dec		-08:40:17				
Magnitude		10.9				
Spectral type		sdB+M				
Discovered in			2008			
Detection method			Eclipse Timing Variations			
Parameter	Unit	Lee (2009)			Beuermann (2012)	
Mass A	M_s	0.485±0.013				
Mass B	M_s	0.142±0.004				
Total binary mass	M_s	0.627±0.017		0.01861844		
Separation a_{bin}	AU	0.00399833	0.0468±0.0066	0.1551±0.0054		
Eccentricity	e	-				
Inclination i_{bin}	◦	80.92±0.36				
Distance	pc	181±20				
T	HJD	2 445 730.557123±2.5E-5	2 449 840 ± 63	2 454 500 ± 39	2 452 401	2 461 677 :
P	d	0.11671959933±5.5E-10	3316 ± 80	5786 ± 51	4638.675 ± 73.1	20088.75 (fixed)
M sin i	M_s		0.00809 ± 0.00040	0.01836 ± 0.000031	0.0136 ± 0.0009	0.062 ± 0.014
a sin i	AU		3.62 ± 0.52	5.30 ± 0.23	4.69 ± 0.06	12.8 ± 0.2
e	-		0.31 ± 0.15	0.46 ± 0.05	0.40 ± 0.10	0.05 :
ω	◦		60.6 ± 7.1	90.8 ± 2.8	-18 ± 10	0 :

Table 9. Parameters for the HW Vir system, from Lee et al. (2009) and Beuermann et al (2012).

The eccentricity of the orbit of the binary is unknown. However, there is a direct correlation between the period of revolution of a binary star and the eccentricity of its orbit, with systems of short period having a lower eccentricity. It has been shown that for binaries with periods less than ~4.3 d (log P < 0.6), the individual eccentricities are

not significantly different from zero as a result of tidal interactions, as shown in Figure 9 (Abt 2005).

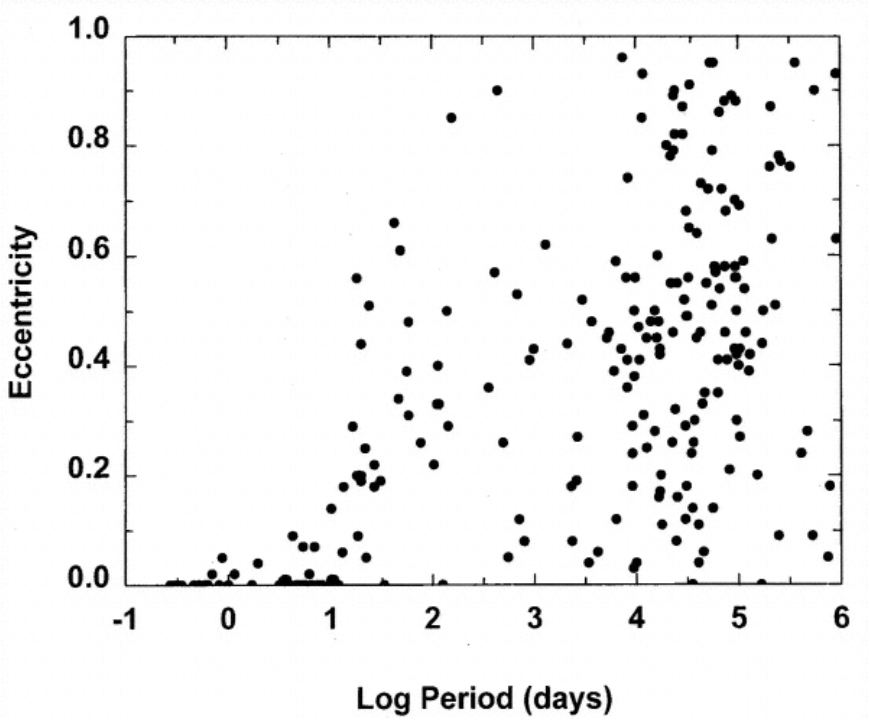

Figure 9. Eccentricities for 155 B0–B9.5 main-sequence spectroscopic and visual binaries against the logarithms of their periods. Note that systems with zero eccentricity are frequent in systems with periods of 0.5 – 10 days (log P = -3 to 1) and extend to 10^5 days.

An eccentricity of zero for the binary was therefore assumed.

The fitted parameters for the planet and outer companion show they are both very large, with masses comparable to a gas giant and brown dwarf respectively, and have highly eccentric, probably mutually crossing orbits with separations that could see close encounters. Significant mutual gravitational interactions may therefore be likely, with dynamic instability being possible. These factors could make it a good test for the integrators.

Modelling the binary system

In our modelling, HW Vir A was always considered the central body or Body 1, with HW Vir B denoted as Body 2.

The benchmark used was the output from the Fortran program TwoStars (Carroll & Ostlie 2007), a binary star code available from the book's site www.aw-bc.com/astrophysics. Since this model calculates the Keplerian orbits analytically, the only sources of cumulative error over time would be due to numerical precision and roundoff.

The inputs to the program were the binary's parameters, which were input using the same number of significant figures as in Table 9, except for the period, which was truncated to four decimal places. The orientation of periastron was arbitrarily selected as zero for convenience and the binary's center of mass velocity vector was also chosen to be zero.

Examining the literature showed that the traditional number of time steps used in integrations is around 20 per orbit. A total number of time steps of 10^6 was chosen to ensure reasonable run times. This was therefore equal to $10^6/20 = 50\,000$ orbits, equivalent to $50\,000 \times 0.1167/365 \approx 16$ yr.

A few code modifications were made to TwoStars's default program settings:

(1) The binary parameters were hardcoded into the program for convenience.

(2) The number of orbits was made the (only) input variable.

(3) The time step was changed to 20 steps per orbit.

(4) A timer was inserted to provide the elapsed (wall clock) computation time.

The program was run on a laptop with the specifications shown in Table 10.

System	
Processor	Intel(R) Core(TM) i7-3630QM CPU @ 2.4GHz
Total amount of system memory	16 GB RAM
System type	64-bit
Number of processor cores	4
GPU	
Display adapter type	NVIDIA GeForce GTX 670M
Total available graphics memory	10.984 GB

Table 10. Specifications of computer used for simulations.

The program was then compiled and run, requiring a computation time of 602s, as shown in Table 13.

Running the program resulted in the z' and y' coordinates of the two bodies, shown by the inner orbit in Figure 10. The z' - y' plane lies in the plane of the sky and the x-axis points towards the observer. However, the z' and y' coordinates returned by TwoStars are from the observer's perspective. Because of the 80.9° inclination (which makes the system an eclipsing binary) the perspective is highly elongated, as seen in Figure 10. In the other algorithms we used a Cartesian coordinate system centred on HW Vir A, and to make them comparable we needed to transform TwoStars's coordinates. This was easily done by inverting equations K1 to K3 in (Carroll & Ostlie 2007) Appendix K, which results in

$$x = x' \sin i - z' \cos i \quad (3)$$

$$z = x' \cos i + z' \sin i \quad (4)$$

where i is the inclination.

Applying this transformation to the output data lead to the modified coordinates x and z shown in Figure 10. Since we chose an eccentricity of zero, the orbit was now circular, as expected.

We then needed to compare the output from the various algorithms in Mercury6 with this result.

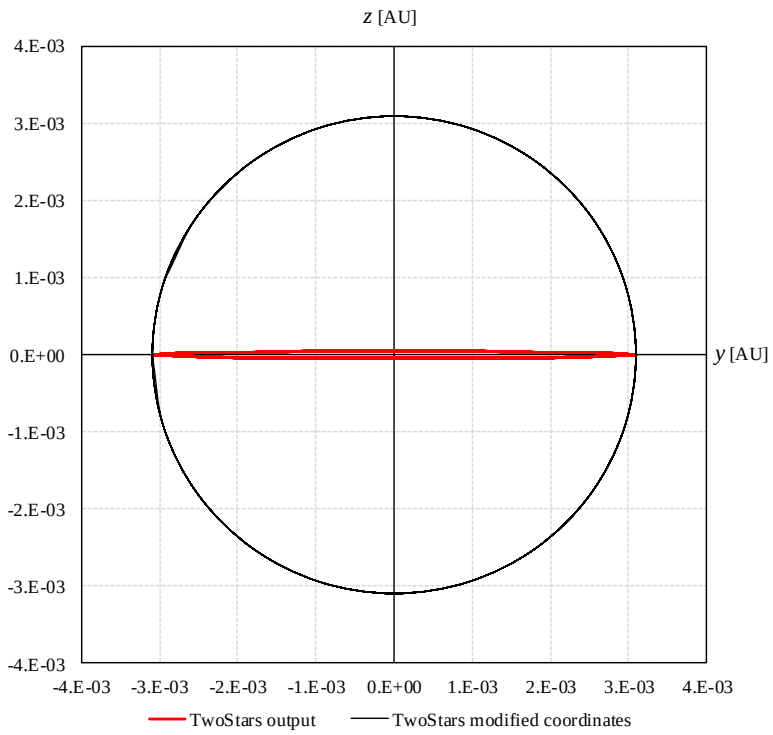

Figure 10. TwoStars: the binary's orbit in two coordinate systems.

Before using Mercury6, it was first updated with a fix for a minor bug that had been discovered (de Souza Torres & Anderson 2008).

The program was also modified with the insertion of a timer to provide computation time. Each of the Mercury6 algorithms was then run for 50 000 orbits. The code used for the timer and a typical set of input parameters are shown in Appendix C. The reference manual that discusses the algorithms, the parameters and some of their recommended values may be found at http://star.arm.ac.uk/~jec/home.html#publications.

For convenience we often used Keplerian orbital elements for input and output, but in this particular comparison we selected Cartesian elements for the output in order for them to correspond with the output from TwoStars.

We selected the argument of pericentre, the longitude of the ascending node and the mean anomaly to all be zero for convenience. Other key data are the masses of the

bodies and their density; these were calculated from the published masses and radii and are shown in Table 11.

System density estimate		Body 1 HW Vir A	Body 2 HW Vir B	Combined HW Vir AB
Mass	M_s	0.485	0.142	0.627
Radius	R_s	0.183	0.175	0.226
Density ρ (calculated)	g/cm^3	111.70	37.40	77.03

Table 11. HW Virginis components - mass and density.

The maximum distance from the body (in Hill radii[3]) that constitutes a close encounter was set to its default of one. No external user-defined forces on the bodies were used. An initial time step of 0.00584 days, corresponding to 1/20th of an orbit, was used in each of Mercury6's algorithms. Variable time step algorithms such as Bulirsch-Stoer and Radau may subsequently choose different time steps. The integration accuracy parameter was chosen as the default 10^{-12}. It is ignored by the MVS algorithm. Medium precision, corresponding to roughly nine significant figures, was used. An escape distance from the central body of 4 AU, much smaller than for planetary systems, was chosen because of the much smaller mass of the central body and the very close orbit of its companion. For the output we chose a central origin for the elements rather than barycentric or Jacobi elements, since this is appropriate to this system and the approximation to it that will be made later. The usual Keplerian output elements were

[3] An astronomical body's Hill (or Roche) sphere approximates the gravitational sphere of influence of this body in the face of perturbations from a more massive body – it is the region in which it dominates the attraction of satellites. The Hill radius R_H for a small body of mass *m* orbiting a larger body of mass *M* with a semi-major axis *a* and eccentricity *e* is defined as $R_H = a(1-e)\sqrt[3]{\frac{m}{3M}}$.

selected, together with the Cartesian positions for the orbiting body.

A typical Mercury6 output is also shown in Appendix C. There were no close encounters reported in any of the simulations and none of the output files showed any changes in the orbital parameters of the bodies, except in the case of the hybrid algorithm, which showed a very small change in eccentricity, shown in Table 12.

Algorithm	*a* [AU]	*e*	*i* [°]	Mass [*Ms*]	Rot/day	Obl
bs	0.00400	0.00000	90.80000	0.14200	0.00000	90.80000
bs2	0.00400	0.00000	90.80000	0.14200	0.00000	90.80000
hyb	0.00400	0.00040	90.80000	0.14200	0.00000	90.80000
mvs	0.00400	0.00000	90.80000	0.14200	0.00000	90.80000
rad	0.00400	0.00000	90.80000	0.14200	0.00000	90.80000

Table 12. Orbital elements at end of the integration.

Any orbital changes were therefore very small in this undemanding and therefore probably very accurate simulation and we had to devise another method for measuring them.

The performance of the algorithms was measured in two ways. First, the intrinsic error or drift of an algorithm was measured by comparing the coordinates of the calculated orbit at the beginning and at the end of the simulation. Second, on the assumption that the analytical TwoStars computation is exactly "correct", the orbits calculated by the other algorithms were compared with it, at the end of the simulations.

In order to quantify the intrinsic error in the program, we compared the first and last orbits, represented by the plain line and marked line respectively in Figure 11, and measured the difference between them. In order to avoid too much dependence on just the first and last 20 points representing each orbit, we took the last 10 orbits of each, i.e. compared the first and last 200 points.

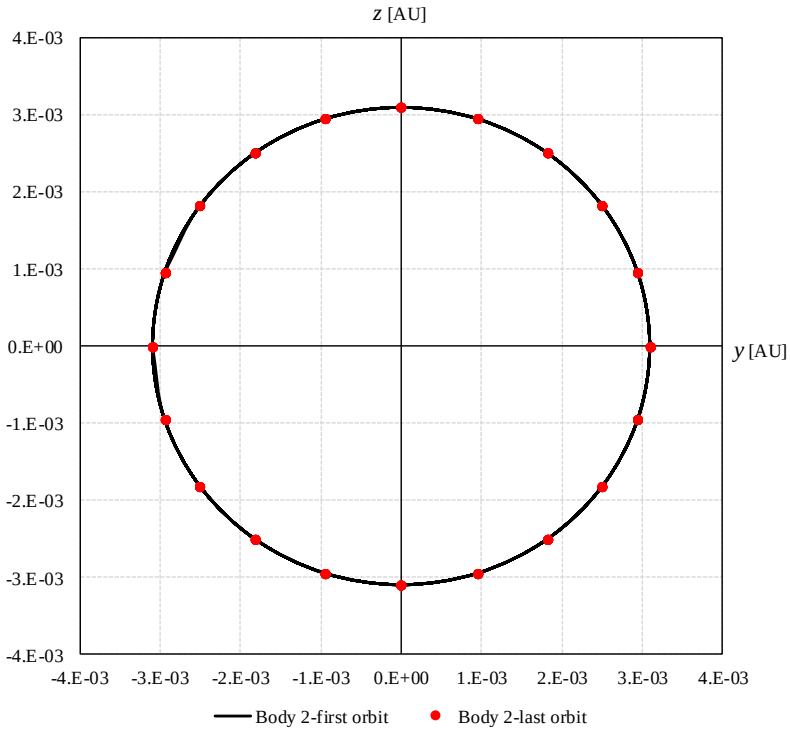

Figure 11. Orbits at the beginning and end of the simulation.

For the difference between orbits we selected as our goodness-of-fit metric the root mean square error (RMSE), represented for the *z* coordinates by

$$RMSE_z = \sqrt{\frac{\sum_{t=1}^{n}(z_{1,t}-z_{2,t})^2}{n}} \tag{5}$$

where $z_{1,t}$ and $z_{2,t}$ represent the *z*-coordinates for the first and last orbits respectively at each time step *t* around the orbit and *n* is the total number of time steps.

Similarly, for the *y* coordinates,

$$RMSE_y = \sqrt{\frac{\sum_{t=1}^{n}(y_{1,t}-y_{2,t})^2}{n}} \tag{6}$$

and we measured the total error between the two orbits as

$$RMSE_{total} = \sqrt{(RMSE_z)^2 + (RMSE_y)^2} \tag{7}$$

Applying this method to TwoStars resulted in an $RMSE_{total}$ of 4.32×10^{-3} AU.

The procedure was repeated for the other Mercury6 algorithms and the results are shown in Table 13.

Algorithm	Description		Run time (s)	Change in: Energy (dE/E)	Change in: Momentum (dL/L)	Intrinsic error: HW Vir B: Total RMSE difference between: First and last orbits*, for algorithm.	Algorithm error: HW Vir B: Total RMSE difference between: Bulirsh-Stoer bs and algorithm, for last orbit
TwoStars	Analytical	2s	602	-	-	4.32E-03	-
Mercury6	Bulirsh-Stoer (general)	bs	2638	1.89E-10	9.46E-11	9.74E-04	0.00E+00
	Bulirsh-Stoer (conservative systems)	bs2	2639	6.83E-10	3.42E-10	9.73E-04	7.55E-07
	Hybrid (symplectic/Bulirsh-Stoer)	hyb	2530	1.61E-07	2.90E-13	8.56E-04	1.61E-03
	Second order mixed-variable symplectic	mvs	2637	2.72E-13	1.36E-13	9.68E-04	5.29E-06
	Radau 15th order	rad	2654	3.64E-08	1.82E-08	1.00E-03	2.68E-05

* Comparison of first and last 20 orbits

Table 13. Binary stars – comparison of integration algorithms.

In terms of computation time, the simple analytical calculations of TwoStars made it faster than the other algorithms by a factor of over four.

The difference between the run times of the Mercury6 integration algorithms was very small. This suggested that in this very undemanding problem, where there were only two bodies, no close encounters, collisions or ejections, the algorithms did not need to use their special capabilities, were all doing essentially the same elementary thing and were not fully utilised.

The algorithms' performance in terms of changes in energy and angular momentum is shown in Figure 12.

These two measures were usually fairly closely aligned. The smallest changes by far were from the MVS algorithm, followed by the two Bulirsch-Stoers (with the one for conservative systems performing slightly more poorly on both energy and angular momentum) and then Radau, which was roughly two orders of magnitude worse. The hybrid algorithm was quite different, with very dissimilar changes in energy and angular momentum; it produced the second-best performance on angular momentum but the worst one on energy.

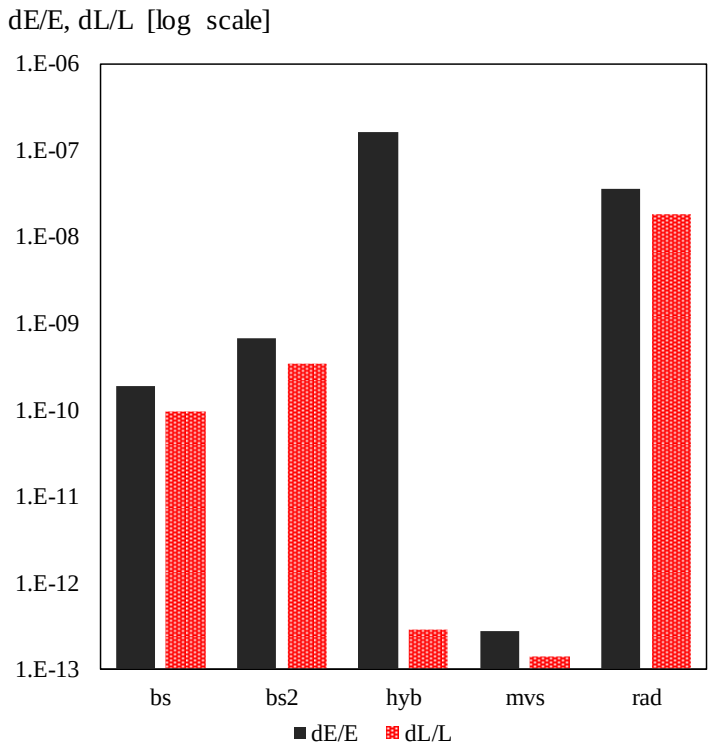

Figure 12. Binary stars – changes in energy and angular momentum for the algorithms.

Nevertheless, all performances were very good – simulations are usually ignored only if these changes become as large as 10^{-4}.

Figure 13 shows the intrinsic errors for the various codes. The units of RMS error are AU.

Surprisingly, however, TwoStars showed the highest drift, by a factor of over four. Even though it is written in double precision, it appears that roundoff errors may have had a negative effect over the duration of the simulation. Because of this high intrinsic error, our earlier assumption that this is the exactly "correct" solution to use as the benchmark for comparing the integration algorithms' accuracies became questionable. It was therefore replaced by the general Bulirsch-Stoer as the benchmark against which the other algorithms' orbits were compared.

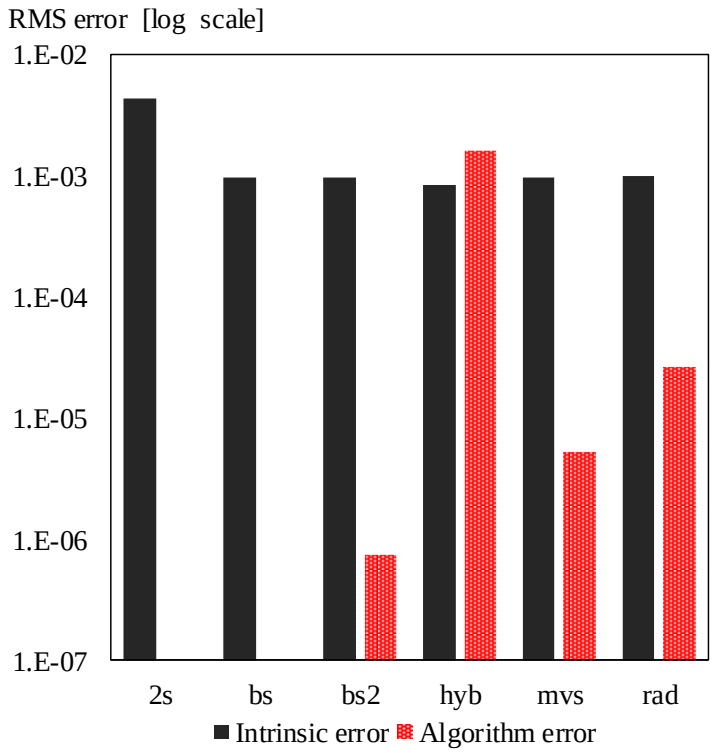

Figure 13. Intrinsic and algorithm error for the algorithms.

In terms of intrinsic error or drift, all the integrations had very similar RMS errors after 50 000 orbits.

At the end of these simulations, the conservative Bulirsch-Stoer showed the smallest RMSE difference from this benchmark, followed by MVS and Radau, with these three approximately an order of magnitude apart, and then the hybrid scheme, with an error over two thousand times larger. Nevertheless, all these RMS errors remain acceptable. For example, in the highest-error hybrid scheme, the maximum difference between this orbit and the general Bulirsch-Stoer orbit was less than 0.2%.

The faster algorithms are less accurate. However, in more complex integrations, the algorithms with the larger errors may see these errors remain within acceptable limits but could begin to garner the benefit of faster computation times.

Modelling the binary exoplanet

In this evaluation we modelled an exoplanet in a P-type orbit around the same binary, by approximating the system as a single star and planet.

We first carefully calculated the coordinates of the planet's orbit analytically and assumed this to be the "correct" benchmark. We then ran each of the integration algorithms for a large number of orbits and at the end of the simulations measured the amount by which their orbits differed from this benchmark.

The benchmark used was the output from the program Orbit (Carroll & Ostlie 2007), a binary star code available from the book's site www.aw-bc.com/astrophysics.

The Orbit procedure is a stepwise calculation of the planet's orbital path. Subject to a sufficiently small time step, the allowable error at the end of the calculated orbit is defined as the fractional amount by which either time or angular distance differ from that given for one full orbit, and is explicitly defined in the program as 10^{-15}. We retained this value for the benchmark orbit.

Since this model calculates the planet's Keplerian orbit analytically over many small time steps, the only sources of cumulative error over time would again be due to numerical precision and roundoff. This error is affected by the size of the time step used and the error tolerance selected.

The inputs to the Orbit program were the mass of the central "single" star, the semimajor axis of the planet's orbit and its eccentricity. Approximating the system as a single star and planet, the mass of the central star was taken as the sum of the masses of HW Vir A and HW Vir B. It is assumed that this mass is located at the centre of mass of the two stars. It is actually unimportant whether it is located here or at HW Vir A or B, since this difference, of $0.003998/2 \approx 0.002$ AU, is very small compared with the planet's semimajor axis of 3.62 AU, amounting to only 0.06% of this distance. The

notional radius and density of this single central star was calculated from the two components, as shown in Table 11. The radius and density of the planet are unknown and were set to the program default values of one.

The orbital parameters were entered using the same number of significant figures as in Table 9, except for the period, which was truncated to four decimal places. For the input data asteroidal elements were again used and the central "single" body was chosen as the origin for the output elements.

Since the scale of this system is far larger than that of the binary pair of stars, the ejection distance was increased to 100 AU. All the other parameters were retained and the accuracy parameter in particular was kept at 10^{-12}.

One million time steps were used around the orbit, with every $10^6/200 = 5\ 000^{th}$ saved, resulting in an output of 200 points with which to compare the other algorithms.

All these parameter values were hard-coded into the Orbit program for convenience, the program was modified to produce output in days as well as years and a timer was added. Mercury6 was then run and the planet's orbit calculated.

The period of the planet as calculated by the program (using Newton's form of Kepler's third law) for the above parameters is 3 156 days, compared with Lee et al's 3 316 days in Table 9, a 5% difference.

The time step should now be approximately $1/20^{th}$ of the orbital period or ~160 days. An actual value of 157.824 days was selected to make the time steps exactly the same magnitude as in Orbit, so that the coordinates of the orbits from Orbit and Mercury6 could be compared at exactly the same times.

The comparisons were made over exactly one thousand orbits, equivalent to 8 642 yr. The 200 calculated points of the thousandth orbit calculated by the integration algorithms was then compared with the 200 points of the analytical solution. This is

illustrated in Figure 14, which shows the analytical orbit and some of the 200 comparison points for the Bulirsch-Stoer algorithm.

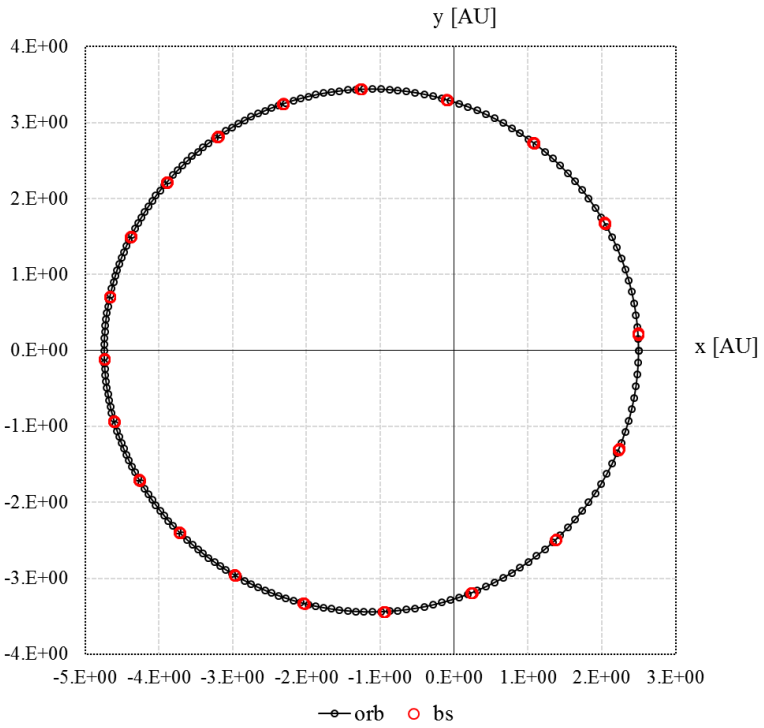

Figure 14. Coordinates of the planet after 1 000 orbits using the Bulirsch –Stoer algorithm, compared with the analytical orbit.

All the other Mercury6 algorithms were then run. There were no close encounters reported in any of the simulations and none of the output files showed any change in the orbital parameters of the bodies, except a small difference for the planet in the case of the hybrid algorithm, as shown in Table 14.

Algorithm	*a* [AU]	*e*	*i* [°]	Mass [*Ms*]	Rot/day	Obl
bs	3.62000	0.31000	0.00000	0.00809	0.00000	0.00000
bs2	3.62000	0.31000	0.00000	0.00809	0.00000	0.00000
hyb	3.61890	0.30954	0.00000	0.00809	0.00000	0.00000
mvs	3.62000	0.31000	0.00000	0.00809	0.00000	0.00000
rad	3.62000	0.31000	0.00000	0.00809	0.00000	0.00000

Table 14. Planet elements after 1 000 orbits.

The differences in the planet's semimajor axis and eccentricity were 0.03% and 0.15% respectively.

The differences between orbits were again measured using RMS error. The results are shown in Table 15.

Algorithm	Description		Run time (s)	Change in: Energy (dE/E)	Change in: Momentum (dL/L)	Algorithm error: HW Vir (AB) b: Total RMSE difference between: Bulirsh-Stoer (general) and algorithm, for last orbit
Orbit	Analytical	orb	0.54	-	-	-
Mercury6	Bulirsch-Stoer (general)	bs	160	1.95E-10	5.00E-11	9.8393E-01
	Bulirsch-Stoer (conservative systems)	bs2	162	1.65E-11	2.26E-12	9.8393E-01
	Hybrid (symplectic/Bulirsh-Stoer)	hyb	162	3.17E-04	2.91E-14	6.4289E+00
	Second order mixed-variable symplectic	mvs	162	9.86E-13	1.40E-13	9.8393E-01
	Radau 15th order	rad	157	2.13E-12	1.25E-12	9.8393E-01

Table 15. Binary exoplanet – comparison of integration algorithms.

The analytical calculation of the planet's orbit was very fast, with the integrations taking 300 times longer. There were no material differences between the times taken by the various algorithms. The changes in energy and angular momentum are shown in the table and also plotted in Figure 15.

Generally, changes in energy were larger than changes in angular momentum. Taking a rough average of these two measures, the smallest changes were for the MVS algorithm, followed by Radau, the conservative Bulirsch-Stoer and then the general Bulirsch-Stoer.

The hybrid scheme was again anomalous, with the lowest change in angular momentum (by three orders of magnitude compared with the next highest) but the highest on energy (by a large seven orders of magnitude compared with the next worst).

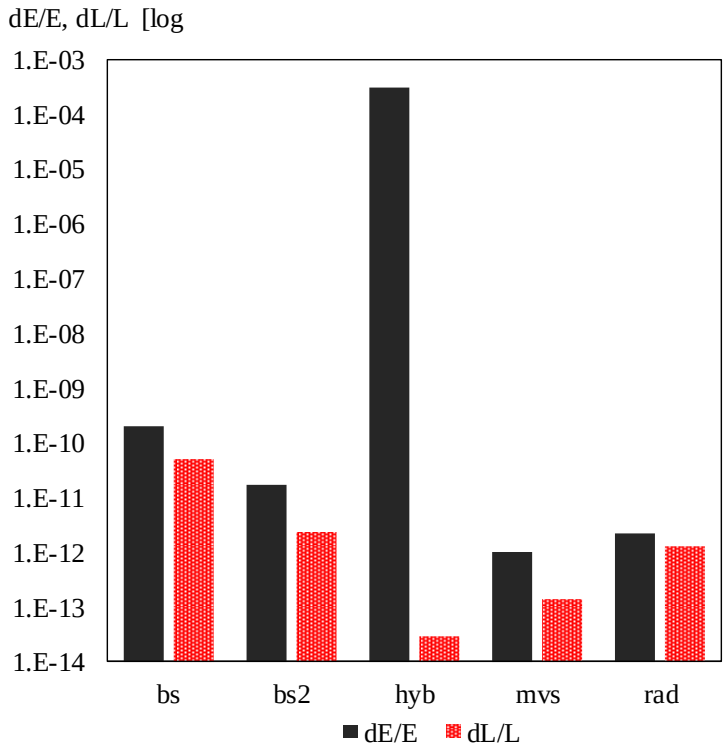

Figure 15. Binary exoplanet – changes in energy and angular momentum for the algorithms.

Turning to the algorithm errors or differences between orbits as shown in Table 15, the RMS errors are generally larger than for the binary star model, which was not unexpected given that we were using over three times as many orbits before evaluating the coordinate differences.

More interesting is the fact that all the errors are exactly the same (to four significant digits) for all the algorithms except the hybrid scheme. In other words, the orbits produced by most of the integrations were exactly the same. Given the simplicity of this model, it would probably be more surprising if they were not.

Justification of the approximation of a single star

Treating the two binary stars as a single central object with a mass equal to the sum of the component masses is a very reasonable assumption, since the semimajor axis of the

planet is a thousand times larger than that of the two binary stars and its period is 28 000 times longer. As pointed out by Beuermann et al, who used an integration time step of 35 d, "The gravitational field at the position of a distant companion can be represented as the sum of the constant field created by the combined mass of the binary components and a gravitational wave, emanating from the revolving binary with periods of 2.8 h for the fundamental and 1.4 h for the first harmonic. The relative strength of the wave field is 4×10^{-8} and closely averages to zero over the 300 or 600 periods that occur in a time step of 35 d. The retroaction of the companion tends to excite an eccentricity in the binary, but with a relative strength of 10^{-8} this effect is also entirely negligible." (Beuermann et al. 2012).

A three-body model of the HW Virginis system

We then went a step further in examining the capabilities of Mercury6, by retaining this assumption but expanding the model of the system by including HW Vir C in the integrations.

The parameters used for HW Vir C's mass (M sin *i)*, semimajor axis and eccentricity were those proposed by Lee et al (2009) and shown in Table 9. This body was assumed to be coplanar with HW Vir (AB) b, i.e. to also have an inclination of 80.92°. The integrations were begun with HW Vir C and HW Vir (AB) b at maximum periastron separation, i.e. the longitude of periastron of the outer body's orbit with respect to the periastron of the inner body's orbit was fixed at 180° initially. The unknown density of the outer body was set at the Mercury6 default value. The Bulirsch-Stoer algorithms was used in this simulation, with the same time step of 157.824 d as in the previous integration.

The results for the two bodies, showing their semimajor axes, radial distances and eccentricities over time, are presented in Figure 16. The fractional changes in the energy and angular momentum of the three-body (central "body" and two companions) system at the end of the integration were very good, at 10^{-11} and 10^{-12} respectively.

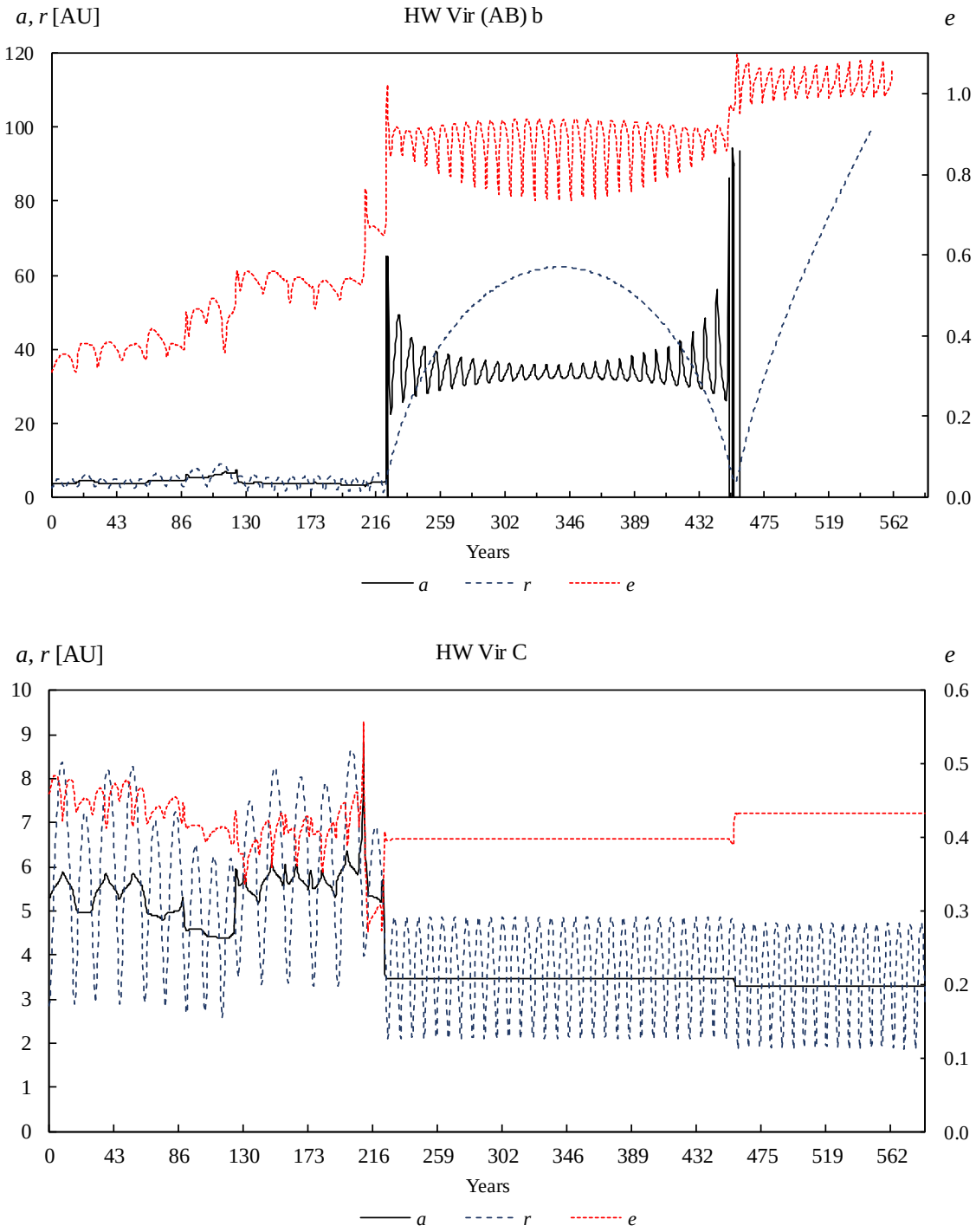

Figure 16. Three-body Bulirsch-Stoer integration: Lee et al (2009) proposed parameters.

The system was unstable, with HW Vir (AB) b being ejected at 205 171 days or 562 yr. As shown in the figure, its orbit was initially reasonably stable up to around 220 yr. However, over this period its eccentricity increased steadily from 0.31 to over 0.90. At this stage its semimajor axis expanded dramatically to over 30 AU and then at around 450 yr it expanded further, to over 90 AU, before passing the program's 100 AU limit a hundred years later and being deemed to be ejected.

Clearly, HW Vir C was gravitationally affected by HW Vir (AB) b up until the planet's orbit expanded at 220 yr, after which the planet's considerably diminished gravitational influence allowed the dwarf's motion to become a very stable Keplerian orbit, undergoing only a small further adjustment at the next and final expansion of the planet's orbit. HW Vir C's eccentricity ended up at 0.43, close to the 0.41 where it began, but the size of its orbit contracted from 5.3 AU to 3.3 AU with the ejection of the planet. The inclination of its orbit was unaffected.

This simulation therefore supported the contention by Beuermann et al that Lee et al's proposed orbits for the two bodies in this system are unstable.

The simulation was then repeated using the parameters proposed by Beuermann et al, also shown in Table 9. The Bulirsch-Stoer algorithm was again used, as well as the assumption of coplanarity. The first simulation was done over a period of 165 yr, equivalent to three of the proposed orbital periods for HW Vir C.

The results are shown in Figure 17.

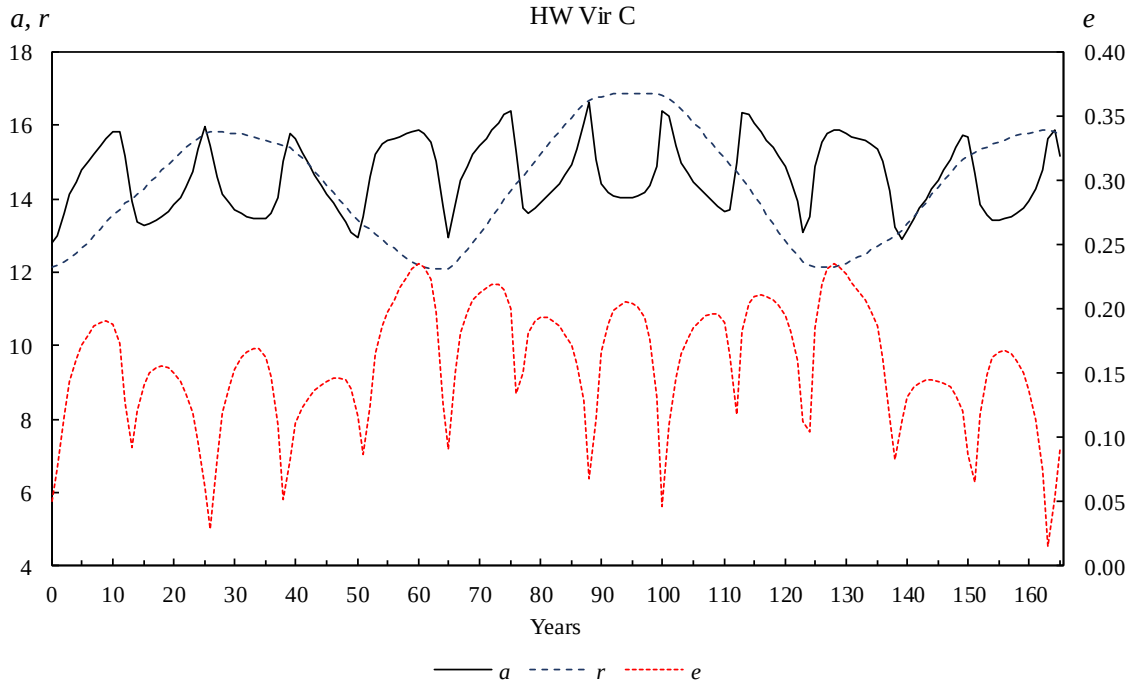

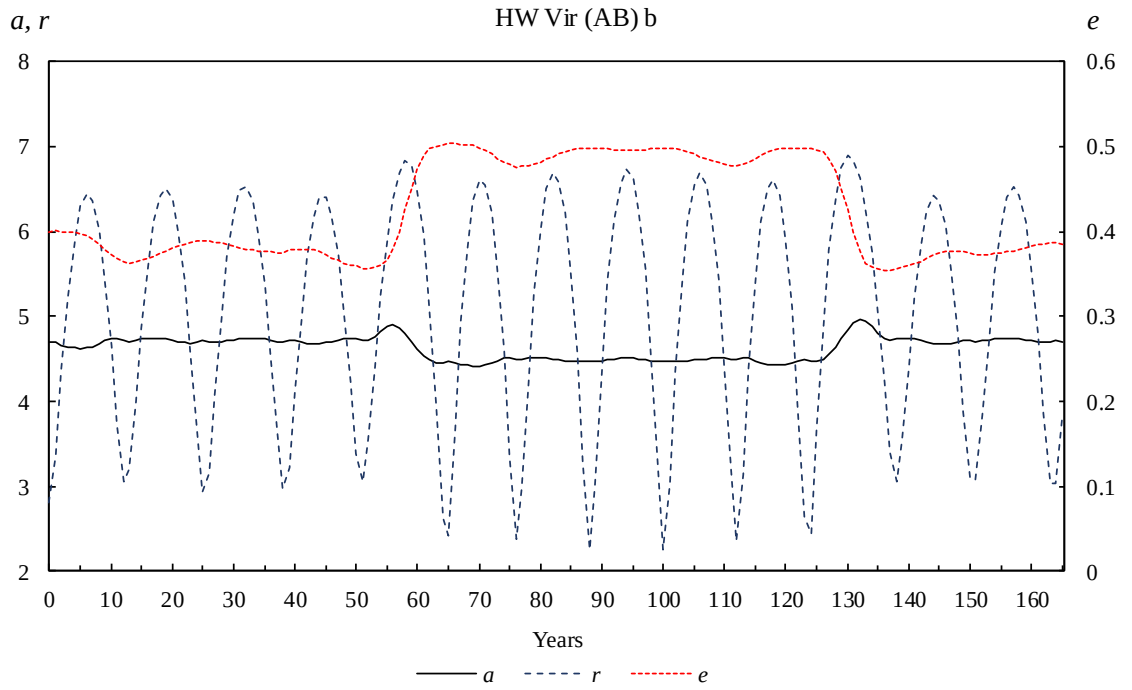

Figure 17. Three-body Bulirsch-Stoer integration using Beuermann et al's proposed parameters – short term.

The orbit of HW Vir (AB) b is stable over this period, with its eccentricity ranging from approximately 0.35 to 0.50 and it semimajor axis varying between 4.4 AU and 4.9 AU.

The orbit of HW Vir C is also stable, but periodic. Over short time intervals, the periodicity is at the synodic period of the planet, i.e.

$$P_{\text{syn}} = \left(P^{-1}_{\text{HW Vir (AB) b}} - P^{-1}_{\text{HW Vir C}}\right)^{-1} \tag{8}$$

and is approximately 16 yr. The graphs shown are essentially identical to those published by Beuermann et al, 2012 and shown in Figure 18, confirming the correct operation of Mercury6.

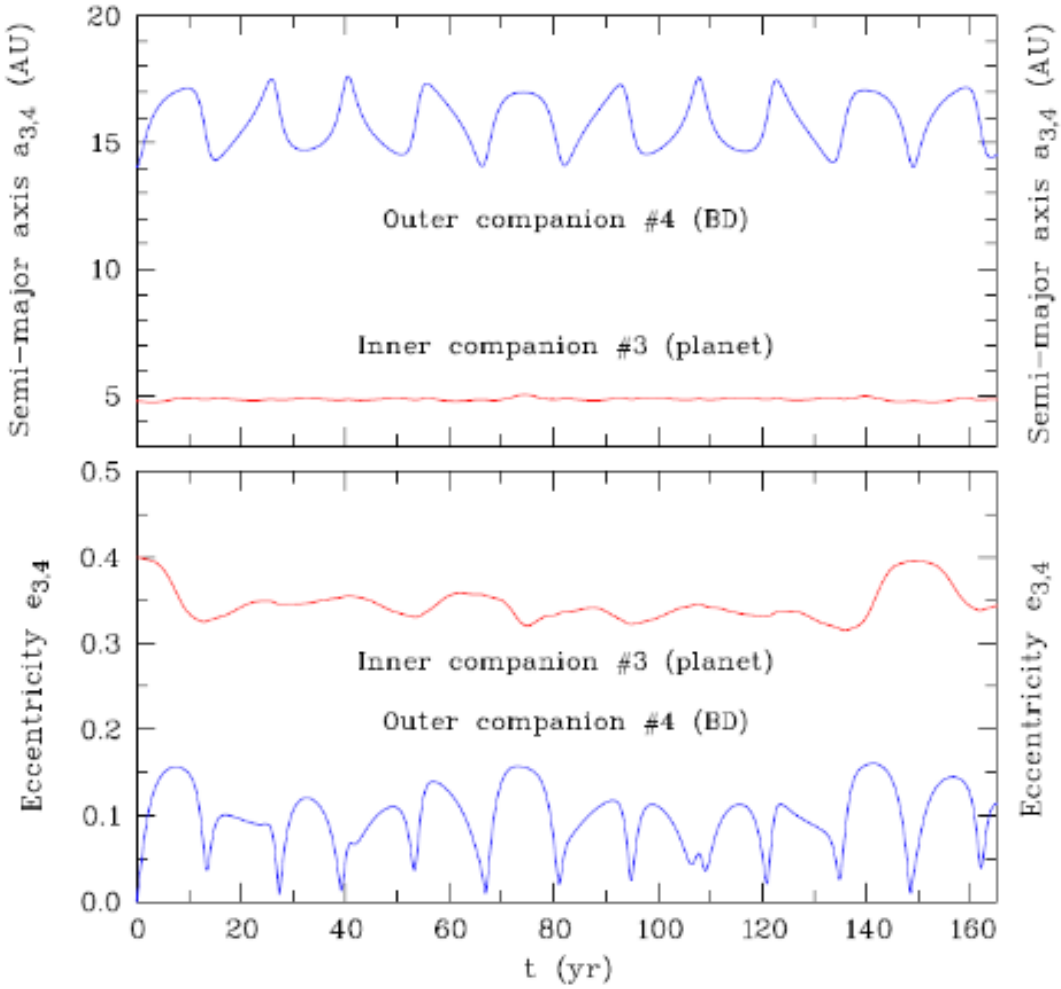

Figure 18. Temporal variation of the semimajor axes and the eccentricities of the osculating orbits of the companions to HWVir as calculated with Mercury6 (Beuermann et al, 2012).

The next step was to extend the integrations to 10 000 yr. In this case HWVir (AB) b collided with the central binary at 3 359 299 days or 9 197 yrs. The evolution of the orbits of the two bodies is shown in Figure 19.

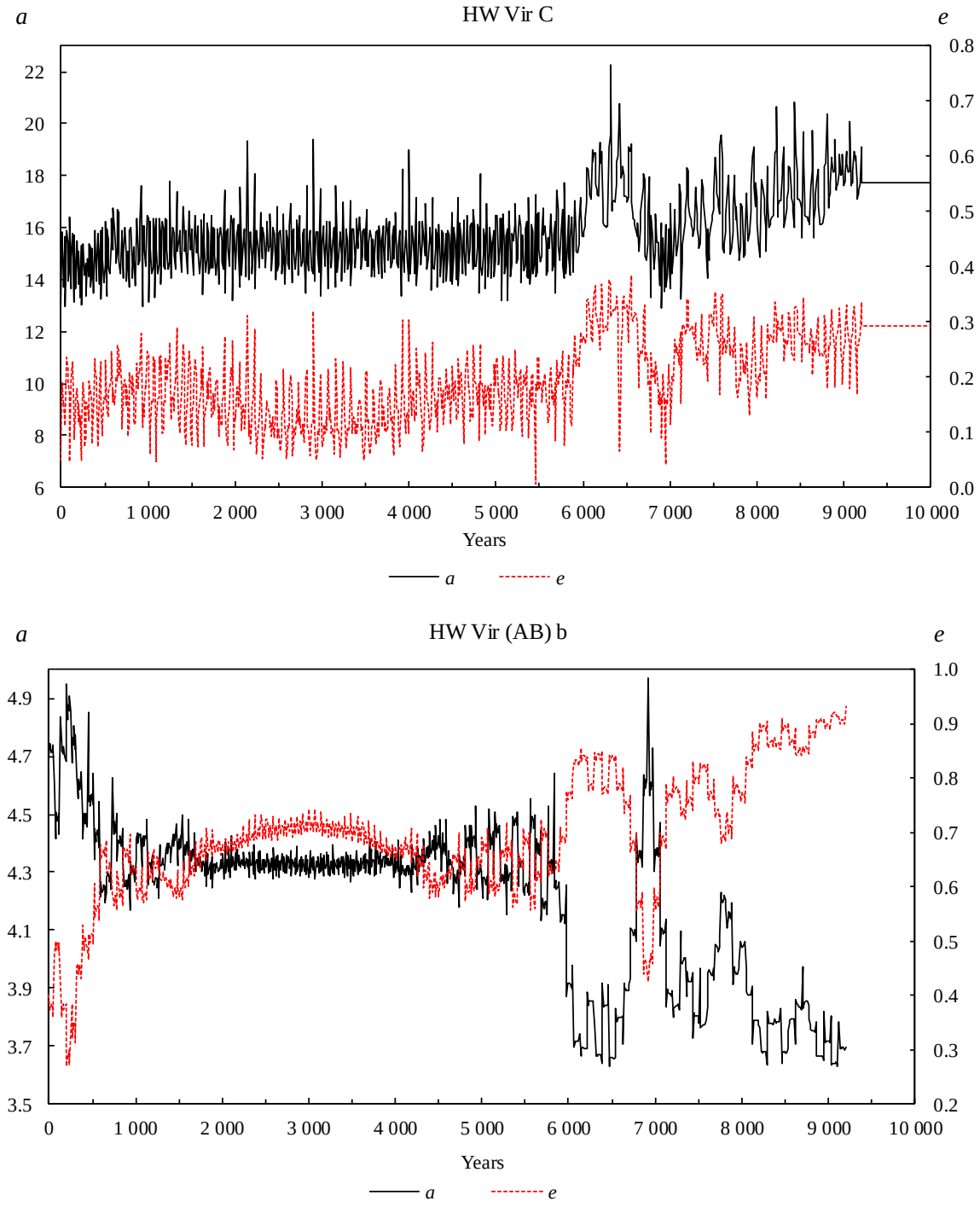

Figure 19. Three-body Bulirsch-Stoer integration using Beuermann et al's proposed parameters – longer term.

For the planet, instability begins to set in after about 4 000 yr, with its semimajor axis contracting from 4.7 AU to 3.7 AU prior to collision and its eccentricity rising from an initial 0.41 to an highly elliptical 0.90. There were 17 close encounters with the central binary pair before the ultimate collision.

For the dwarf, the planet's instability began to affect it after 5 500 yr, with its semimajor axis increasing from an initial 12.8 AU to 17.7 AU and it's eccentricity from a (notional) 0.05 to 0.30. On the removal of the planet it entered a stable Keplerian orbit at those values.

It was useful to repeat the simulation using all the integration schemes and to compare their performance, as shown in Table 16.

Algorithm	Description		Run time (s)	Time to collision/ ejection (yr) $d=10^{-12}$	$d=10^{-16}$	Change in: Energy (dE/E)	Momentum (dL/L)
Mercury6	Bulirsch-Stoer (general)	bs	140	9 197	7 630	5.68E-10	1.24E-11
	Bulirsch-Stoer (conservative systems)	bs2	155	None	9 293	7.31E-10	5.16E-13
	Hybrid (symplectic/Bulirsh-Stoer)	hyb	566	1 953	2 448	2.12E-01	3.98E-14
	Second order mixed-variable symplectic	mvs	578	8 346	8 346	2.66E-05	4.21E-15
	Radau 15th order	rad	376	None	7 974	6.38E-14	1.37E-14

Table 16. Three-body Bulirsch-Stoer integration using Beuermann et al's proposed parameters – longer term: comparison of algorithms.

Surprisingly, the fastest algorithms are the two Bulirsch-Stoers, with the hybrid and MVS schemes taking 3-4 times longer, and the Radau lying somewhere in between.

Looking at the changes in energy and angular momentum, also highlighted in Figure 20, while changes in angular momentum are similar to those in the two-body case, the change in energy was poor in both the hybrid case (as usual), but also for the MVS algorithm. *Contrary to expectations, the non-Bulirsch-Stoer algorithms are both slower and perform worse on this measure, as well as taking longer.*

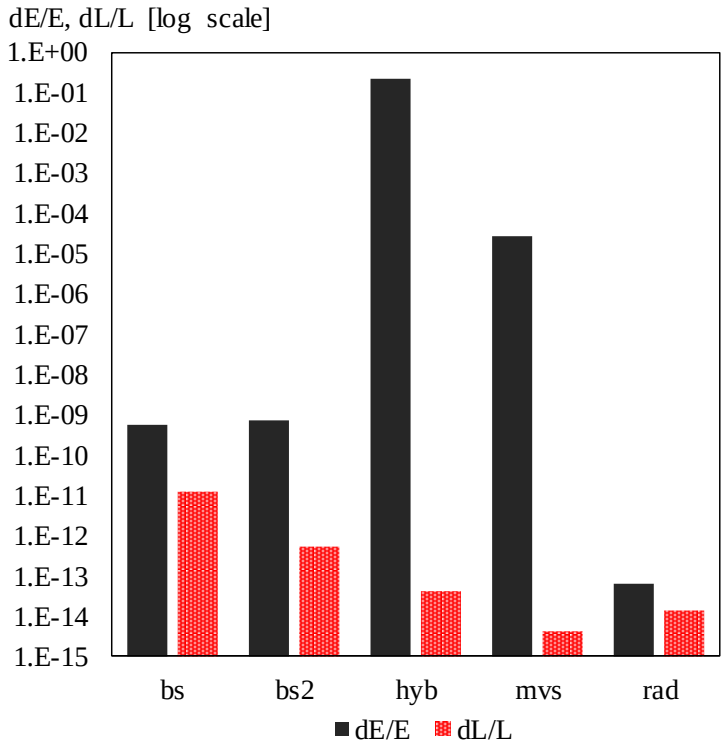

Figure 20. Three-body system – changes in energy and angular momentum for the algorithms.

Three of the algorithms saw a collision occur with the central binary, after times ranging from around 2 000 yr to 9 000 yr, while two algorithms did not experience any collisions in the 10 000 yr simulation. It is interesting that the two Bulirsch-Stoer schemes gave different outcomes.

Beuermann et al used Mercury6's hybrid algorithm, and found no instability over 10 000 yr, or indeed over 10^8 yr.

The above simulations were run using an integration accuracy parameter of 10^{-12}. Since Beuermann et al used a more demanding 10^{-16}, the simulations were repeated using this value and the results also tabulated in Table 16. In this case all algorithms lead to the removal of the planet, mostly by collision with the central binary but also through an ejection in the case of the hybrid algorithm. The times to collision given by the MVS algorithm were unchanged; this was because this scheme ignores the

integration accuracy parameter. The other exit times differed from the previous ones by up to 25%.

These results are therefore more aligned with those of Horner et al, who were unable to find any dynamically feasible orbits for the HW Vir system.

It is sobering that while our results appear to be identical to Beuermann et al's over a few orbits, they reach completely opposite conclusions on stability over longer periods, with these periods being much shorter than the commonly accepted 10^8 yr criterion for stability, even when the parameters used are the "best" ones chosen by Beuermann et al from their various simulations. As mentioned at the beginning of this section, these integrations appear quite sensitive to initial conditions, raising some concern about their robustness.

Clearly, a lot more work can be done to establish the (in)stability characteristics of this system.

Having examined the characteristics of the various algorithms in Mercury6, we then proceeded to use it to investigate HD 1818068.

3. Results

3.1 Stability of the HD 181068 stellar system

Before searching the stability landscape for planets around the compact hierarchical triple system HD 181068, also known as the Trinity system, we first needed to check the stellar system's dynamics using the published parameters (Borkovits et al. 2013).

The notation used is that of Borkovits. A denotes the red giant, the main component of the wider A−B binary and the most massive and luminous component of the system, while Ba and Bb refer to the members of the close binary formed by the two red dwarfs. These symbols are also used as subscripts to physical quantities.

The system's properties are listed in Table 17 (Borkovits et al. 2013; Derekas et al. 2011), where the numbers in parentheses are the estimated errors in the last digits.

Stellar parameters				
Star		Ba	Bb	A
Description		Red dwarf	Red dwarf	Red giant
Spectral type		G8V	K1V	G
Mass	[M_s]	0.915(34)	0.870(43)	3.0(1)
Radius	[R_s]	0.865(10)	0.800(20)	12.46(15)
	[AU]	0.00402	0.00372	0.05793
Density (calculated)	[g cm^{-3}]	1.995	2.398	2.189E-03
Orbital parameters				
Subsystem		Ba–Bb	A–B	
Period	[d]	0.9056768(2)	45.4711(2)	
a	[R_s]	4.777(39)	90.31(72)	
	[AU]	0.02221	0.41987	
e	[-]	0	0	
ω	[-]	–	–	
i	[°]	86.7(14)	87.5(2)	
$\Delta\Omega$	[°]	0.0(5)		
i_m	[°]	0.8(14)		

Table 17. Properties of the HD 181068 system, as measured by Borkovits et al. (2012).

The binary red dwarfs Ba and Bb orbit each other with period of 0.906 d and the red giant A orbits the binary with a period of 45.5 d. Its mass of $3M_s$ is 1.7 times the total mass of the binary and its semimajor axis is eighteen times that of the binary.

In binary systems the eccentricity is correlated with period; circular orbits dominate for periods below 10 days while longer-period systems have eccentricities ranging from 0.1 to almost 1.0, with an absence of circular orbits. Note that the proposed orbits of both subsystems are circular, with orbital inclinations of $i \cong 90°$, and the mutual inclination of $i_m = 0.8° \pm 1.4°$ suggests an exact coplanarity. This is not surprising given that the system is triply eclipsing.

Because we were calculating orbital elements with respect to a single star in a triple star system of three objects of almost equal mass, Keplerian orbital elements with

respect to one star did not make much sense. We could, however, use Cartesian coordinates (i.e. x, y, z, v_x, v_y and v_z) instead. (While it probably made most sense to use barycentric coordinates, this was not important since we were not interested in looking at the actual orbits *per se*, but simply measuring the number of years of stability, i.e. no collisions or rejections, at any coordinate point.)

As the Cartesian coordinates we selected modified Herschel astrocentric coordinates, which are commonly used for exoplanets. The formulas for converting Keplerian elements into these coordinates are shown in Appendix D. Astrocentric coordinates have a few drawbacks, e.g. in numerical integrations all bodies must be integrated with time steps smaller than the innermost body's period, because of the high-frequency forcing this body introduces.

The conservative Bulirsch-Stoer algorithm was chosen for integrating the triple; this is the only algorithm that will work for the multiple, close and massive bodies in this configuration, and it can also provide close encounter data and handle highly eccentric orbits. A time step of one twentieth the period of the binary, 0.05 d, was selected and an accuracy tolerance of 10^{-12} was used. Component Ba was chosen as the central body and central coordinates were used. An ejection was deemed to occur if a body's distance from Ba exceeded 50 AU or approximately 900 times the outer semimajor axis (i.e. of A). The two bodies Bb and A were always aligned initially with both at pericentre, with their x-coordinates being the proposed semimajor axes distances and their tangential velocity components v_y being the Keplerian velocities implied by the proposed orbital parameters. These were +0.1540 AU d^{-1} for Bb and -0.0580 AU d^{-1} for A. They were launched on opposite sides of Ba, and Bb was given a positive v_y velocity component. A was initially assumed to have a prograde orbit relative to Bb. An initial eccentricity of zero was assumed for both bodies, so their initial velocity

components v_x were both zero. This eccentricity assumption is very probably true for Bb since the inner period is only ~1 d and this orbit is highly likely to have been circularized. The configuration described is shown schematically in Figure 21.

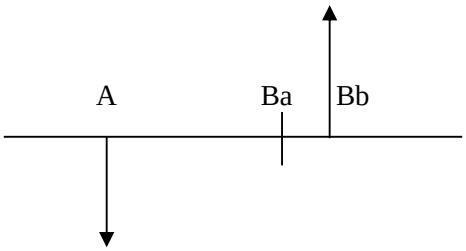

Figure 21. Initial configuration of orbit geometry – stellar system.

The evolution of the orbits of Bb and A relative to Ba over the first 10 days of the integration are shown in Figure 22, which plots the six relevant cartesian coordinates for each body.

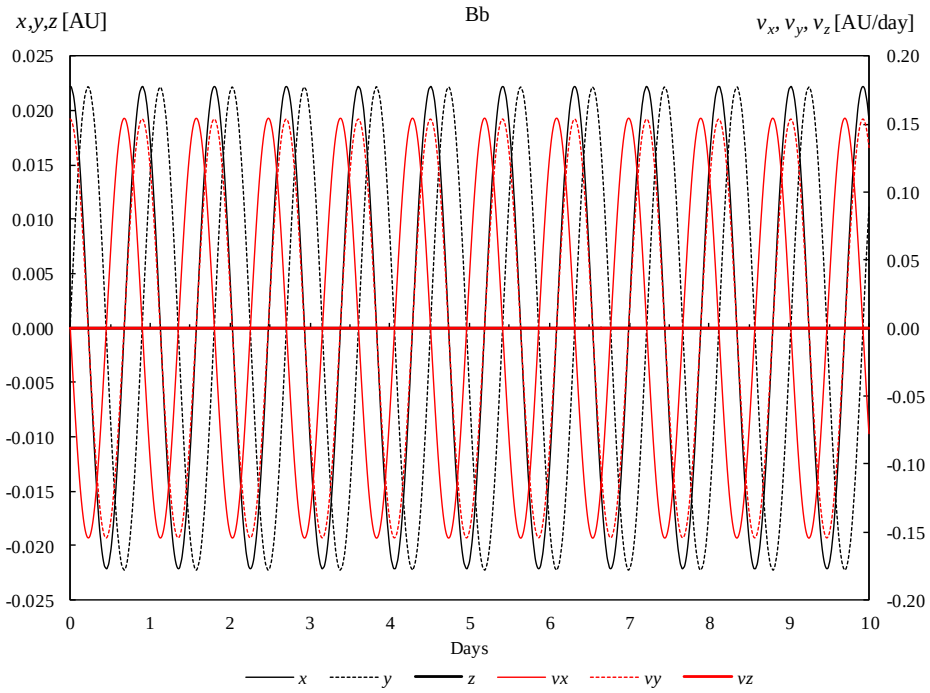

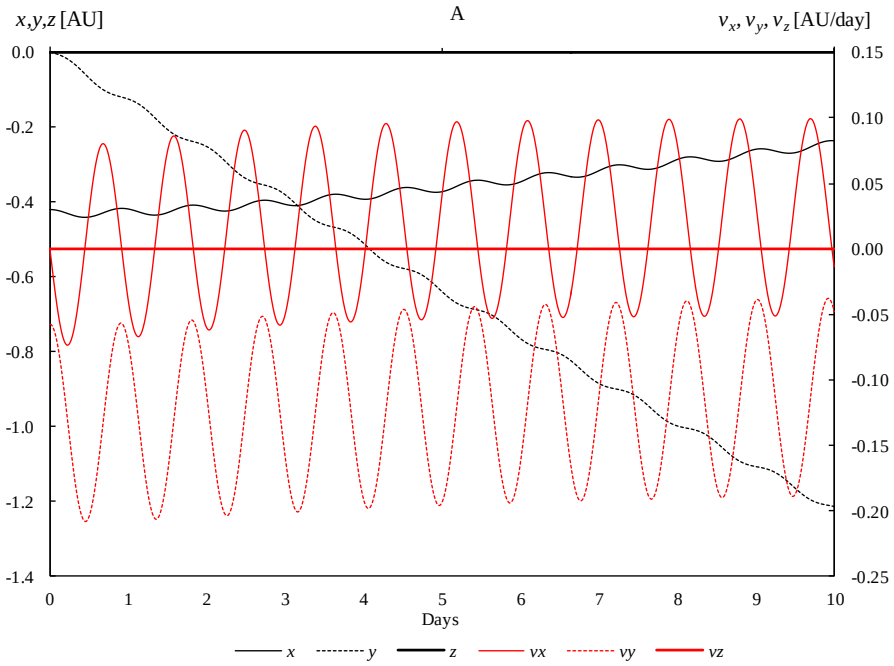

Figure 22. Orbits of HD 181068 Bb and A - first ten days.

The orbit of Bb is stable over this period. However, A's *x*-coordinate immediately begins to slowly rise, with its *y*-coordinate increasing even more rapidly: A is being ejected. This is more clearly seen on the *x*-*y* plot in Figure 23.

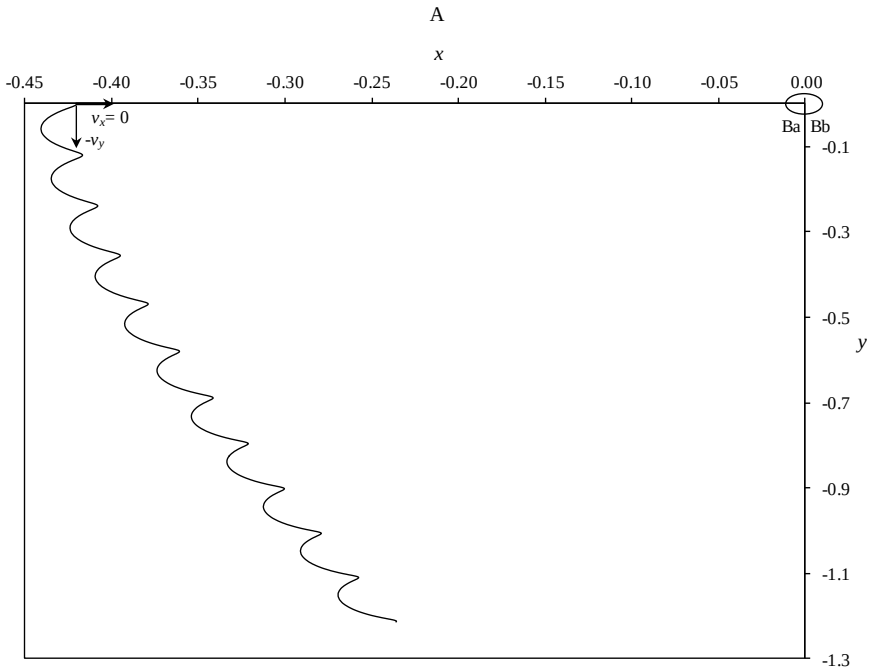

Figure 23. Orbital motion of A over ten days.

Here the binary is located at the origin and the arrows show the initial position and velocity components of A. The perturbation of A's path by the ~1 d period of Bb is clearly evident. The results of extending the integration for a longer time are shown in Figure 24.

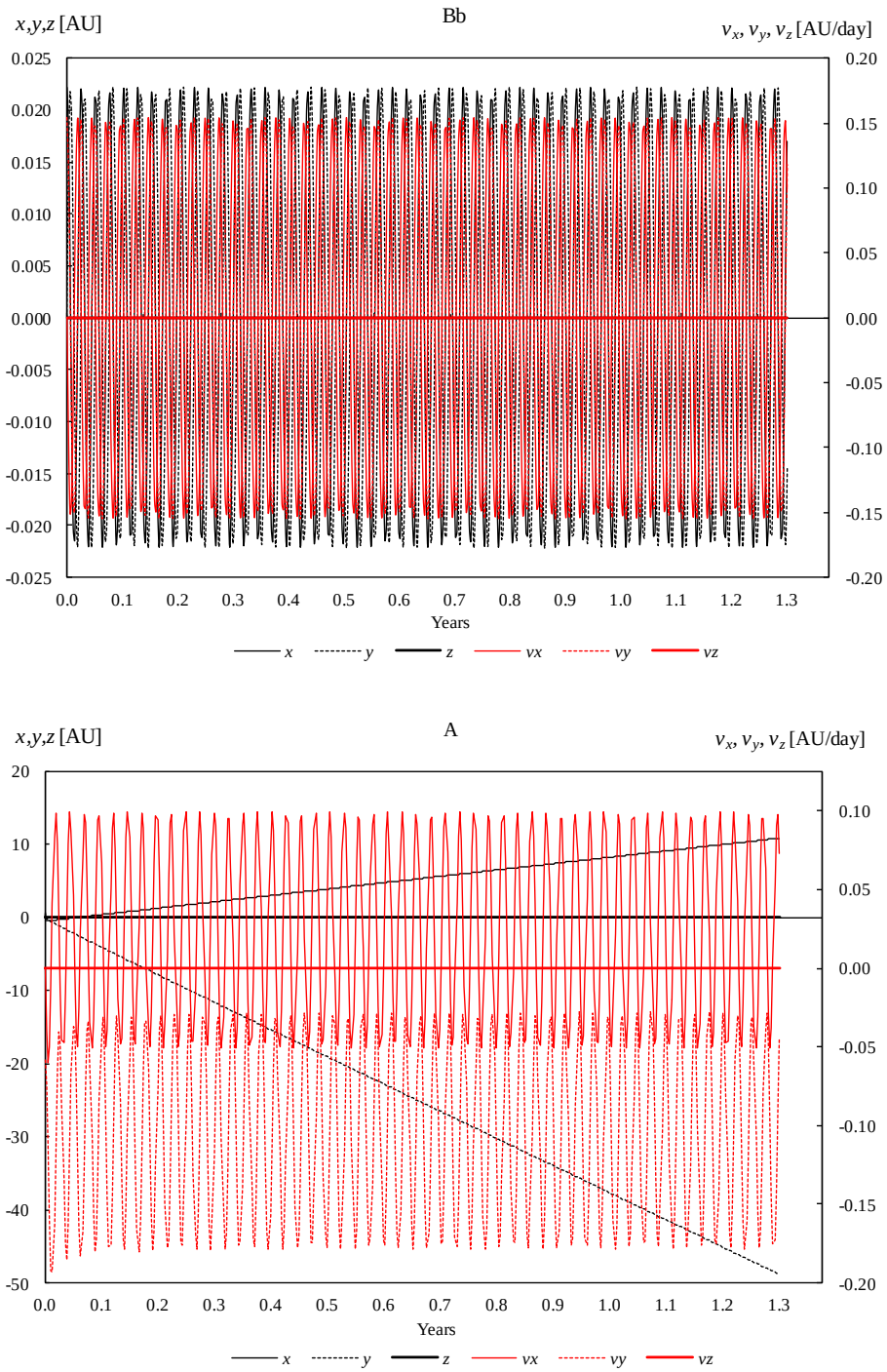

Figure 24. Orbits of HD 181068 Bb and A – longer term.

The orbit of the binary remained stable over this period, while A continued to move away, being classified as ejected on reaching the 50 AU limit after 469 days.

Since the proposed orbital parameters did not produce a stable orbit, it therefore became necessary to examine the stability region for the third star in this system.

In investigating the stability region for body A, we noted that the uncertainty given by Borkovits et al for its period is 4.4×10^{-5} %, while that for its semimajor axis is two orders of magnitude larger at 8.0×10^{-3} %. We therefore assumed the period was correct and varied the semimajor axis. In Mercury6, while bodies defined as "small bodies" do not affect one another gravitationally, they do affect any "big bodies". One therefore cannot use a large number of massive test particles to check the orbit of, for example, A - they have to be massless test particles, otherwise they will all perturb Bb.

The generation of large numbers of test particles for the program's input files is fairly straightforward, and an example is given in Appendix G.

We therefore launched 600 massless test particles with semimajor axes ranging from 0.1 AU to 0.7 AU into initially circular orbits around the binary, assuming an inclination of zero, and integrated for 25 yr (~9 200 d). No stable orbits were found. The subsequent unsuccessful searches for stable orbits are detailed in Appendix E. Finally, we explored the possibility that A's initial velocity was different to that implied by the published parameters.

We then launched 333 test particles from the same initial location, the system's published semimajor axis of 0.4198 AU, with velocities v_y ranging from -0.0015 AU d^{-1} to -0.5 AU d^{-1} (compared with the implied Keplerian value of -0.0580 AU d^{-1}), and with $v_x = 0$. These test particles were integrated for 200 yr.

After this period 39 particles remained. These were then integrated for 500 yr, after which 37 remained. Integrating these for 10^4 yr resulted in 36 survivors and further integrations of 4×10^4 yr and 10^5 yr saw no further ejections or collisions, indicating probable stability. Longer integration times were constrained by available computing power. However, this was compensated to some extent by the compactness of the system, since the number of orbits in any time period is higher than for the wider systems for which most dynamical analyses have been done.

The initial velocities of the stable orbits found ranged from -0.027 AU d^{-1} to -0.123 AU d^{-1}. So velocities significantly greater than the Keplerian velocities implied by the orbital parameters resulted in stable orbits. The implication is that A's eccentricity is not zero.

On examining these orbits we found that while orbits that are stable up to 4×10^4 yr are found over the initial velocity range from -0.027 AU d^{-1} to -0.123 AU d^{-1}, this range is discontinuous, with stable regions from -0.027 AU d^{-1} to -0.045 AU d^{-1} and from -0.09 AU d^{-1} to -0.123 AU d^{-1}, with an unstable gap from -0.045 AU d^{-1} to -0.09 AU d^{-1}.

Using the uncertainties given for the published period and semimajor axis, the resulting uncertainty around body A's implied velocity can be calculated to be -0.05848±0.00046 AU d^{-1}. The published orbital parameters imply a velocity that, together with its uncertainty range, falls well inside this unstable region. This explained the difficulty in finding stable orbits using this value as a starting point.

It was also substantially easier to find stable retrograde orbits than stable prograde orbits. In an initial investigation of the parameter space for orbits, we took 1000 massless test particles, with semimajor axes a = 0.4198 AU, eccentricities e = 0 and tangential orbital velocities v_y ranging from -0.0002 AU d^{-1} to -0.2 AU d^{-1} (i.e. with

velocity increments -2×10^{-4} AU d^{-1}) and launched them in both prograde and retrograde orbits.

All the prograde test particles either collided with the central body or were ejected past a 500 AU ejection limit, with none surviving longer than 39 yr. However, of the retrograde particles, 279 or over a quarter were still in stable orbits after 10^4 yr.

This was noted in the literature some time ago, e.g. (Donnison & Mikulskis 1995), and in the specific case of hierarchical triples with an inner binary it was found that retrograde systems are more stable for all mass ranges. It was also found that for those systems in which the binary eccentricity is small the retrograde orbits are more stable, while for systems with both large binary and outer-body eccentricities the prograde orbits tend to be more stable.

A wider, higher-resolution search was then made for the prograde case - over the range -0.0001 AU d^{-1} to -1.0 AU d^{-1} using 10 000 test particles (i.e. with a velocity increment of -10^{-4} AU d^{-1}). Again, no stable orbits were found.

(A minor modification to the Mercury6 code was necessary to do this, as the number of bodies is limited to 2 000.)

Usefully, these large parameter space searches are in fact quite fast, since most end in failure, and the collisions and ejections usually occur quite soon. This is illustrated in Figure 25, which shows, for a typical simulation that had no survivors, the attrition of an initial set of test particles over time. Over 97% of the 695 test particles failed in the first 11 d or 4% of the simulation time.

There was often a clear demarcation in velocity where the cause of failure changes from collisions to ejections, with this transition usually showing longer survival times, making this a possibly promising region.

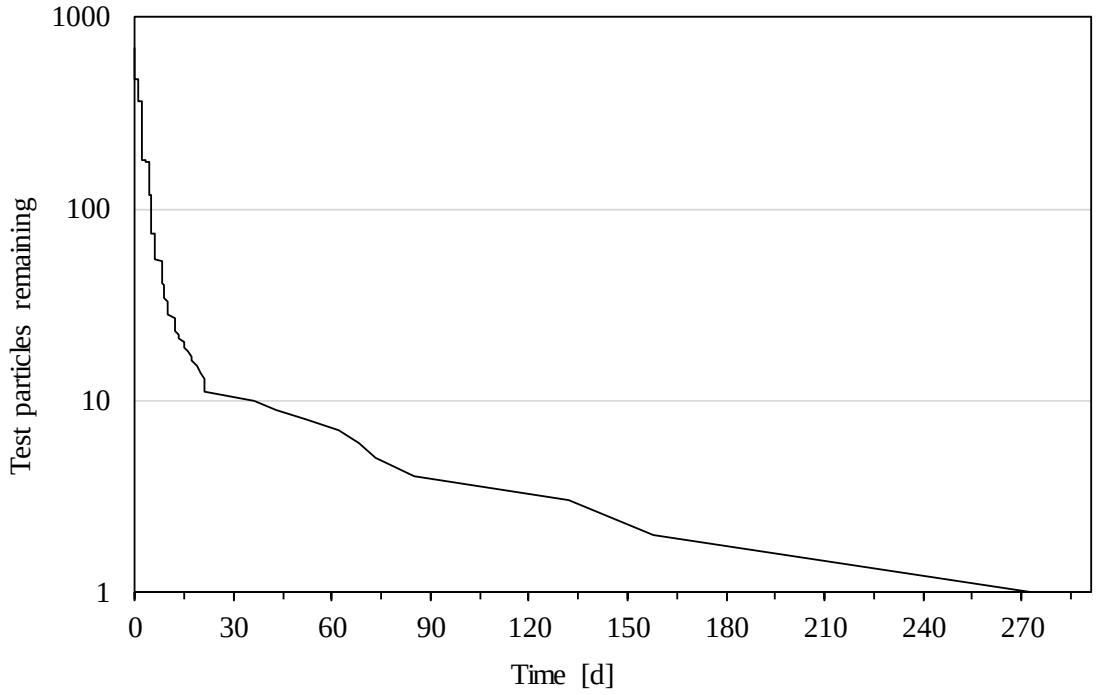

Figure 25. Attrition over time of a group of test particles.

This transition was at -0.0145 AU d^{-1}, so the range -0.014 - -0.015 AU d^{-1} was investigated with another10 000 test particles, giving a velocity increment of -10^{-7} AU d^{-1}. However, no orbits survived for more than 1 200 yr.

Having made a detailed search of the velocity space from 0.001 AU d^{-1} to 10 AU d^{-1} in increments ranging from ~10^{-3} to 10^{-7} AU d^{-1} without finding a single stable orbit, *we were therefore forced to conclude that despite the determinations of Borkovits et al, it appears that there may be a higher probability that stable orbits of body A are retrograde rather than prograde.*

It was therefore decided to proceed with the retrograde situation, and then to investigate the stability landscape for planets based on this assumption.

The stable retrograde velocity ranges are shown in Figure 26.

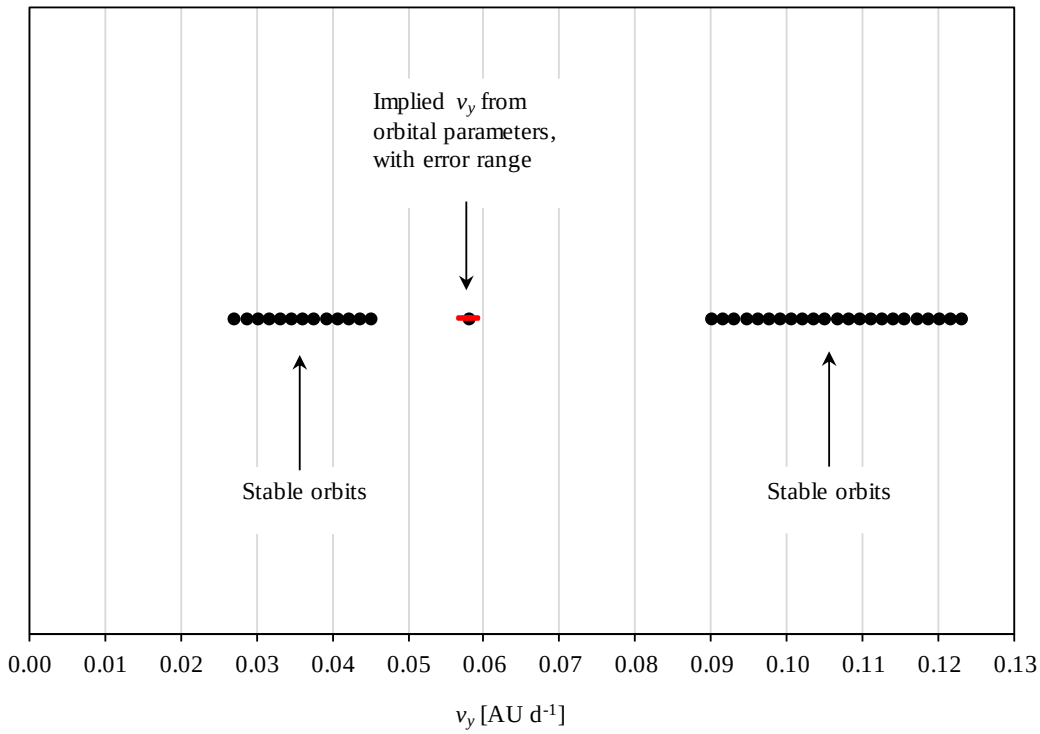

Figure 26. Initial velocities for which stable retrograde orbits result.

The implications were that:

- If the orbital parameters of body A were correct, its orbit was unstable, or
- If its orbit was stable, the orbital parameters for A (and/or for Ba-Bb) were incorrect.

Since the ages of all three stars in the system are estimated at 200 – 500 Myr and assuming they were formed together rather than one component being captured, the second possibility appeared more likely.

If we assume that the orbital period of body A is correct, then the only way for the orbital velocity v_y to fall into the low-velocity range shown in Figure 26 is for the body's semimajor axis to be smaller than the given 0.4198 AU, assuming the given eccentricity of zero is correct. It can be calculated that this semimajor axis would lie in the range 0.195 AU - 0.326 AU. If the eccentricity was greater than zero, this semimajor axis could be smaller.

Similarly, the only way for the orbital velocity to fall into the high-velocity range would be for its semimajor axis to be materially higher than the given value, again assuming an eccentricity of zero. This higher value can be calculated to be above 0.65 AU. Again, higher eccentricities would allow this value to be smaller.

If, however, we assume that the published value of the semimajor axis is correct, then the only way a higher orbital velocity can be achieved (at the same coordinate point) is for the eccentricity to be greater than zero. Again, this can be calculated, which shows that for the low-velocity range an eccentricity greater than 0.42 would be required.

These simulations used test particles in order to quickly survey a wide range of orbital velocities, since one can integrate a number of test particles simultaneously but have to do massive test bodies one by one. We now needed to integrate the dwarf body A as a massive body of 3.0 M_s over the velocity ranges that appeared stable using the test particles.

The logical next step was therefore to formally examine the stability landscape of the system for body A by constructing an *a* - *e* stability diagram.

Since there are six orbital elements for each star, the system constitutes a $6 \times 6 \times 6$ dimensional space, so some simplifying assumptions were needed to make the investigation feasible. First, all orbits were taken as coplanar; this assumption is probably correct, as discussed earlier. Second, the initial orientation of the three stars was fixed. This leaves only the semimajor axes and the eccentricities as free parameters. These were taken as given for the binary, so we needed only to vary these two parameters for body A. The two bodies Bb and A were always initially aligned with both at pericentre.

We monitored conservation of total energy and angular momentum for the integration. Using an initial time step of 0.05 d (~1/20 of the binary's period) and an error tolerance of 10^{-12} leads to an overall fractional change in the system energy $\Delta E/E$ of about 10^{-7} or better over a 10^5 yr integration. This can be considered the maximum time the system can be followed accurately. The fractional angular momentum change was usually around 10^{-8}. With the computing power available, the practical upper limited on integration time was 10^5 yr and the simulations discussed are typically for this time.

A grid of values of semimajor axis *a* ranging from 0.10 AU to 1.00 AU incrementing by 0.005 AU, and eccentricities from 0 to 0.9 incrementing by 0.1, was used and was integrated for 10^5 yr. An orbital period of 45.4711 d was used and the other orbital elements were fixed at: argument of pericentre $w = 0$, mean anomaly $M = 0$ and, assuming coplanarity as discussed, inclination $I = 0$. Stability was then measured by computing the survival time in years of the orbit at each grid point.

Orbits were deemed to have failed if body A collided with the binary or was ejected. An ejection distance of 5 AU was set. Most failures were collisions with the central binary rather than ejections.

It was again found that orbital failures tend to occur very quickly - if an orbit did not fail within 10 yr, it was usually stable up to 10^5 yr. While longer integration times are always desirable, the fact that the system is compact works in our favour: 10^5 yr is equivalent to over 800 000 orbits of the outer body A.

The results are shown in Figure 27.

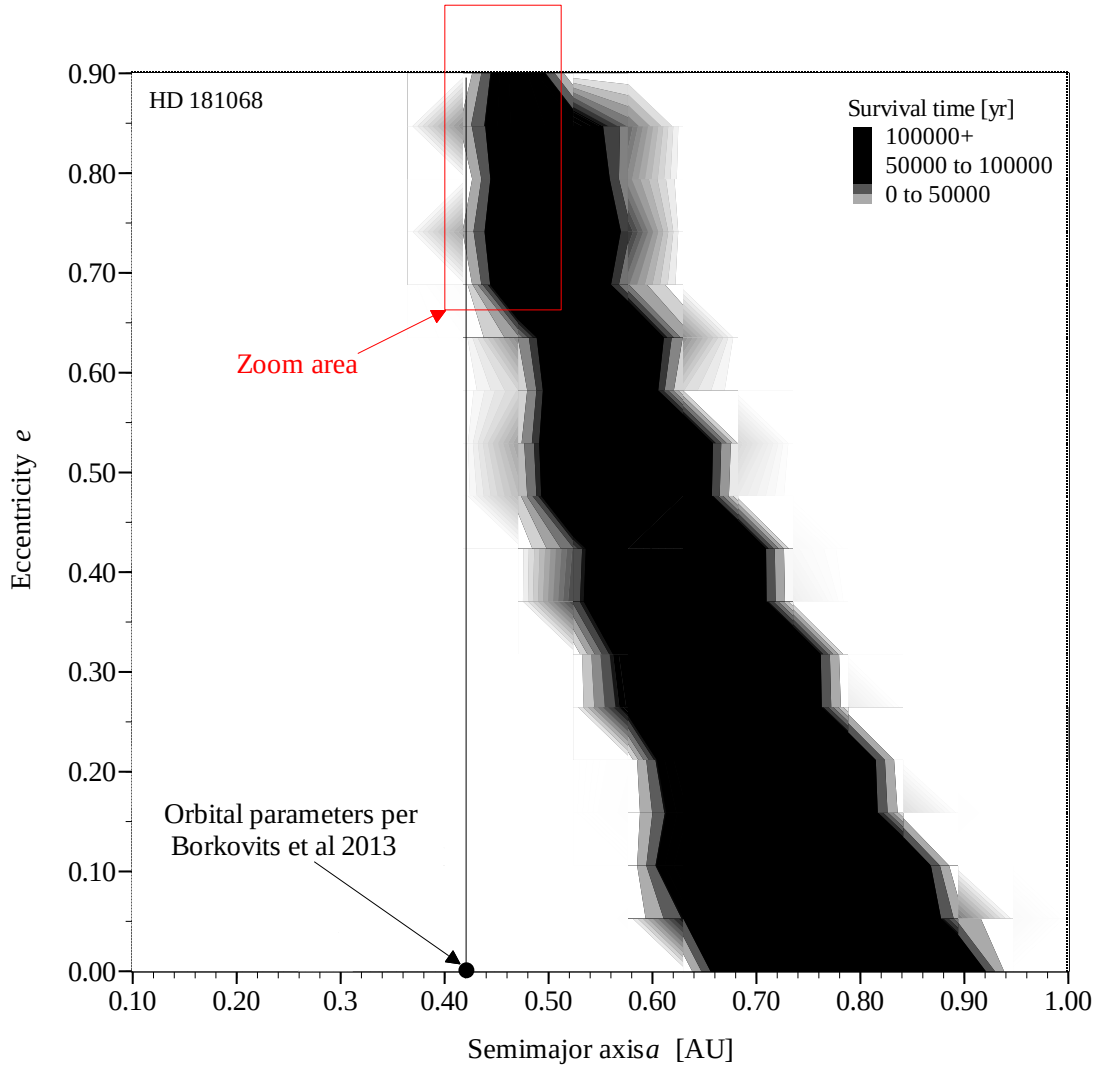

Figure 27. Stability map of HD 181068.

Stable orbits were found in only a minor portion of the parameter space examined. The region of stability reflected an inverse relationship between the semimajor axis and the eccentricity of stable orbits. For orbits of zero eccentricity the region of stability lay between semimajor axes of ~0.70 AU – 0.90 AU. For high eccentricities approaching one, the semimajor axis of stable orbits declined to around 0.40 AU.

The orbital parameters given by Borkovits et al of a = 0.4198 AU and e = 0 represent a point that appears to lie well outside the region of stability. The implication is that if this semimajor axis is correct, the eccentricity of the orbit must be very high, or, if the eccentricity is correct, the semimajor axis must be significantly larger, possibly

around 0.80 AU. We assumed that the given semimajor axis was more likely to be correct and investigated the eccentricities required for stability.

It appears from Figure 27 that this semimajor axis may lie inside the stable region at high eccentricities, so we constructed a higher-resolution map of the area enclosed by the box in Figure 27. This zoomed-in region of the stability map is shown in Figure 28.

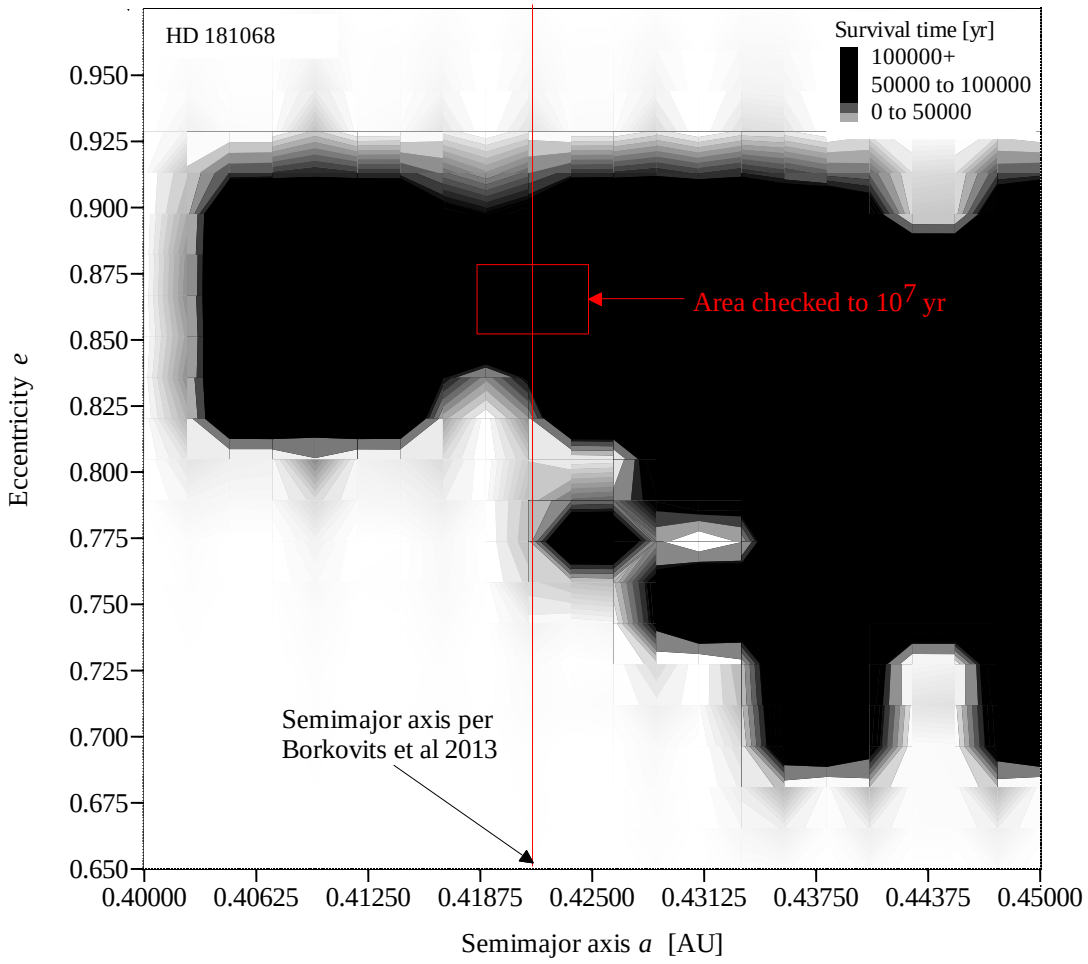

Figure 28. Stability map of HD 181068 – zoomed-in region.

The semimajor axis of 0.4198 AU intersects the stable region at eccentricities lying between 0.825 and 0.900. The most probable value is estimated as 0.856±0.015. Note that the survival times in the stability maps are smoothed. The actual data is in Appendix G.

While this is an intriguing result, there are some caveats.

First, integration times of 10^5 yr are insufficient. With an estimated age of the stellar system of 300 Myr -500 Myr, integration times should be comparable to this. Therefore, as a further check, the point representing our most probable parameters and another four points immediately surrounding it, as indicated by the boxed region in Figure 28, were integrated for 10^6. All these orbits were found to be stable over this period.

Second, the maps are of relatively low resolution, which may leave some large areas of stability or instability unrevealed.

Third, each point in the stability maps consist of only one simulation. It was noticeable that even small changes in the input parameters can have a large effect on survival times, sometimes even changing a point from being stable to unstable and vice versa. It is good practice to take the average of multiple survival times at each point using slightly different initial conditions; some research has used an average of 40 simulations. This was not done here because of computational limitations.

Also, the influence of orbital inclination on these results was not examined. High inclinations will lead to Kozai instability, resulting in even larger variations in the stellar orbits

The final caveat arises from the wide variety of trajectories of the stable orbits. For example, Figure 29 shows the trajectory of a particle with initial velocity v_y = -0.12 AU d^{-1} over its first 362 days, which brings it almost to a full orbit around the binary.

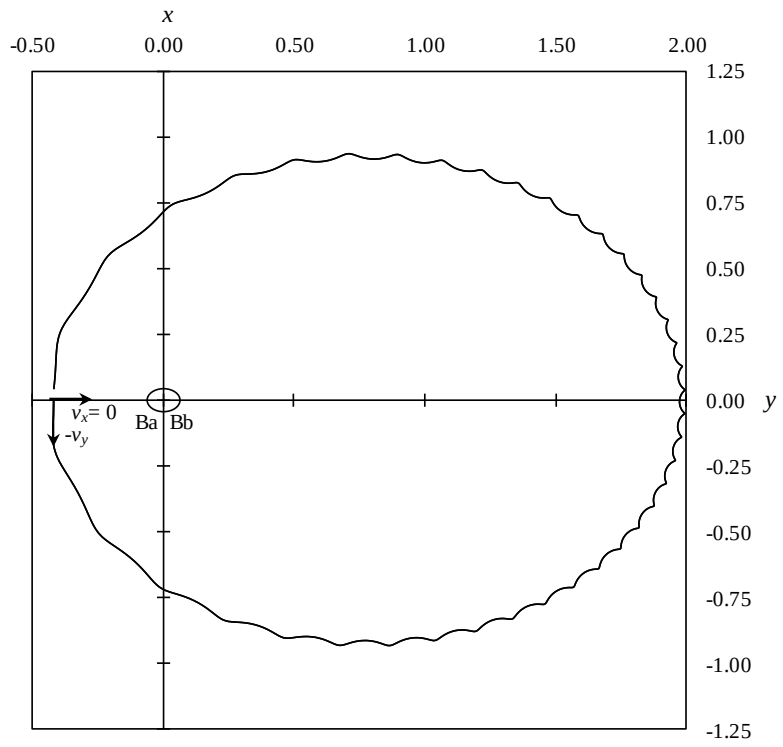

Figure 29. Body A: v_y = -0.120 AU d^{-1}, orbit over 362 d.

This is clearly not an "osculating" Keplerian orbit. Because it is plotted using central coordinates centred on Ba, the body shows a scalloped trajectory arising from the gravitational influence of Bb's orbit, with the wavelength of this scalloping increasing as its orbit speeds up close to the binary and vice versa. In barycentric coordinates the trajectory would be a smooth ellipse. Note that the eccentricity of this orbit is not zero as suggested by the published orbital parameters, and the semimajor axis is much larger than the 0.4198 AU of these parameters.

Because the period of the orbit of the inner binary is not an exact multiple of the orbital period of A, subsequent orbits precess, and their evolution over 200 yr is shown in Figure 30.

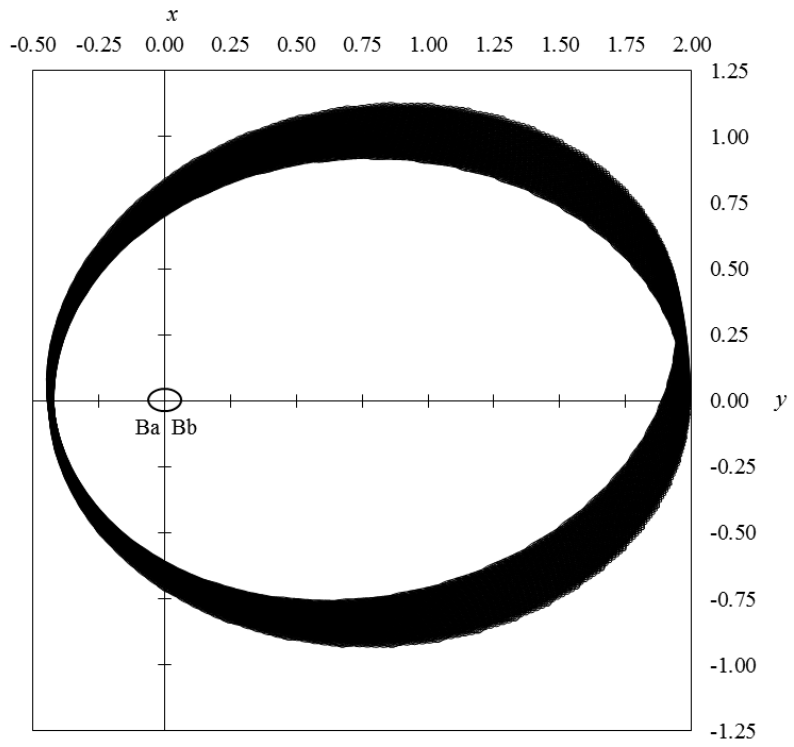

Figure 30. Body A: v_y = 0.120 AU d^{-1}, orbits over 200 yr.

The movement of the precessing orbits is bounded. While all the orbits we found for the triple were well-behaved, this will not necessarily be true for any planets. Their orbits could be chaotic. Nevertheless, if chaotic orbits completely fill an orbital space, although they are not “stable” in the traditional sense, they are bounded.

Chaos is a term used to describe a system with nonrepeating motion over a given timescale - it is deterministic but unpredictable because of high sensitivity to initial conditions. Stability describes the ‘‘boundedness’’ of a system; a system is stable if changes in its evolution are confined to a certain range. Therefore, one of the most fundamental features of a chaotic system is stability. For example, a chaotic system can be stable in that the orbits of the bodies do not interchange or become unbound, and the oscillations of orbital elements such as eccentricity occur over a finite range. This illustrates an important dichotomy in chaotic systems - a system may be formally unstable, but, for all practical purposes, it is in fact stable. With “stable chaos” one can

predict the general orbital evolution reasonably well but not the exact position of the bodies in their orbits.

To determine the type of motion of the computed orbits, one has to use either long-term orbital computations and analysis, or a chaos indicator, such as the fast Lyapunov indicator, which is quite a quick tool to distinguish between regular and chaotic motion.

While all the orbits indicated as such in the stability map are stable, even small differences in the estimated orbital parameters may result in large differences in orbital trajectories. Since these stellar orbits are variable, the initial orbital configurations may not define the stable regions well. This could lead to different stability landscapes for any planets in the system. It is therefore probably very important to establish the orbital parameters of stellar component A precisely.

Borkovits et al believe there is strong evidence that the orbits of Bb and A are both circular, based on:

(1) The radial velocity solution of Derekas et al. 2011, which suggested that both orbits are circular. Derekas et al calculated their orbital solutions by the method of differential corrections. The eccentricity from the fit was $e = 0.022 \pm 0.023$, consistent with zero, and in the final solution they set $e = 0$ because its inclusion as a free parameter did not improve the solution.
(2) By the observed locations and shapes of the secondary minima with respect to the primary minima in both the close and wide orbits.

However, our admittedly rudimentary analysis suggests that, in addition to the direction of A's orbit, the combination of semimajor axis and eccentricity proposed by Borkovits et al may be incompatible with dynamic stability.

We therefore made the provisional assumption that the orbit of body A is described by a = 0.41986 AU and e = 0.856, with the remaining parameters as given by Borkovits et al, and used this as the geometry of the compact stellar system around which we investigated the stability landscape for planets.

The trajectories of the orbits using these selected parameters are interesting. The time series for the first few orbits of body Bb are shown in Figure 31

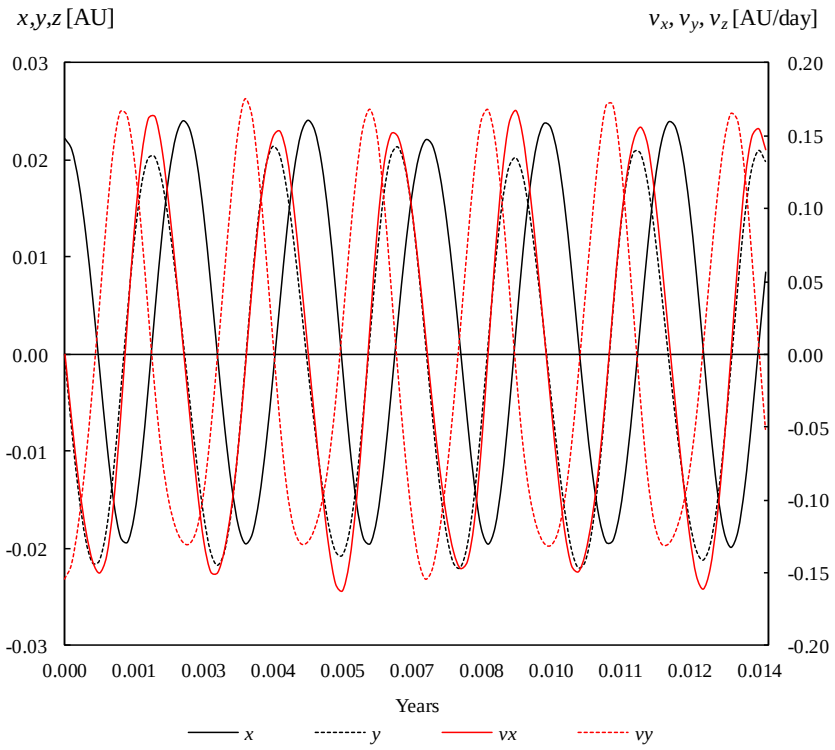

Figure 31. Position and velocity of body Bb over time.

The orbit of Bb is almost, but not perfectly, circular. This is more clearly seen by plotting its $x - y$ coordinates, as shown in Figure 32. The starting point and direction of Bb's orbits are indicated by the arrow.

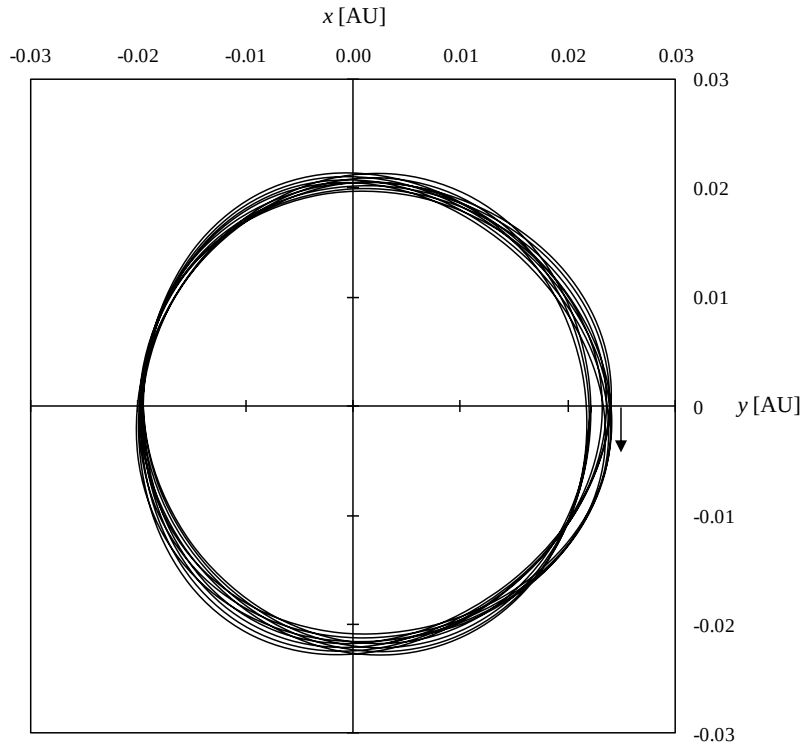

Figure 32. Initial orbits of Bb.

Bb's orbit is not perfectly circular because we are using central coordinates centred on Ba, and Bb (as well as Ba) is actually orbiting around their mutual centre of mass. Over time, these orbits cover a well-defined region, as shown in Figure 33.

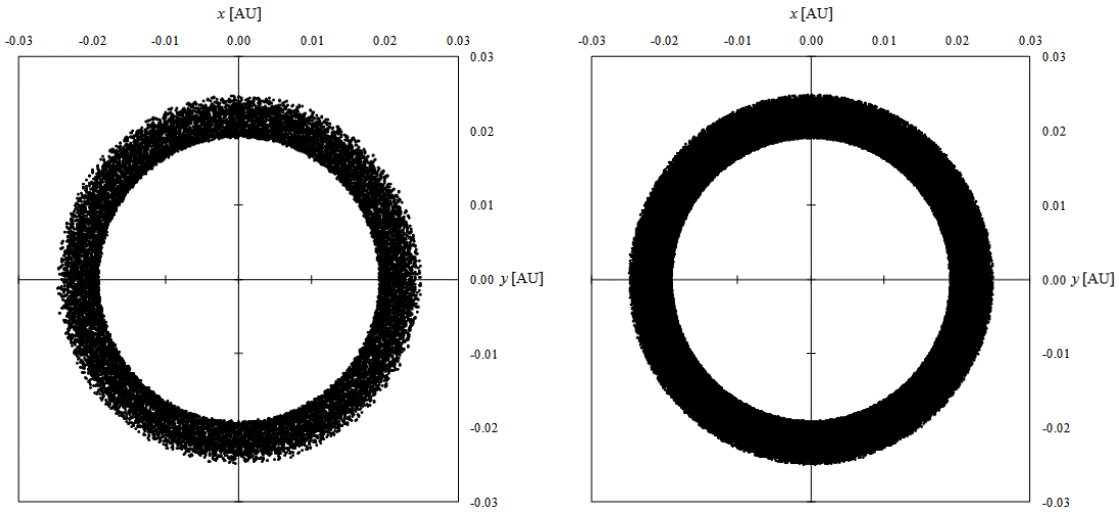

Figure 33. Region filled by the orbits of Bb over (a) 2.7 yr and (b) 19.8 yr.

Figure 33(a) shows the location of Bb at each of the first 20 000 time steps. Since each

time step is 0.05 d, this represents the first 2.74 yr of this body's evolution.

This cloud map shows that the region that the orbits fill becomes perfectly circular and it also defines the width of the annular space that the orbits fill. Using a longer period of time defines this region more crisply. For example, using 145 000 time steps, equivalent to 19.8 yr, resulted in the region shown in Figure 33(b).

The width of the annulus, i.e. the radial variation in Bb's orbit, is approximately 0.006 AU, or 28% of its average orbital radius of 0.0221 AU.

Turning to body A, the evolution of its first few orbits is shown in Figure 34.

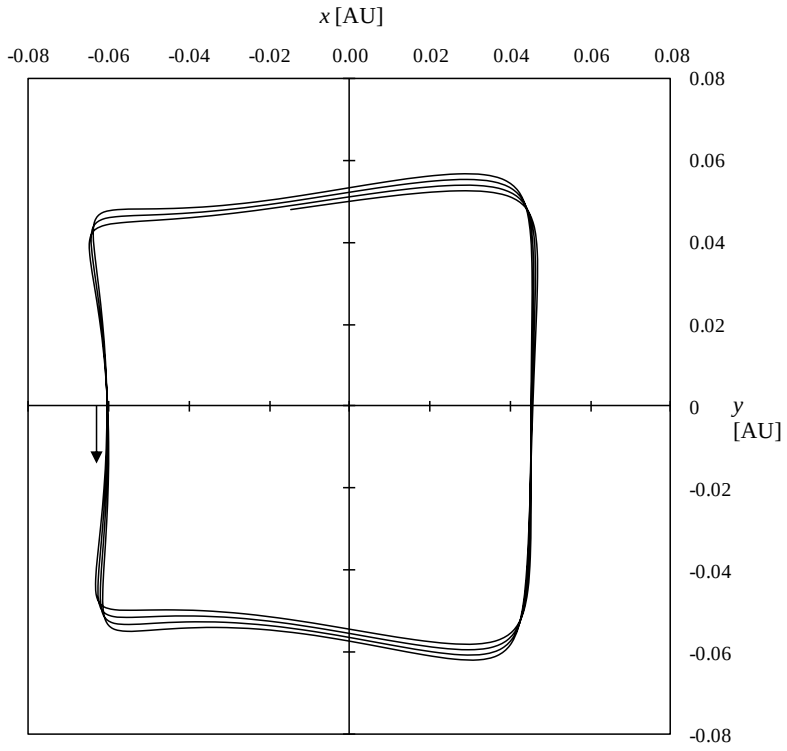

Figure 34. Initial orbits of A.

This unusual-looking orbit approximates a square, and at first sight appeared quite improbable. However, it is in a non-inertial reference frame, and is consistent with, and simply a more extreme version of, the scalloped orbit shown in Figure 29. Here the size of the orbit has been reduced to the extent that the central binary completes

approximately only four orbits in the orbital period of A, compared with the numerous orbits it completed within the far larger orbit shown in Figure 29. (In fact, reducing the size of A's orbit even further, so that the binary completes only three orbits in A's orbital period, could in principle lead to a triangular orbit!) There is only one mention of square orbits in the literature (also in a non-inertial frame), which has received only one citation (Stagg 1984).

Again, the shape of the orbit is because we are calculating orbital elements with respect to one star in what is a triple star system with 3 almost equal mass objects (3.0, 0.915 and 0.87 solar masses). Using barycentric coordinates, as shown in Figure 35, results in elliptical orbits as expected.

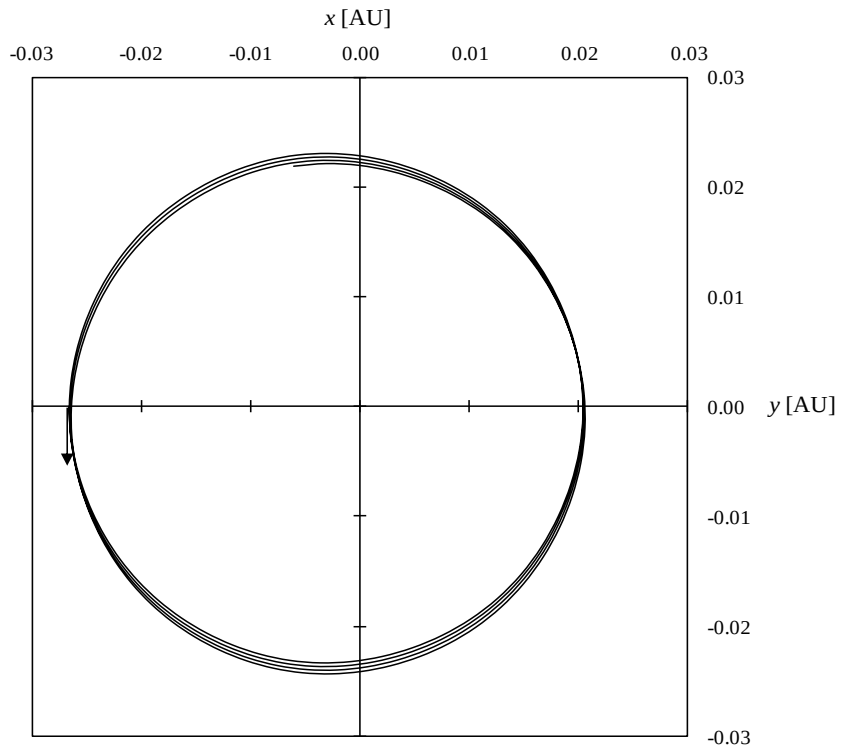

Figure 35. Initial orbits of A – barycentric coordinates.

Again, the orbit is not perfectly circular and show some precession. Over time this results in the cloud map shown in Figure 36(a), which plots the position of A over the

first 2.7 yr or 20 000 points.

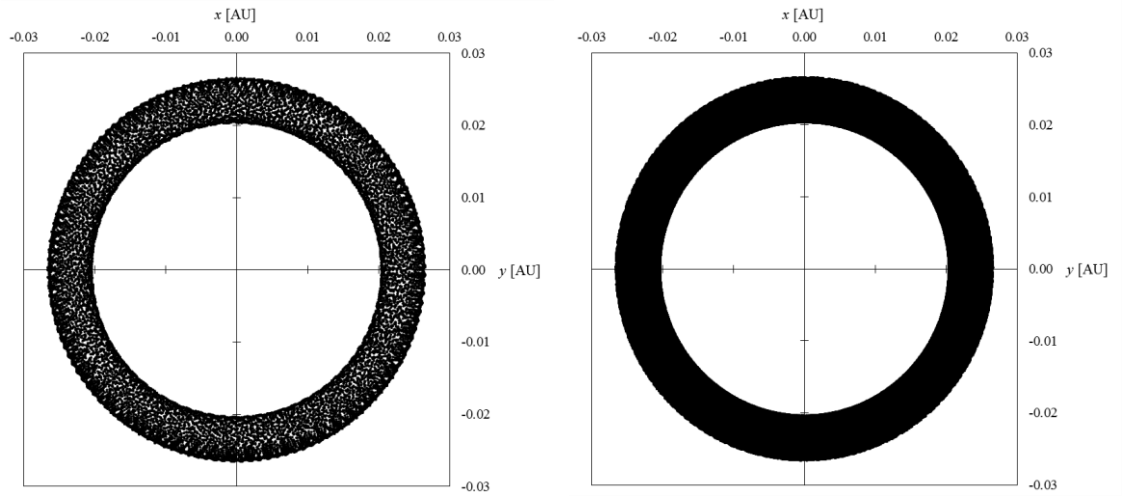

Figure 36. Region filled by the orbits of A over (a) 2.7 yr and (b) 19.8 yr.

Generating more points by following the body for just under 20 yr resulted in a better-defined orbital region for A, as shown in Figure 36(b).

Here the width of the annulus is wide, at approximately 0.034 AU or 55% of the average orbital radius of 0.063 AU.

A few examples illustrating the wide variety of stable orbits (in central coordinates) and their space-filling regions are shown in Figure 37. All these orbits were stable to 10^5 yr.

The shape of orbits, while interesting, is, however, irrelevant to our purpose, which is to find stable orbits. The stability of an orbit is, of course, independent of the coordinate system one elects to view it in.

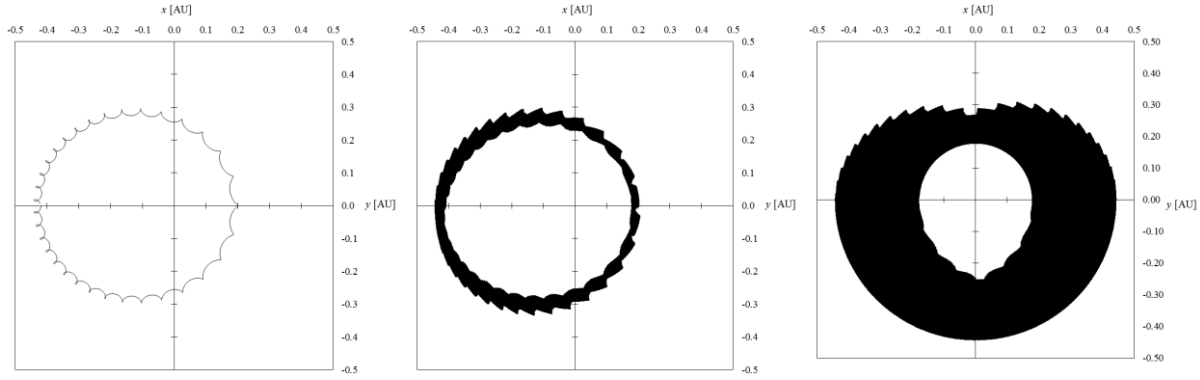

a = 0.4198 AU, *e* = 0.60

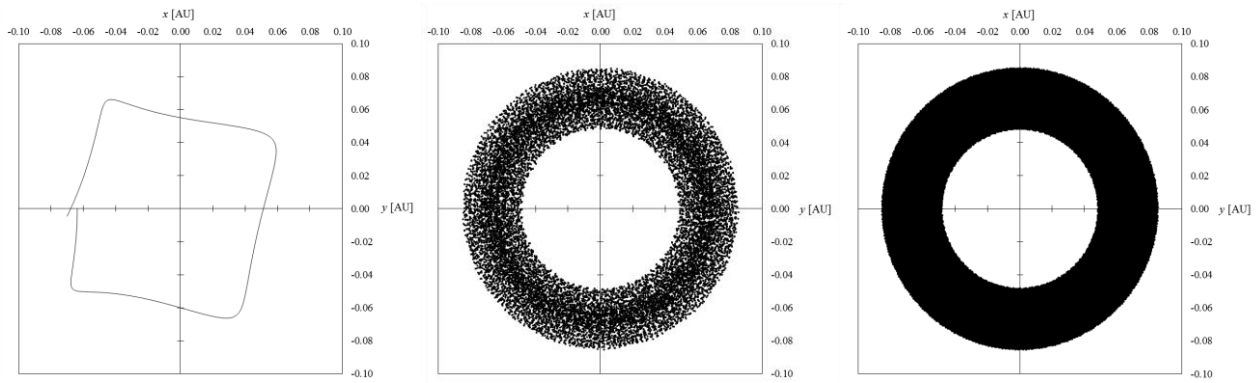

a = 0.4250 AU, *e* = 0.00

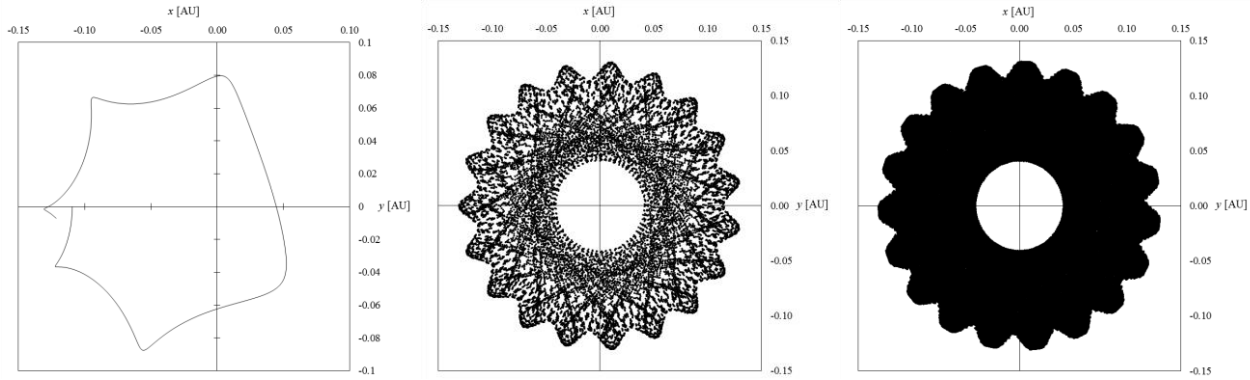

a = 0.4375 AU, *e* = 0.00

Figure 37. Stable orbits for body A – (a) first orbit, (b) cloud map of 20 000 time steps (~3 yr), (c) cloud map of 226 500 points (~30 yr).

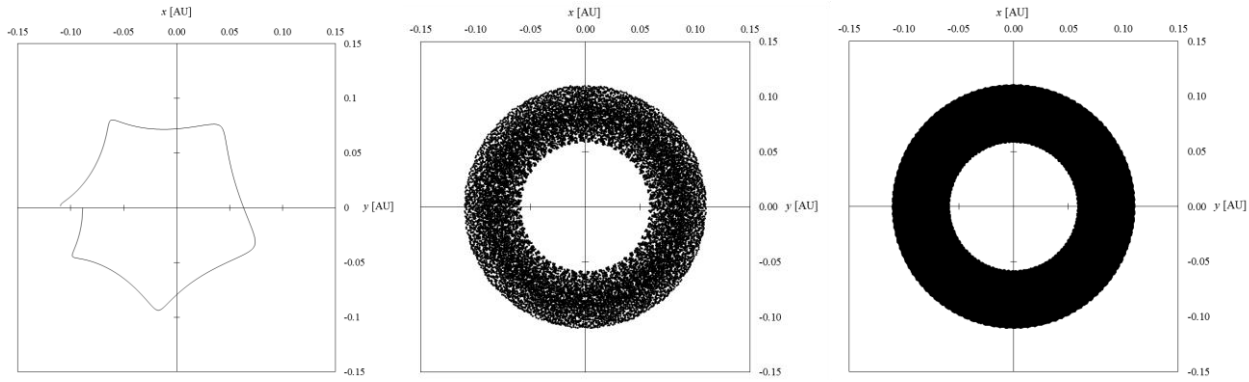

a = 0.4437 AU, *e* = 0.80

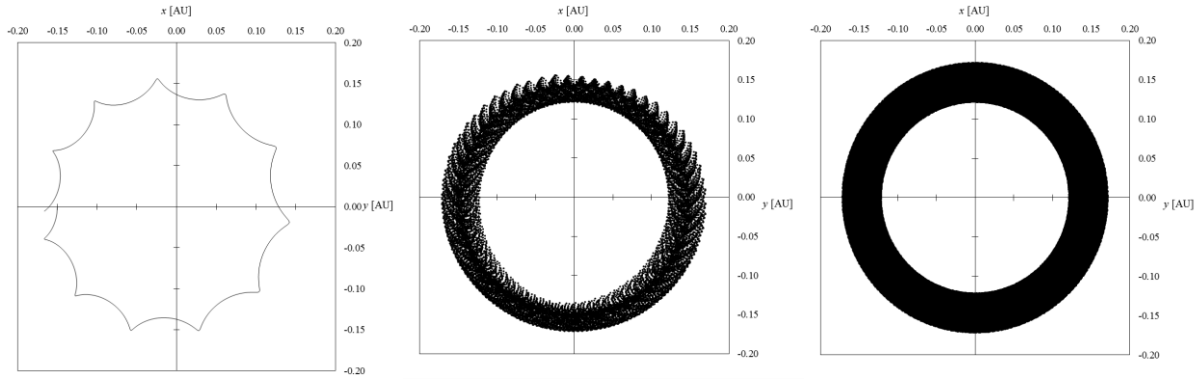

a = 0.5000 AU, *e* = 0.70

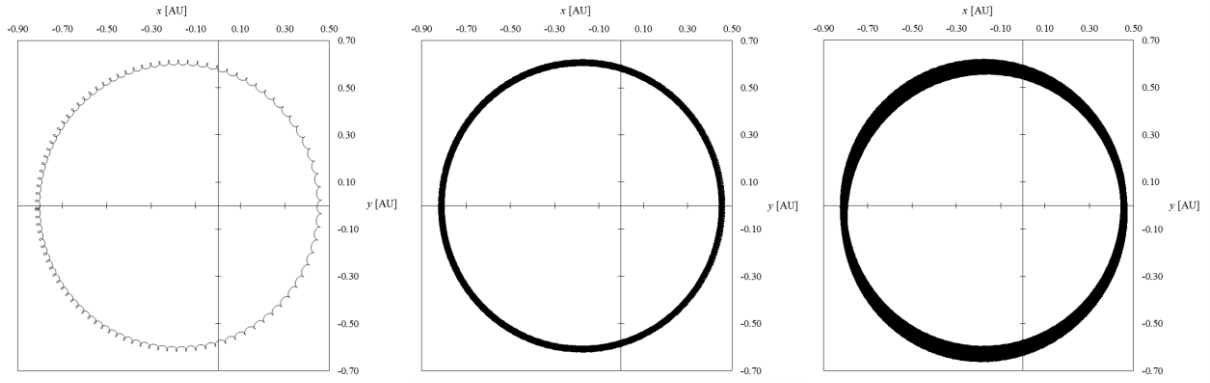

a = 0.7000 AU, *e* = 0.20

Figure 37 (continued). Stable orbits for body A – (a) first few orbits (b) cloud map of 20 000 time steps (~3 yr) and (c) cloud map of 226 500 points (~30 yr).

3.2 The habitable zone of HD 181068

Before establishing any regions of orbital stability for planets around the compact triple, we calculated the bounds of the habitable zone (HZ), since we would want to know where these stable regions intersected the HZ of the system.

The HZ of a star is given by the distances of an annulus around it where, with sufficient atmospheric pressure, water on the surface of a planet can remain liquid. A more general concept that takes into account the average time a planet spends in the HZ is the eccentric habitable zone (EHZ). Definitions of the habitable zone are given in, e.g. (Elser, Grimm & Stadel 2013) and (Jones, Sleep & Chambers 2001). A habitable planet is then often defined as a rocky planet of mass ~1 $M_{\oplus}$ up to that of a super-earth (~10$M_{\oplus}$), located in the habitable zone of its host star.

The HZ for single star systems defined by stellar irradiation has been discussed by a number of sources, most notably by Kasting (Kasting, Whitmire & Reynolds 1993), recently updated by Kopparapu (Kopparapu et al. 2013), who provide formulas for the inner and outer boundaries of the habitable zone. The HZ of planets in S-type orbits has been considered in detail by Eggl (Eggl et al. 2013). The above principles have been generalised to circumbinary systems (Kane & Hinkel 2013) and can be similarly extended to multistellar systems.

For a single star, the extent of the habitable zone is primarily controlled by the star–planet separation, and is calculated as a function of both the flux received and the peak wavelength of the energy distribution, but it is also affected by orbital eccentricity, planet rotation, heat sources other than stellar irradiation and atmospheric properties including circulation.

For a multistellar system, the multiple sources of flux results in the locus of the HZ no longer being spherical and becoming more complex. The apparent HZ bounds

will also be time-dependent as a result of the orbital motion of the central stars. An additional perturbation will also be caused by the changing separation between the stars, which will result in a complex insolation of the HZ as the stars orbit around their centre of mass. In addition, the flux received by the planet varies as a result of its orbit. For example, the variation in flux resulting from the factors mentioned previously will be enhanced at the planet's periastron.

For compact triples specifically, the HZ can often be approximated by considering the triple as a single star. It has been demonstrated for binaries that the circumstances under which this approximation holds depends only on the stellar masses and separations (Kane & Hinkel 2012).

The effective temperature and luminosity of the three components of HD 181068 are shown in Table 18, together with the limits of their individual HZs assuming they were isolated. The HZ limits were calculated from the equations given by Kopparapu et al. 2013, which require effective temperature and stellar luminosity as inputs, using his calculator provided at www3.geosc.psu.edu/~ruk15/planets/.

Star		Ba	Bb	A
Mass	[M_s]	0.915(34)	0.870(43)	3.0(1)
Radius	[AU]	0.00402	0.00372	0.05793
Effective temperature T_{eff}	[K]	5100(100)	4675(100)	5100(100)
Luminosity L/L_s	[-]	0.447(37)	0.270(27)	92.812(7615)
HZ distance from star - max	[AU]	0.68	0.54	9.83
- min	[AU]	1.20	0.96	17.25

Table 18. Stellar parameters and habitable zones for HD 181068 bodies. Data from Borkovits et al. 2013, estimate of habitable zone from Kopparapu et al. 2013.

Since star A dominates in terms of luminosity, as a first approximation its habitable zone provided us with a lower bound of ~10 AU-17 AU for the width of the HZ of the system.

As a better approximation we assumed that the luminosity of the three stars of the triple are additive. The total luminosity was therefore 93.529 L_s. We could then calculate the equivalent effective temperature from the Stefan-Boltzmann Law for a blackbody

$$T_{eff} = \left(\frac{L}{4\pi R^2 \sigma}\right)^{\frac{1}{4}} \quad (9)$$

where $T_{eff} =$ temperature of body [K]

$L =$ total luminosity of the body [W]

$R =$ radius of equivalent body [m^2]

$\sigma =$ Stefan $-$ Boltzmann constant [5.67×10^{-8} W m^{-2} K^{-4}]

The equivalent radius R in terms of the individual stellar radii is given by

$$R^2 = {r_{Ba}}^2 + {r_{Ba}}^2 + {r_A}^2 \quad (10)$$

R and T_{eff} were calculated to be 0.0582 AU and 5 078 K respectively. *Using these values moved the HZ out only marginally, with inner and outer limits increasing to 9.87 AU and 17.35 AU.*

3.3 The search for planets

While component A had to be represented by a massive body in the analysis of the stellar system as it affects the other stars, since planets are significantly smaller they could be represented by massless test particles, which are defined in Mercury6 as particles which perturb and interact with all the large, massive bodies in the system but do not perturb one another and cannot collide with each other.

In the search for planets the conservative Bulirsch-Stoer algorithm was again used, with a time step of one twentieth the period of the binary or 0.05 d and an

accuracy tolerance of 10^{-12}. The central body was component Ba, the "big" body was Bb, and central coordinates were again used.

The upper limit of semimajor axes used in the simulations was chosen to have the same gravitational influence as our Solar System has as far out as Pluto. Since the total stellar mass of the triple is 4.785 M_s, and Pluto's mean distance from the Sun is 40.7 AU, from the inverse square law this limit of influence for the triple is $\sqrt{4.785}\,(40.7\text{ AU}) \approx 90$ AU. An ejection limit of 500 AU was used.

The lower limit for the semimajor axes used was determined by the stability zone. From equation (2) and Figure 2, for the system's mass ratio of 1.68, if the eccentricity is 0.856, the semimajor axis stability ratio is 44.3. The stability zone will therefore have an inner limit of 44.3×0.02221 AU ≈ 1 AU - *the stable region begins well inside the HZ.* The region between the binary and body A at 0.4198 AU was therefore not searched for planets.

A full eccentricity range, from 0 to almost 1 was used. Low eccentricities are more likely for planets closer to the triple, as shown in Figure 38.

A quick survey of a few similar analyses (Holman & Wiegert 1999; Horner et al. 2012; Verrier & Evans 2007; Wittenmyer et al. 2011) showed that the average increment used for semimajor axes was 0.8 AU and the average increment in eccentricity was 0.08. For this analysis increments of 1.0 AU and 0.10 respectively were selected.

The resolution of the stability map would therefore be similar to these previous studies, but computational constraints restricted the upper limit on survival times to 10^5 yr. As mentioned previously, the compactness of the stellar system results in a relatively high number of orbits within any time period, which mitigates the effect of this restriction to some extent.

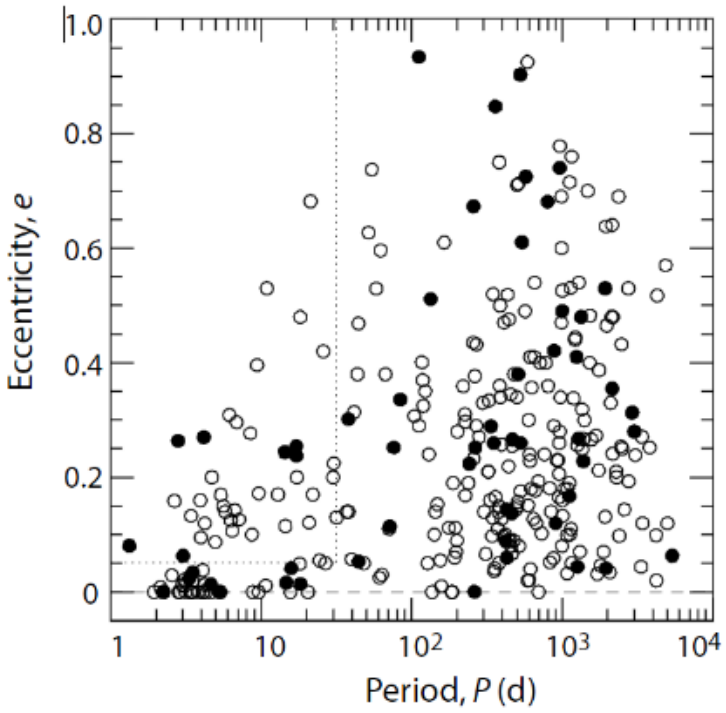

Figure 38. Exoplanet eccentricity versus period. Planets detected from radial velocity observations (317 planets from exoplanets.org, 2010), with those orbiting single stars shown as open circles and those in binary or multiple systems as filled circles. (Perryman, 2011)

Once again, coplanarity was assumed, giving orbital inclinations of zero, and the other orbital parameters were fixed at zero as before. Test particles were launched in initially circular orbits, with all bodies beginning from their pericentre. Both prograde and retrograde orbits (relative to A) were investigated.

In calculating the Cartesian orbital elements, test particles' periods in years were derived directly from Kepler's third law

$$T = \sqrt{\frac{4\pi^2 a^3}{GM}} \tag{11}$$

where a is the semimajor axis, G is the gravitational constant, M is the total mass of the stellar triple, all in consistent units, and it was assumed that there are 365.25 days in a year.

The plane around the triple was first searched using *a* and *e* as parameters.

The initial, preliminary search launched 100 test particles between 1 AU and 10 AU in increments of 1 AU, with eccentricities ranging from 0 to 0.9 in increments of 0.1. Prograde orbits were used, with the particles being launched on the opposite side of the binary to body A. This is shown schematically in Figure 39.

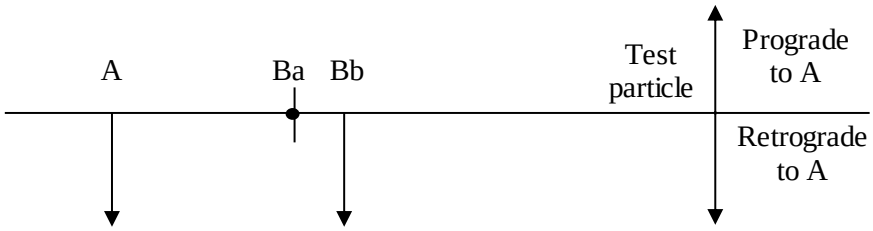

Figure 39. Initial configuration of orbit geometry – planet search.

The region 100 AU - 200 AU was then similarly searched, with all the other parameters remaining unchanged, using 1 010 test particles.

Then the area close to the triple, from 0.1 AU to 10 AU, was searched in smaller increments of 0.1 AU and also finer increments of eccentricity of 0.05. A total of 1 900 test particles were used.

The region 1 AU - 90 AU was then searched using various combinations of prograde and retrograde orbits and with test particles being launched on both the same and opposite sides of the binary relative to A. Each of these six simulations used 900 test particles.

The next simulation selected the most likely scenario, i.e. retrograde orbits with an opposite-side launch, and examined the same region at a higher resolution, using semimajor axis increments of 0.5 AU and eccentricity increments of 0.02, requiring a total of 8 771 test particles. In this case the ejection limit was raised from 500 AU to 1000 AU.

Finally, an even higher resolution search was conducted in the habitability zone of 10 AU - 20 AU using a smaller semimajor axis increment of 0.1 AU.

No stable orbits were found in any of these simulations. The longest survival times were only of the order of hundreds of years.

The next searches were conducted using a different approach, by selecting various arbitrary semimajor axis distances and searching a range of orbital velocities v_y at these points, with test particles again being launched on initially circular orbits.

The distances selected were 1 AU, 10 AU and 100 AU. The ejection limits used were 500 AU, 1 000 AU and 10 000 AU respectively. At each point the velocities selected ranged from approximately one quarter the implied Keplerian velocity to four times this value. The factor of four was used because this was the multiple by which the actual velocity of body A exceeded its Keplerian value in the analysis of the stellar system.

The first four simulations used retrograde orbits and opposite-side launches. In each case 1 000 test particles were used. These simulations were then repeated for prograde orbits.

The range of velocities was then expanded, with the upper limit becoming a factor of 10 greater than the Keplerian value. This range was applied to the 10 AU case, for both retrograde and prograde orbits with opposite-side launches, using 3 290 test particles in each case.

Again, no stable or even long-lived orbits were found.

A summary of the parameters used in the simulations is shown in Table 19.

Table 19. Summary of planet searches.

Run	File name	Direction relative to A	Side of binary relative to A	Test particles [No.]	Range of a Min [AU]	Range of a Max [AU]	Δa [AU]	Range of e Min	Range of e Max	Δe	Keplerian v_y (approx.) [AUd^{-1}]	Range of v_y Min [AUd^{-1}]	Range of v_y Max [AUd^{-1}]	Δv_y [AUd^{-1}]	Ejection limit [AU]	Stable orbits found	Longest survival [yr]
Searching a-e space																	
1	Case 1	Prograde	Opposite	100	1	10	1.0	0.00	0.90	0.10	-	-	-	-	500	None	512
2	Case 1 Close in	Prograde	Same	1 900	0.1	10	0.1	0.00	0.90	0.05					500	None	49
3	Case 1 100-200	Prograde	Opposite	1 010	100	200	1.0	0.00	0.90	0.10	-	-	-	-	500	None	294
4	Case 2	Prograde	Same	900	1	90	1.0	0.00	0.90	0.10	-	-	-	-	500	None	71
5	Case 2 100yr	Prograde	Same	900	1	90	1.0	0.00	0.90	0.10	-	-	-	-	500	None	695
6	Case 3	Prograde	Opposite	900	1	90	1.0	0.00	0.90	0.10	-	-	-	-	500	None	0
7	Case 4	Retrograde	Opposite	900	1	90	1.0	0.00	0.90	0.10	-	-	-	-	500	None	75
8	Case 5	Retrograde	Same	900	1	90	1.0	0.00	0.90	0.10	-	-	-	-	500	None	6
9	Case 6 Higher res	Retrograde	Opposite	8 771	1	90	0.5	0.00	0.96	0.02	-	-	-	-	1 000	None	184
10	Habitable zone	Prograde	Opposite	4 949	10	20	0.1	0.00	0.96	0.02	-	-	-	-	500	None	1185
Searching v_y space																	
11	Retrograde 1 AU	Retrograde	Opposite	1 000	1	-	-	-	-	-	0.0300	-0.0075	-0.1200	-1.125E-04	500	None	13
12	Retrograde 10 AU	Retrograde	Opposite	1 000	10	-	-	-	-	-	0.0100	-0.0025	-0.0400	-3.750E-05	1 000	None	360
	Retrograde 10 AU vy+-	Retrograde	Opposite	3 290	10						0.0100	0.0025	0.1258	3.750E-05	500	None	96
13	Retrograde 100 AU	Retrograde	Opposite	1 000	100	-	-	-	-	-	0.0040	-0.0010	-0.0160	-1.500E-05	10 000	None	22
15	Prograde 1 AU	Prograde	Opposite	1 000	1	-	-	-	-	-	0.0300	0.0075	0.1200	1.125E-04	500	None	363
16	Prograde 10 AU	Prograde	Opposite	1 000	10	-	-	-	-	-	0.0100	0.0025	0.0400	3.750E-05	1 000	None	367
	Prograde 10 AU vy++	Prograde	Opposite	3 290	10						0.0100	0.0025	0.1258	3.750E-05	500	None	186
17	Prograde 100 AU	Prograde	Opposite	1 000	100	-	-	-	-	-	0.0040	0.0010	0.0160	1.500E-05	10 000	None	980
	Total, min/max			33 810	0	1 000		0	0.96			0.001	0.1258				

In total, the region 1 AU - 100 AU was searched in increments ranging from 1 AU to 0.1 AU and eccentricities varying from 0 to 0.96 in increments ranging from 0.1 to 0.02, and orbital velocities spanning 0.001 AU d^{-1} - 0.1258 AU d^{-1}, using a total of 33 810 test particles, without success.

There is no reason why there should not be stable orbits - if one goes out far enough, distant particles should see the stellar system essentially as a point mass, and there is absolutely no fundamental reason why all bodies should be ejected. There are a few puzzling aspects to this lack of stable orbits.

(1) Most orbit failures are ejections. Most of these trajectories are straight lines away from the initial position and perpendicular to the line joining the three bodies, irrespective of the test particle's initial velocity. Figure 40, in barycentric coordinates, shows a few initial time steps (of 0.05 d) in a test particle's typical ejection path. The arrows indicate the initial position and velocity for the bodies.

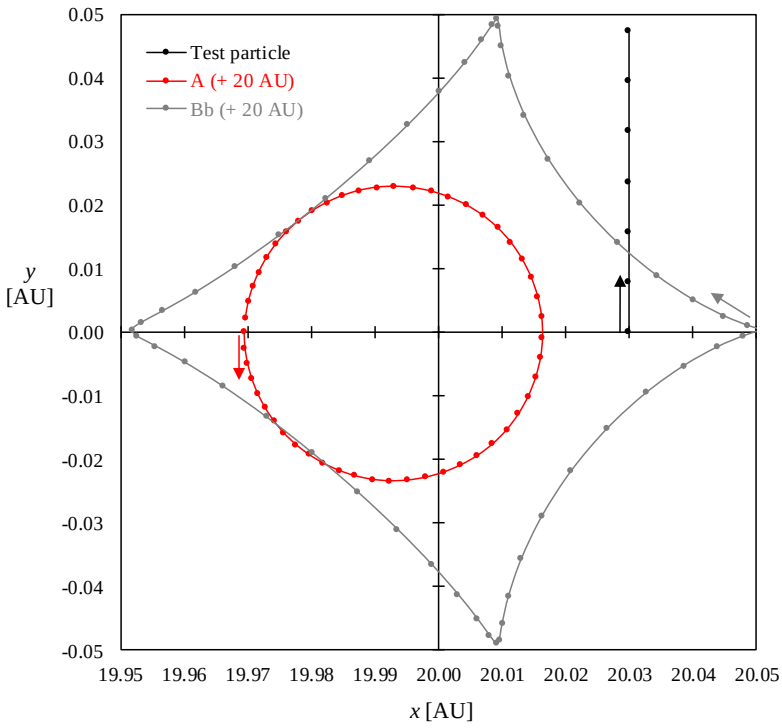

Figure 40. Initial time steps in an ejection: *x*-*y* position coordinates.

In this example the test particle was placed at its starting point with no velocity at all. In the very first time step it acquired a v_y velocity component which remained constant thereafter, and no x-velocity, despite the initial location of the other two bodies on the x-axis. The velocities are shown in Figure 41, where the arrows indicate the initial velocities. After one time step, A's velocity remained where shown.

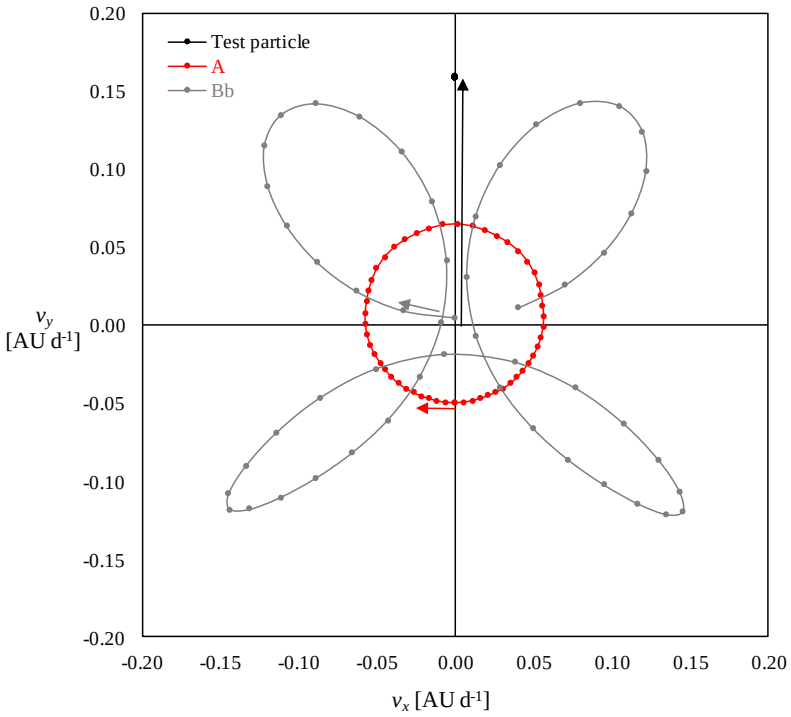

Figure 41. Initial time steps in an ejection: v_x-v_y velocity coordinates.

How the particle acquired a v_y velocity component, and a positive one, is not clear.

(2) We then went back to the HW Virginis simulation and removed the approximation of the binary being a point mass, splitting it into its two binary components but keeping everything else unchanged. The simulation then failed.

(3) The HD 181168 triple was then simplified by consolidating the central binary into a single mass, and some of the previous searches shown in Table 19 repeated. For example, picking an arbitrary semimajor axis of 20 AU and searching a wide range of orbital velocities at that point *resulted in no stable prograde orbits. However, many retrograde orbits were stable up to* 10^5 *yr*. The two regions of stable orbital velocities are shown in Figure 42.

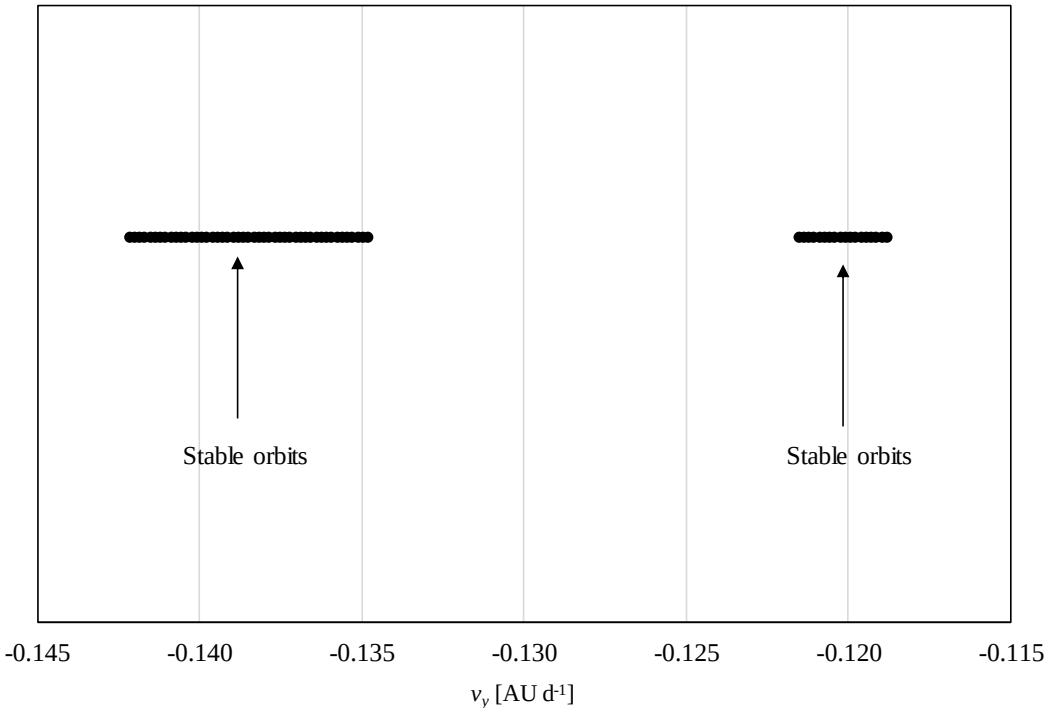

Figure 42. At 20 AU - initial velocities for which stable retrograde orbits resulted.

The key point is that these velocities are approximately 16 times the appropriate Keplerian value. The only way these high velocities can be achieved is if the orbits are highly eccentric. To generate the lowest velocity shown in Figure 42, an eccentricity of over 0.998 is required. This may be related to the high eccentricity of the stellar component A.

Why only highly eccentric orbits are stable, for both A and for the test particles, remains a puzzle.

These puzzling aspects suggest that perhaps the algorithm is not appropriate to the problem. While Mercury6 worked well in configurations such as the original HW Virginis approximation and appeared to model the three components of the triple well, the addition of a fourth body in both these cases led to seemingly unrealistic results. As mentioned previously, the different coordinate scheme used for test particles may not work for objects such as compact, comparable-mass triples. Mercury6 was designed to have a dominant body plus much smaller bodies, like a planetary system, which HD 181068 clearly is not. So even while the Bulirsch-Stoer algorithm is robust, it has been embedded in a package structured for systems unlike the compact triple.

We can, of course, simplify the triple even further, by consolidating all three components into a single central mass. This would provide a first-order approximation of the stability landscape around the central mass. Doing this for 1 000 test particles covering semimajor axis distances from 1 AU to 90 AU and eccentricities from 0 to 0.9 lead to orbits with a wide range of survival times, with a large number surviving beyond 10^6 yr. It must be noted, however, that while momentum conservation $\Delta L/L$ was 10^{-12}, energy conservation $\Delta E/E$ was poor at 10^{-2}. The resulting *a*-*e* stability map is shown in Figure 43.

The data does not appear to contain much information. The broadest trend is that for the stable regions, eccentricity increases with semimajor axis distance, which is consistent with the data in Figure 40. The region of stability is divided by a finger of instability at around 50 AU, suggesting two separate islands of stability, one centred at around 20 AU with eccentricities in the region of 0.4, and another at about 75 AU with much higher eccentricities of around 0.6.

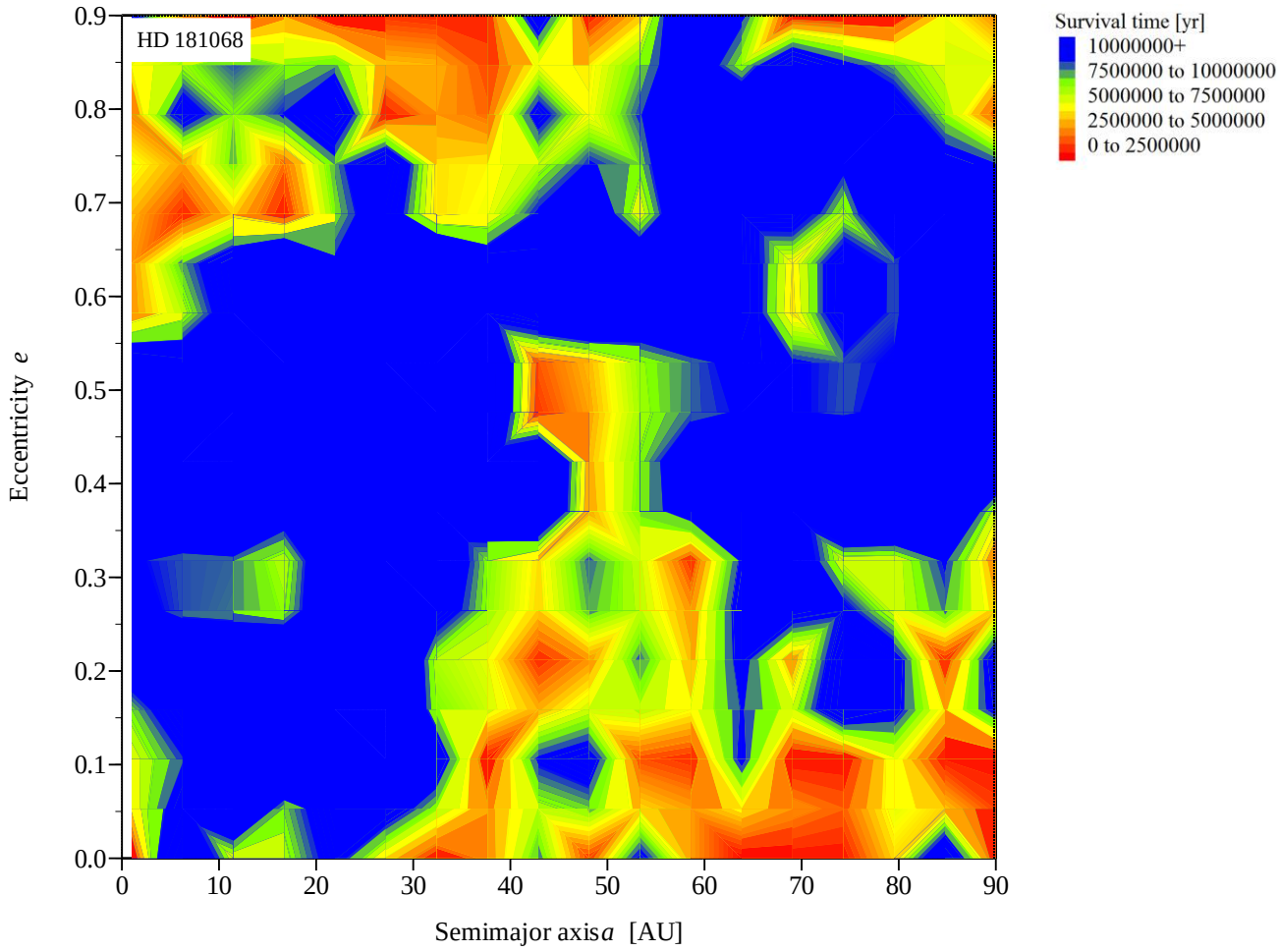

Figure 43. Stability map for HD 181068 as a point mass.

4. Summary and conclusions

In this study we identified the small number of stellar triples that are compact enough to possibly harbour exoplanets in P-type orbits around them. From these we selected and analysed the hierarchical triple HD 181068, using the *N*-body integrator Mercury6 to determine the stability of the stellar triple as well as of possible planetary orbits around it. Published empirical stability criteria suggested that the stellar system should be stable. For the system to become unstable, the triple's outer orbit would have to be quite eccentric, with an eccentricity of over 0.67.

However, a stability map of the stellar system, using orbits stable to 10^5 yr, showed a stability zone for the outer body which differed from the published orbital parameters of $e = 0$ and $a = 0.4198$. For orbits of zero eccentricity the region of stability lay between semimajor axes of ~0.70 AU - 0.90 AU, while for the given semimajor axis the stable region had eccentricities in the region of 0.825 - 0.900. Generally, retrograde orbits were found to be more stable than prograde ones. While the analysis had relatively low resolution and survival times, the general pattern was unambiguous. The reason for this difference from the published parameters is unknown.

We therefore made the provisional assumption that the orbit of body A is described by $a = 0.41986$ AU and $e = 0.856$, with the remaining parameters as published. Orbits in this region were shown to be stable up to 10^6. We then used this as the geometry of the compact stellar system around which we investigated the stability landscape for planets.

The limits of the habitability zone were calculated to be 10 AU - 17 AU. The plane around the triple was then comprehensively searched for planets, using 33 810 test particles. The region 1 AU - 100 AU was searched in increments ranging from 1 AU to 0.1 AU and eccentricities from 0 to 0.96, in increments ranging from 0.1 to 0.02; orbital velocities spanned 0.001 AU d^{-1} - 0.1258 AU d^{-1}. No stable orbits were found.

It appears that the addition of a fourth body leads to poor performance from the algorithm; this was also found when tested in the case of HW Virginis. So although the most robust algorithm within the Mercury6 integrator was used, we concluded that this package, which was originally designed for configurations comprising one central dominant body, probably became inappropriate for a compact triple system of three almost equal-mass stars, possibly in the coordinate system for its test particles, i.e. in the original splitting of the Hamiltonian for the assumed configuration.

Simplifying the model by consolidating the central binary into a single body resulted in stable but very highly eccentric orbits. Again, the reason for this is unclear and may be related to the high eccentricity of stellar body A. Further simplification of the stellar system yielded a planetary stability map out to 90 AU, but computational limitations meant that its resolution was not sufficient to extract detailed conclusions. The analysis needs to be extended by identifying the best *N*-body algorithm for this particular system and by increasing the resolution of its output.

5. Further work

There are two key aspects to tackle.

The first is to crosscheck these results using a different algorithm. The best candidate is Herve Beust's HJS (Hierarchic Jacobi Symplectic) add-in for Hal Levison's Swift package. HJS was specifically designed to symplectically integrate multiple stellar systems, i.e. systems with more than one massive centre, provided they have an hierarchical structure. However, attempts to compile Swift under Windows were problematic; it will probably be better to use a Linux environment for this.

The second is to address the fact that a large constraint in the study was computational. The integrations were slow because of the algorithm used and also the computational power available.

(1) The Bulirsch-Stoer algorithm is very robust but slow. The faster symplectic algorithms in Mercury6 cannot be used for this particular problem. Again, the Swift/HJS package should be significantly faster.

(2) On the computing platform used, integrating 100 test particles over 10^5 yr used 28 hours of running time, equivalent to ~0.01 sec particle^{-1} year^{-1}. To construct a reasonably high-resolution $a - e$ plot would need around 1 000 points on each

axis, or 10^6 test particles. Smoothing the results by averaging over, say, 20 simulations using different initial conditions would therefore be equivalent to 20×10^6 test particles. Integrating these for the commonly accepted 10^8 yr on the current platform would therefore take around 5×10^9 yr of computation time, which would be tedious. Access to more computing power is necessary. This more limited study required computing power approximately five orders of magnitude greater than that available.

Nevertheless, this application remains a small-*N* problem and this computing requirement is far less demanding than for large-*N* problems such as galaxy evolution.

Acknowledgments

The author would like to acknowledge:

- The Mercury6 code from John Chambers and his assistance in applying it to the stellar system investigated.
- The SWIFT and HJS codes from Hal Levison and Herve Beust respectively, together with helpful comments from both.
- Useful input from Patricia Verrier and Rosemary Mardling.
- Many patient answers from Rachel Akeson of the NASA Exoplanet Archive team.

This research made use of NASA's Astrophysics Data System.

Appendices

Appendix A: Exoplanet nomenclature

From medbib.com/Extrasolar_planets#cite_ref-EPE55Can_57-0

Multiple-star standard

The standard for naming exoplanets is an extension of the one used by the Washington Multiplicity Catalog (WMC) for multiple-star systems.

The brightest member of a system receives the letter "A." Distinct components not contained within "A" are labelled "B", "C", etc. Sub-components are designated by one or more suffixes with the primary label, starting with lowercase letters for the 2nd hierarchical level and then numbers for the 3rd. For example, if there is a triple star system in which two stars orbit each other closely while a third star is in a more distant orbit, the two closely orbiting stars would be considered a component with two subcomponents. They would receive the designations Aa and Ab, while the third star would receive the designation B. (For historical reasons, this standard is not always strictly followed. For example, the three members of the Alpha Centauri triple star system are conventionally referred to as Alpha Centauri A, B and C while the formal standard would give their designations as Alpha Centauri Aa, Ab and B respectively.)

Extrasolar planet standard

Following an extension of the above standard, an exoplanet's name is normally formed by taking the name of its parent star and adding a lowercase letter. The first planet discovered in a system is given the designation "b" and later planets are given subsequent letters. If several planets in the same system are discovered at the same time, the closest one to the star gets the next letter, followed by the other planets in order of

orbit size.

For instance, in the 55 Cancri system the first planet – 55 Cancri b – was discovered in 1996; two additional farther planets were simultaneously discovered in 2002 with the nearest to the star being named 55 Cancri c and the other 55 Cancri d; a fourth planet was claimed in 2004 and named 55 Cancri e despite lying closer to the star than 55 Cancri b; and the most recently discovered planet, in 2007, was named 55 Cancri f despite lying between 55 Cancri c and 55 Cancri d.

If a planet orbits one member of a binary star system, then an uppercase letter for the star will be followed by a lowercase letter for the planet. Examples are 16 Cygni Bb and HD 178911 Bb. Planets orbiting the primary or "A" star should have 'Ab' after the name of the system, as in HD 41004 Ab. However, the "A" is sometimes omitted; for example the first planet discovered around the primary star of the Tau Boötis binary system is usually called simply Tau Boötis b.

If the parent star is a single star, then it may still be regarded as having an "A" designation, though the "A" is not normally written. The first exoplanet found to be orbiting such a star could then be regarded as a secondary sub-component that should be given the suffix "Ab". For example, 51 Peg Aa is the host star in the system 51 Peg; and the first exoplanet is then 51 Peg Ab. Since most exoplanets are in single star systems, the implicit "A" designation was simply dropped, leaving the exoplanet name with the lower-case letter only: 51 Peg b.

A few exoplanets have been given names that do not conform to the above standard. For example, the planets that orbit the pulsar PSR 1257 are often referred to with capital rather than lowercase letters. Also, the underlying name of the star system itself can

follow several different systems. In fact, some stars (such as Kepler-11) have only received their names due to their inclusion in planet-search programs, previously only being referred to by their celestial coordinates.

Circumbinary planets and the 2010 proposal

Hessman et al. state that the implicit system for exoplanet names utterly failed with the discovery of circumbinary planets (Hessman et al. 2010). They note that the discoverers of the two planets around HW Virginis tried to circumvent the naming problem by calling them "HW Vir 3" and "HW Vir 4", i.e. the latter is the 4th object – stellar or planetary – discovered in the system. They also note that the discoverers of the two planets around NN Serpentis were confronted with multiple suggestions from various official sources and finally chose to use the designations "NN Ser c" and "NN Ser d."

The proposal of Hessman et al. starts with the following two rules:

Rule 1. *The formal name of an exoplanet is obtained by appending the appropriate suffixes to the formal name of the host star or stellar system. The upper hierarchy is defined by upper-case letters, followed by lower-case letters, followed by numbers, etc. The naming order within an hierarchical level is for the order of discovery only. (This rule corresponds to the present provisional WMC naming convention.)*

Rule 2. *Whenever the leading capital letter designation is missing, this is interpreted as being an informal form with an implicit "A" unless otherwise explicitly stated. (This rule corresponds to the present exoplanet community usage for planets around single stars.)*

They note that under these two proposed rules all of the present names for 99% of the planets around single stars are preserved as informal forms of the IAU-sanctioned provisional standard. They would rename Tau Boötis b formally as Tau Boötis Ab,

retaining the prior form as an informal usage (using Rule 2, above).

To deal with the difficulties relating to circumbinary planets, the proposal contains two further rules:

Rule 3. *As an alternative to the nomenclature standard in Rule 1, a hierarchical relationship can be expressed by concatenating the names of the higher order system and placing them in parentheses, after which the suffix for a lower order system is added.*

Rule 4. *When in doubt (i.e. if a different name has not been clearly set in the literature), the hierarchy expressed by the nomenclature should correspond to dynamically distinct (sub-) systems in order of their dynamical relevance. The choice of hierarchical levels should be made to emphasize dynamical relationships, if known.*

They submit that the new form using parentheses is the best for known circumbinary planets and has the desirable effect of giving these planets identical sub-level hierarchical labels and stellar component names which conform to the usage for binary stars. They say that it requires the complete renaming of only two exoplanetary systems: the planets around HW Virginis would be renamed HW Vir (AB) b and (AB) c, while those around NN Serpentis would be renamed NN Ser (AB) b and (AB) c. In addition, the previously known single circumbinary planets around PSR B1620-26 and DP Leonis can almost retain their names (PSR B1620-26 b and DP Leonis b) as unofficial informal forms of the "(AB) b" designation where the "(AB)" is left out.

The discoverers of the circumbinary planet around Kepler-16 followed Hessman et al.'s proposed naming scheme when naming the body Kepler-16 (AB)-b, or simply Kepler-16b when there is no ambiguity.

Appendix B: Extracting star system frequencies from the NASA Exoplanet Archive

The object was to extract discoveries by the type of star system, i.e. to list planets:

(1) orbiting one star of a binary system,

(2) orbiting two stars of a binary system (circumbinary orbit),

(3) orbiting one star of a triple system,

(4) in a circumbinary orbit of the two stars of a triple system,

(5) orbiting three stars of a triple system (circumtriple orbit).

While the NASA Exoplanet Archive database includes information on stellar multiplicity, this is not currently searchable from the confirmed planet table.

The easiest way to identify planets which may fall into these categories is to look at the host name column in exoplanetarchive.ipac.caltech.edu/cgi-bin/ExoTables/nph-exotbls?dataset=planets. Stars with a capital letter at the end are part of a multiple system. One can then click twice on the *i* icon, and click on *Confirmed Planet Overview*. The stellar multiplicity information is under *Stellar Information* in the column control panel on the left. One must click the *Stellar Companions* box and then update.

The new information appears at the bottom of the page and lists the known companions. The Washington Double Star Catalog (WDS) (where much of the companion information comes from) includes some very wide separations where the stars may not be dynamically bound. By comparing the stellar separations and the planet-star separation, one can distinguish between circumbinary planets and planets around one star in a binary system.

Appendix C: Mercury6 timer code and input/output files

Timer code added

```
!Timer variables
real(4) :: time1, time2
!Start timer
time1=secnds(0.0)

<Bulk of program>

! Stop timer and write
time2=secnds(time1)
WRITE (*,'(A,F8.2)') "Time (sec):", time2
```

Input files

File big.in

```
)O+_06 Big-body initial data  (WARNING: Do not delete this line!!)
) Lines beginning with `)' are ignored.
)---------------------------------------------------------------------
 style (Cartesian, Asteroidal, Cometary) = Asteroidal
 epoch (in days) = 2451000.5
)---------------------------------------------------------------------
 HWVIRB    m=0.142 r=1. d=37.4
 0.00399833 0. 80.9 0. 0. 0.
  0. 0. 0.
```

File element.in

```
)O+_06 element  (WARNING: Do not delete this line!!)
) Lines beginning with `)' are ignored.
)---------------------------------------------------------------------
 number of input files = 1
)---------------------------------------------------------------------
) List the input files, one per line
 xv.out
)---------------------------------------------------------------------
 type of elements (central body, barycentric, Jacobi) = Central
 minimum interval between outputs (days) = 0.005835
 express time in days or years = days
 express time relative to integration start time = yes
)---------------------------------------------------------------------
) Output format? (e.g. a8.4 => semimajor axis with 8 digits & 4 dec. places)
 a8.5 e8.6 i8.4 r8.4 y8.6 z8.6 x8.6
)---------------------------------------------------------------------
) Which bodies do you want? (List one per line or leave blank for all bodies)
```

File param.in

```
)O+_06 Integration parameters  (WARNING: Do not delete this line!!)
) Lines beginning with `)' are ignored.
)------------------------------------------------------------------
) Important integration parameters:
)------------------------------------------------------------------
 algorithm (MVS, BS, BS2, RADAU, HYBRID etc) = bs
 start time (days) = 2451000.5
 stop time (days) = 2454503.5
 output interval (days) = 5.835e-3
 time step (days) = 5.835e-3
 accuracy parameter = 1.d-12
)------------------------------------------------------------------
) Integration options:
)------------------------------------------------------------------
 stop integration after a close encounter = no
 allow collisions to occur = no
 include collisional fragmentation = no
 express time in days or years = days
 express time relative to integration start time = yes
 output precision = medium
 < not used at present >
 include relativity in integration= no
 include user-defined force = no
)------------------------------------------------------------------
) These parameters do not need to be adjusted often:
)------------------------------------------------------------------
 ejection distance (AU)= 4.
 radius of central body (AU) = 8.5079d-4
 central mass (solar) = 0.485
 central J2 = 0
 central J4 = 0
 central J6 = 0
 < not used at present >
 < not used at present >
 Hybrid integrator changeover (Hill radii) = 3.
 number of time steps between data dumps = 1
 number of time steps between periodic effects = 1
```

Output files

File element.out

Time (days): 3503.00000 a e i mass Rot/day Obl
HWVIRB 0.0040 0.00000 80.900 1.4200E-01 0.000 80.900

File info.out

Integration parameters

Algorithm: Bulirsch-Stoer (general)

Integration start epoch: 2451000.5000000 days
Integration stop epoch: 2454503.5000000
Output interval: 0.006
Output precision: medium

Initial time step: 0.006 days
Accuracy parameter: 1.0000E-12
Central mass: 4.8500E-01 solar masses
J_2: 0.0000E+00
J_4: 0.0000E+00
J_6: 0.0000E+00
Ejection distance: 4.0000E+00 AU
Radius of central body: 8.5079E-04 AU

Includes collisions: no
Includes fragmentation: no
Includes relativity: no
Includes user-defined force routine: no

Number of Big bodies: 1
Number of Small bodies: 0

Integration details

Initial energy: -2.54850E-03 solar masses AU^2 day^-2
Initial angular momentum: 9.46056E-05 solar masses AU^2 day^-1

WARNING: No Small bodies are present.

Integrating massive bodies and particles up to the same epoch.

Beginning the main integration.

Integration complete.

Fractional energy change due to integrator: 1.89168E-10
Fractional angular momentum change: 9.45841E-11

Fractional energy change due to collisions/ejections: 0.00000E+00
Fractional angular momentum change: 0.00000E+00
Time (sec): 2638.13

File element.out

HWVIRB

Time (days)	a	e	i	r	y	z	x
0.00000	0.00400	0.000000	80.9000	0.0040	0.000000	0.000000	0.003998
0.00584	0.00400	0.000000	80.9000	0.0040	-.000017	0.001236	0.003802
0.01167	0.00400	0.000000	80.9000	0.0040	-.000033	0.002351	0.003234
0.01750	0.00400	0.000000	80.9000	0.0040	-.000045	0.003236	0.002348
0.02334	0.00400	0.000000	80.9000	0.0040	-.000053	0.003803	0.001232
0.02918	0.00400	0.000000	80.9000	0.0040	-.000056	0.003998	-.000004
0.03501	0.00400	0.000000	80.9000	0.0040	-.000053	0.003801	-.001240
0.04084	0.00400	0.000000	80.9000	0.0040	-.000045	0.003231	-.002355
0.04668	0.00400	0.000000	80.9000	0.0040	-.000033	0.002345	-.003239
0.05251	0.00400	0.000000	80.9000	0.0040	-.000017	0.001228	-.003805
0.05835	0.00400	0.000000	80.9000	0.0040	0.000000	-.000008	-.003998
0.06418	0.00400	0.000000	80.9000	0.0040	0.000017	-.001244	-.003800
0.07002	0.00400	0.000000	80.9000	0.0040	0.000033	-.002358	-.003229
0.07586	0.00400	0.000000	80.9000	0.0040	0.000045	-.003241	-.002341
0.08169	0.00400	0.000000	80.9000	0.0040	0.000053	-.003806	-.001224
0.08752	0.00400	0.000000	80.9000	0.0040	0.000056	-.003998	0.000013
0.09336	0.00400	0.000000	80.9000	0.0040	0.000053	-.003798	0.001248
0.09919	0.00400	0.000000	80.9000	0.0040	0.000045	-.003226	0.002362
0.10503	0.00400	0.000000	80.9000	0.0040	0.000033	-.002338	0.003244
0.11086	0.00400	0.000000	80.9000	0.0040	0.000017	-.001220	0.003808
0.11670	0.00400	0.000000	80.9000	0.0040	-.000000	0.000017	0.003998

…etc

Appendix D: Coordinate conversion

The conversion of Keplerian elements to the modified Herschel astrocentric coordinates that use the sky as the reference plane and are commonly used for exoplanets are described by (Dvorak 2008). A schematic view is shown in Figure D1.

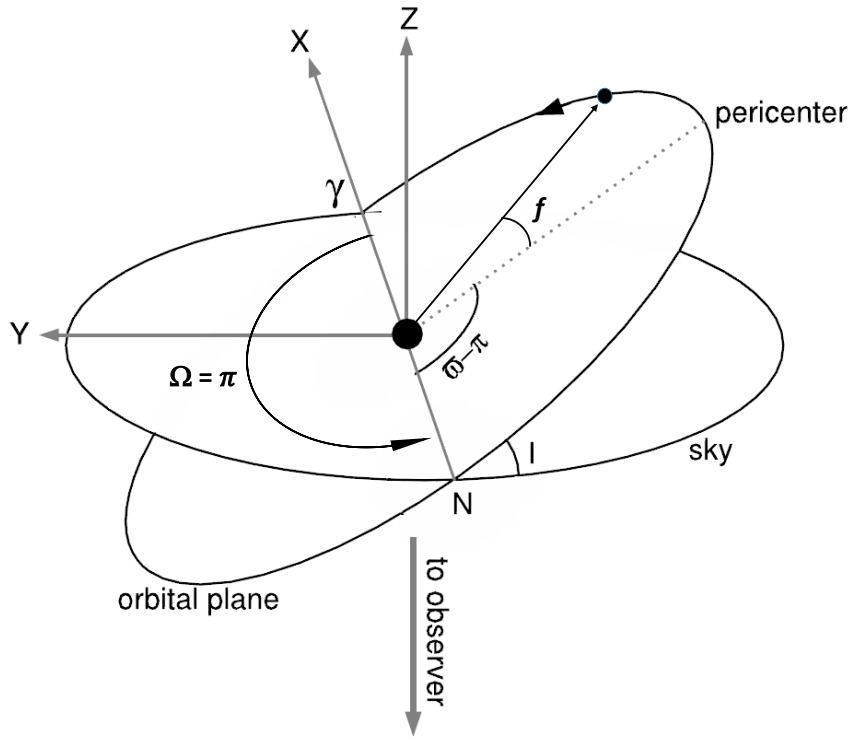

Figure D1. The rotated astrocentric reference frame showing the orbital plane and the plane tangent to the celestial sphere (sky). The origin of the angles is the point γ. Modified from Dvorak 2008.

The cartesian coordinates and velocities are given by

$$x = r[\cos f \cos w - \sin f \sin w]$$

$$y = r[\cos f \sin w \cos I + \sin f \cos w \cos I]$$

$$z = r[-\cos f \sin w \sin I - \sin f \cos w \sin I]$$

$$v_x = -\frac{2\pi a}{T\sqrt{1-e^2}}\,[\sin(f+w) + e \sin w]$$

$$v_y = +\frac{2\pi a \cos I}{T\sqrt{1-e^2}}\,[\cos(f+w) + e\cos w]$$

$$v_z = -\frac{2\pi a \sin I}{T\sqrt{1-e^2}}\,[\cos(f+w) + e\cos w]$$

where r is the magnitude of the radius vector and is given by

$$r = \frac{a(1-e^2)}{1 + e\ cos\ f}$$

$a =$ astrocentric semi $-$ major axis [AU]

$e =$ eccentricity $[-]$

$i =$ inclination [°]

$T =$ orbital period [yr], which may be obtained directly from Kepler's third law

$f =$ true anomaly [°]

$w = g - \pi$ where g is the argument of periapsis/pericentre/perihelion [°]

Note that the longitude of the ascending node Ω is fixed at $\Omega = \pi$.

The true anomaly can be calculated from the eccentric anomaly E by

$$f = \arccos\left(\frac{\cos E - e}{1 - e\ cosE}\right)$$

and E can be calculated iteratively from the mean anomaly M by

$$E - e\sin E = M$$

In the simulations we generally assumed $M = 0$, so $E = 0$.

Note that if $i = 0,\ \Omega$ becomes meaningless.

Appendix E: The search for stable orbits of component A

We first launched 600 massless test particles with semimajor axes ranging from 0.1 AU to 0.7 AU into initially circular orbits around the binary, assuming an inclination of zero, and integrated for 25 yr (~9 200 d).The results are shown in Figure E1.

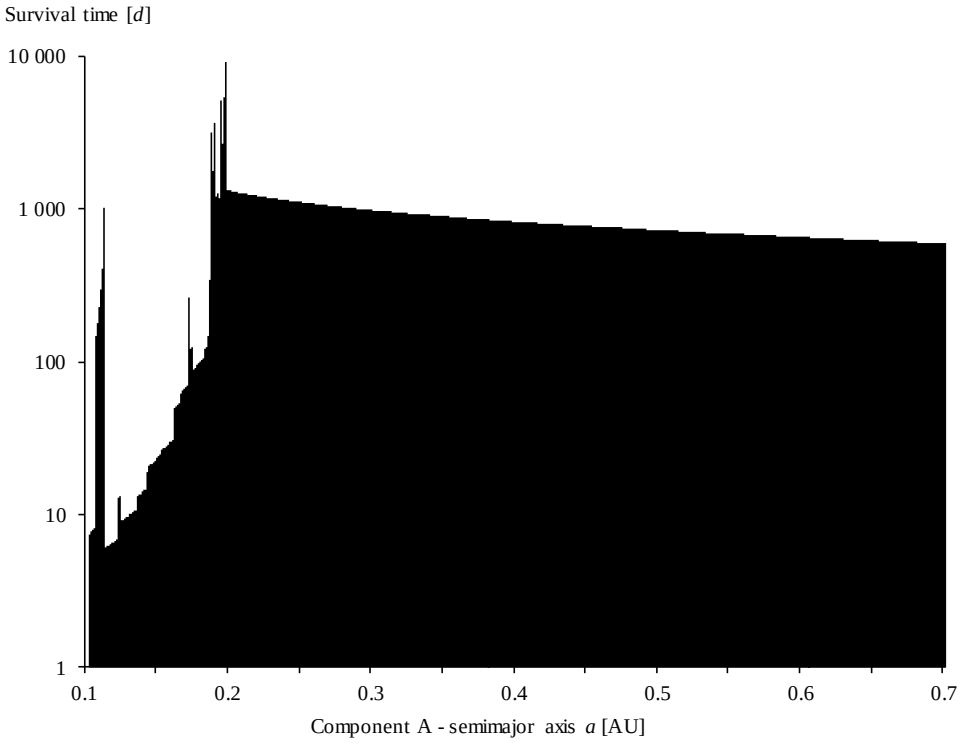

Figure E1. Survival times for test particles with semimajor axes 0.1 AU – 0.7 AU and 50 AU ejection limit, 25 yr.

The orbits were generally unstable, with survival times of less than 10 000 d. Close to the binary, survival times were less than 10 d. They then tended to increase rapidly as one moved away from the binary, as one would expect, with stability peaking above 1 000 d at around 0.2 AU. Subsequently, however, survival times again declined. This was unexpected - the further from the binary one is the more it will behave as a point mass and the more stable the orbits should be.

No orbits were stable - all test particles were either ejected or collided with the central binary, with 83% ejected and 17% colliding.

There was a local peak of relative stability in the region beginning around 0.108 AU and ending close to 0.114 AU, with survival times reaching a peak of just over 1 000 d at 114 AU.

Zooming into this region and integrating for 100 yr (36 525 d) resulted in the distribution shown in Figure E2.

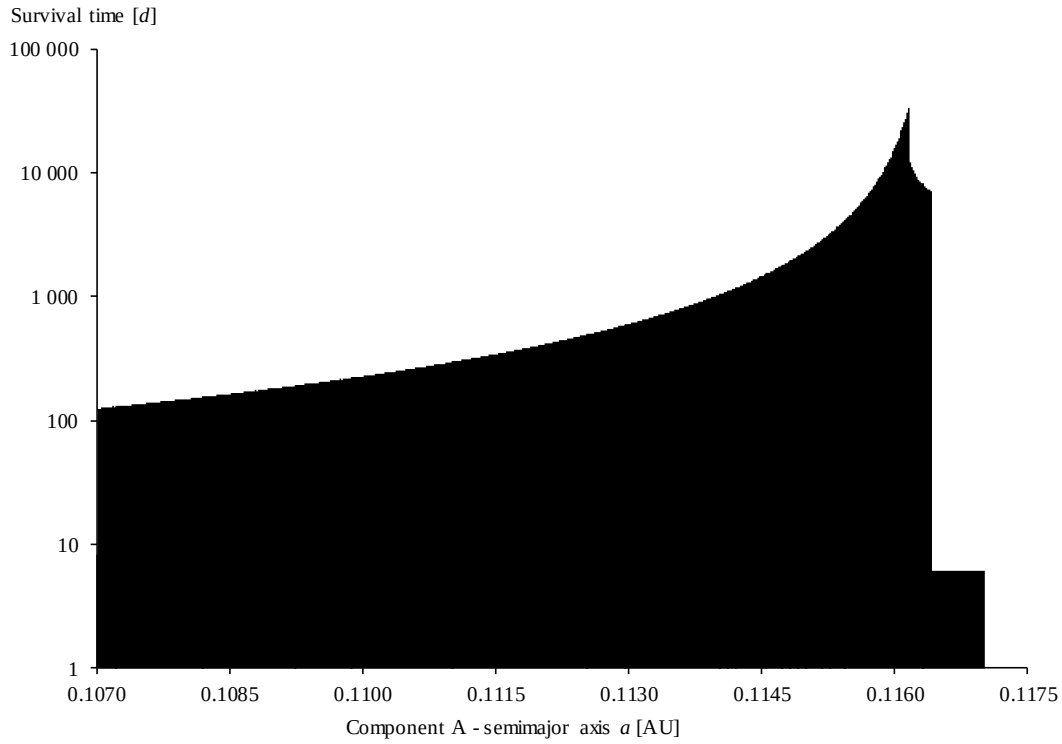

Figure E2. Survival times for test particles with semimajor axes 0.107 AU – 0.117 AU and 50 AU ejection limit, 100 yr.

Survival time increased rapidly in this region, but were still short, peaking at 33 085 d or 90 yr at a distance of 0.11615 AU. The drop-off from high levels of survival times to the new region of six days was instantaneous.

In this region, only 3% of the test bodies were ejected, with 97% colliding.

The global peak began at 0.191 AU, with survival times suddenly jumping tenfold to over 3 000 d and peaking at just over 9 000 d at a semimajor axis of 0.201 AU.

In comparison, the survival time using the semimajor axis given by Borkovits et al of 0.4198 AU was only 810 d. These survival times were too short – it was estimated by Borkovits et al that the age of this system is ~300 – 500 Myr.

Examining the trajectory of the orbit with the longest survival time in the region shown in Figure E2 resulted in the orbit shown in Figure E3.

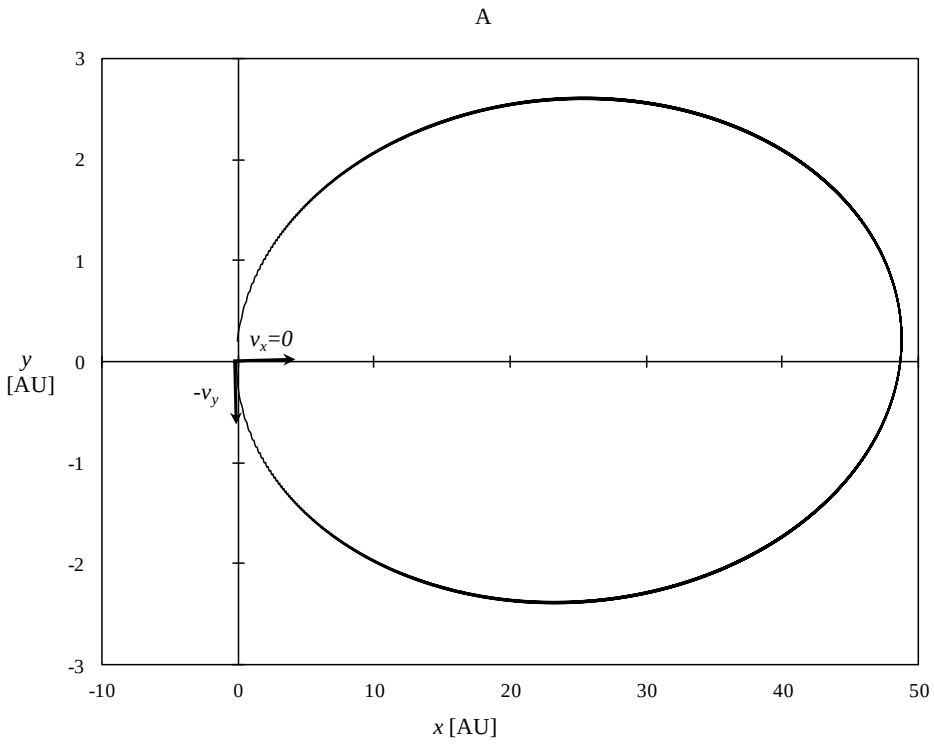

Figure E3. Longest survival time orbit, at 0.11615 AU.

This particle did not actually orbit the binary, it moved away in a very wide and highly elliptical orbit (as can be seen from the axes scales) before returning and colliding with the binary.

It is important to note that no particles were stable - all were ejected or collided. *In fact, it turns out that there were no ejections but only collisions: the ejections were an artefact of the 50 AU limit used, and the very wide orbits that the particles entered*

into exceeded this arbitrary limit. So many "ejections" were extremely wide, eccentric orbits ending in a collision with the binary on their return.

Some of the relatively high survival times were not because the particles were in stable orbits around the binary but were simply reflections of their orbital velocities being relatively low, with the particles therefore taking a longer time to reach the 50 AU ejection cut-off.

The slow decline in survival times after the 0.2 AU peak is a manifestation of this: since the larger the initial semimajor axis of the particle is, the closer it is to the 50 AU cut-off, with a shorter time being required to reach this limit. This may be seen in Figure E4, which covers the region from the binary out to 30 AU.

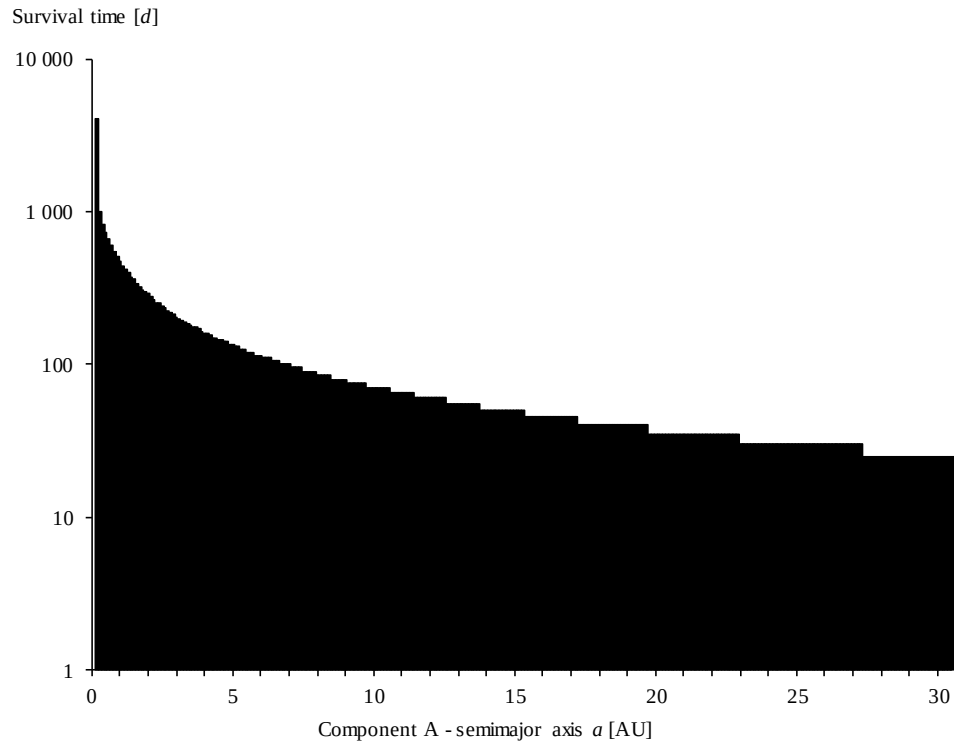

Figure E4. Survival times for test particles with semimajor axes 0.1 AU – 30 AU and 50 AU ejection limit, 25 yr.

We therefore extended the ejection limit out to 10 000 AU and repeated the integration shown in Figure E1, also integrating for a longer period of 200 yr. The results are

shown in Figure E5.

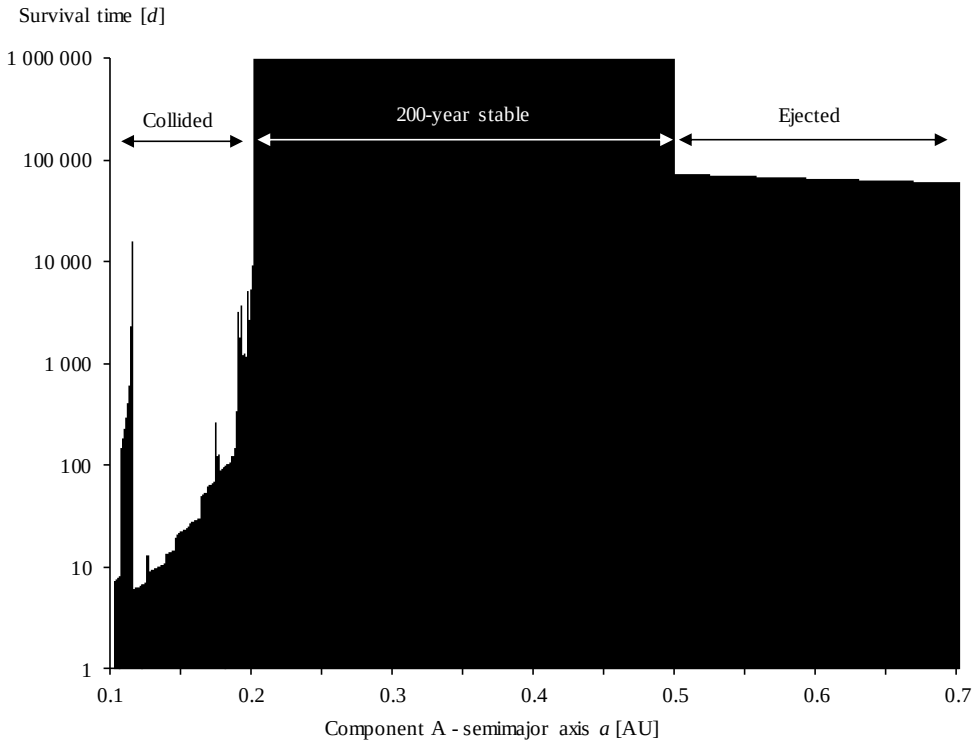

Figure E5. Survival times for test particles with semimajor axes 0.1 AU – 0.7 AU and 10 000 AU ejection limit, 200yr.

Increasing the ejection limit resulted in half the particles appearing “stable" up to 200 yr. Orbits with semimajor axes less than 0.202 AU saw particles colliding with the central binary. The closer the orbit the sooner this collision generally occurred, although again there was a region of relative stability from 0.108 AU - 0.116 AU. For orbits greater than 0.500 AU in semimajor axis, the particles were ejected. Collisions claimed 17% of the particles and ejections 33%. The slow decline in survival times in the ejection region past 0.5 AU was again apparent.

However, once again none of the ostensibly "stable" orbits were circular and repetitive, they were again very wide, highly elliptical orbits that had not yet reached the 10 000 AU ejection limit, but would do so given more time.

This raised the question of what caused these wide orbits, since the particles were initially launched in circular orbits with a velocity of $(-v_y, v_x = 0)$ in Figure E3.

There were two possibilities that required investigation:

(1) Gravitational perturbation from the binary almost immediately introduces a nonzero v_x velocity component, which initiates a highly eccentric orbit.
(2) The magnitude of the initial velocity is too high, directly causing large orbits.

Addressing the first possibility, the nonzero v_x velocity component can be seen in Figure 23 in the main text. Indeed, Figure E3 is Figure 23 extended in time. Since body A of the triple system is relatively close to the binary, any strong nonzero *x*-component of velocity will send a particle on a non-circular orbit, either on a probable collision course with the binary or almost diametrically away from it, resulting in a long, highly elliptical orbit which ends close to where it began, with a correspondingly high probability of collision with the binary.

This implies that the source of orbital instability for the third star is simply its proximity to the other two, and the closer it orbits to them, the greater the likelihood of its instability.

Since always initiating an orbit with a zero v_x component of velocity guarantees that this will become nonzero, initialising with random v_x components may result in some circular orbits. We therefore introduced a v_x velocity component in the initial launch of the orbits. The test particles were again launched from the system's published semimajor axis of 0.4198 AU with 601 different values of v_x. The particles' total velocity was kept constant at the Keplerian value of 0.058 AU d^{-1} implied by the published orbital parameters. The distribution of this velocity between its two components v_y and v_x was varied by changing the argument of pericentre g from -90° to

+90°, resulting in v_x ranging from -0.058 AU d^{-1} through zero to +0.058 AU d^{-1}. The ejection limit was returned to its initial value of 50 AU. Incidentally, it was noticed that when the initial argument of pericentre of the bodies Bb and A were of the same sign, i.e. both bodies were initially on the same side of Ba, the resulting system was more stable than when the arguments of pericentre were of the opposite sign, i.e. the bodies began on opposite sides of Ba. (In all cases Bb and A were in prograde initial orbits.)

Some initial trajectories for different values of v_x are shown in Figure E6.

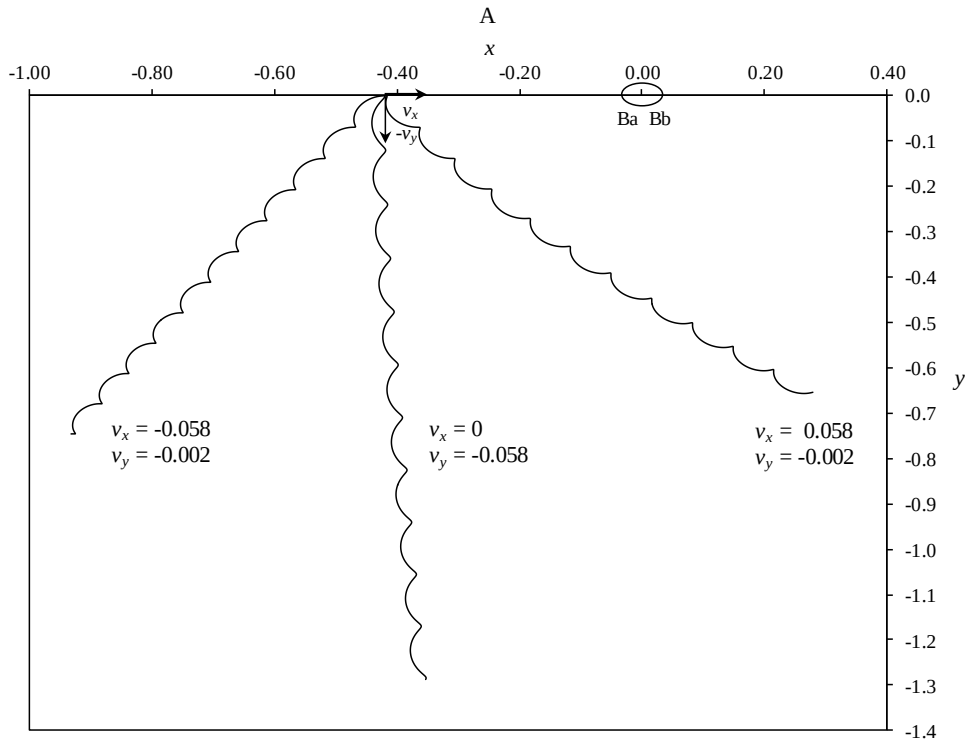

Figure E6. Initial orbital trajectories for different values of v_x.

With v_x equal to zero the initial trajectory was close to circular, so small negative values of v_x were expected to result in an almost circular initial trajectory. *However, once again there were no stable particles; although none collided, all again went into very wide, eccentric orbits.*

We therefore explored the second possibility, that the body's initial velocity was different to that published.

Appendix F: Stellar stability diagram - data

Eccentricity *e*	0.10	0.15	0.20	0.25	0.30	0.35	0.40	0.45	0.50	0.55	0.60	0.65	0.70	0.75	0.80	0.85	0.90	0.95	1.00
0.9	0.00	0.00	0.00	0.00	0.00	0.02	0.04	10^5	0.12	1.37	0.69	1.37	0.55	1.37	0.41	1.37	0.41	1.37	0.27
0.8	0.00	0.00	0.00	0.00	0.00	0.02	0.04	10^5	10^5	10^5	1.51	1.37	0.82	1.37	0.69	1.37	0.55	1.37	0.55
0.7	0.00	0.00	0.00	0.00	0.00	0.00	0.00	10^5	10^5	10^5	8.91	7.82	1.37	1.37	0.96	1.37	0.82	1.37	0.69
0.6	0.00	0.00	0.00	0.00	0.00	0.00	0.00	0.06	10^5	10^5	10^5	5.48	2.06	2.74	1.23	1.37	0.96	1.37	0.82
0.5	0.00	0.00	0.00	0.01	0.01	0.01	0.00	0.09	10^5	10^5	10^5	10^5	4.66	2.74	1.78	1.37	1.23	1.37	0.96
0.4	0.00	0.00	0.00	0.01	0.01	0.01	0.01	0.01	0.11	10^5	10^5	10^5	10^5	5.48	2.47	5.25	1.51	1.37	1.23
0.3	0.00	0.82	1.64	0.83	0.01	0.01	0.01	0.02	0.12	0.08	10^5	10^5	10^5	10^5	4.52	2.74	2.06	2.74	1.51
0.2	0.00	0.00	0.00	0.01	0.01	0.01	0.02	0.00	0.00	0.06	530	10^5	10^5	10^5	10^5	5.48	2.88	2.74	4.01
0.1	0.00	0.69	1.37	0.72	0.08	0.05	0.02	0.02	0.03	0.03	0.10	10^5	10^5	10^5	10^5	10^5	5.62	4.11	2.47
0.0	0.00	0.00	0.00	0.55	1.09	0.56	0.03	0.06	0.03	0.03	0.04	0.35	10^5	10^5	10^5	10^5	10^5	8.21	3.84

Semimajor axis *a* [AU]

Figure F1. HD 181068 stability map data: survival time [yr] (rounded).

Eccentricity *e*	0.40000	0.40625	0.41250	0.41875	0.42500	0.43125	0.43750	0.44375	0.45000
0.975	0.00	0.00	0.00	0.00	0.00	0.00	0.00	0.00	0.00
0.950	0.00	0.02	0.01	0.02	0.56	0.17	0.43	4.11	2.74
0.925	0.17	0.04	0.21	0.11	0.09	0.78	0.29	0.70	0.42
0.900	0.04	100 000	100 000	51 440	100 000	100 000	83 206	9 161	100 000
0.875	0.21	100 000	100 000	100 000	100 000	100 000	100 000	100 000	100 000
0.850	2.74	100 000	100 000	100 000	100 000	100 000	100 000	100 000	100 000
0.825	0.04	100 000	100 000	24.1	100 000	100 000	100 000	100 000	100 000
0.800	0.04	0.26	0.17	0.08	0.17	100 000	100 000	100 000	100 000
0.775	0.02	0.04	0.03	0.09	100 000	159.4	100 000	100 000	100 000
0.750	0.01	0.03	0.07	0.09	0.12	100 000	100 000	100 000	100 000
0.725	0.01	0.04	0.12	2.74	0.05	16.2	100 000	23.3	100 000
0.700	0.00	0.01	0.04	0.08	0.09	0.15	100 000	6.67	100 000
0.675	0.01	0.01	0.04	0.03	0.04	0.26	0.05	2.52	3.96
0.650	0.01	0.01	0.01	0.02	0.02	4.11	0.05	0.19	0.64

Semimajor axis *a* [AU]

Figure F2. HD 181068 stability map data: survival time [yr] (rounded) – zoomed area.

Appendix G: Test particle generation

There are many ways of quickly generating the input files for test particles. One that is surprisingly efficient is to use Excel, as shown in Figure G1.

Particle	T	a Astrocentric semi-major axis	e Eccentricity	I Inclination	g (or ϖ) Argument of pericentre	n (or Ω) Longitude of ascending node (Not used)	M Mean anomaly	x	y	z	v_x	v_y	v_z	d_1 Components of spin angular momentum	d_2	d_3
	[days]	[AU]	[-]	[°]	[°]	[°]	[°]	[AU]	[AU]	[AU]	[AU/day]	[AU/day]	[AU/day]	[AU^2/day]	[AU^2/day]	[AU^2/day]
		Δa =	Δe =	Δi =	Δg =											
		0.00000	0.0000	0.0000	0.0000											
1	45.4711	0.41987	0.0000	0.0000	0.0000	-	0.0000	-0.0015 m=0.0 -0.419870	0.000000	0.000000	0.000000	-0.001500	0.000000	0.000000	0.000000	0.000000
2	45.4711	0.41987	0.0000	0.0000	0.0000	-	0.0000	-0.003 m=0.0 -0.419870	0.000000	0.000000	0.000000	-0.003000	0.000000	0.000000	0.000000	0.000000
3	45.4711	0.41987	0.0000	0.0000	0.0000	-	0.0000	-0.0045 m=0.0 -0.419870	0.000000	0.000000	0.000000	-0.004500	0.000000	0.000000	0.000000	0.000000
4	45.4711	0.41987	0.0000	0.0000	0.0000	-	0.0000	-0.006 m=0.0 -0.419870	0.000000	0.000000	0.000000	-0.006000	0.000000	0.000000	0.000000	0.000000
5	45.4711	0.41987	0.0000	0.0000	0.0000	-	0.0000	-0.0075 m=0.0 -0.419870	0.000000	0.000000	0.000000	-0.007500	0.000000	0.000000	0.000000	0.000000
6	45.4711	0.41987	0.0000	0.0000	0.0000	-	0.0000	-0.009 m=0.0 -0.419870	0.000000	0.000000	0.000000	-0.009000	0.000000	0.000000	0.000000	0.000000
7	45.4711	0.41987	0.0000	0.0000	0.0000	-	0.0000	-0.0105 m=0.0 -0.419870	0.000000	0.000000	0.000000	-0.010500	0.000000	0.000000	0.000000	0.000000
8	45.4711	0.41987	0.0000	0.0000	0.0000	-	0.0000	-0.012 m=0.0 -0.419870	0.000000	0.000000	0.000000	-0.012000	0.000000	0.000000	0.000000	0.000000
9	45.4711	0.41987	0.0000	0.0000	0.0000	-	0.0000	-0.0135 m=0.0 -0.419870	0.000000	0.000000	0.000000	-0.013500	0.000000	0.000000	0.000000	0.000000
10	45.4711	0.41987	0.0000	0.0000	0.0000	-	0.0000	-0.015 m=0.0 -0.419870	0.000000	0.000000	0.000000	-0.015000	0.000000	0.000000	0.000000	0.000000
11	45.4711	0.41987	0.0000	0.0000	0.0000	-	0.0000	-0.0165 m=0.0 -0.419870	0.000000	0.000000	0.000000	-0.016500	0.000000	0.000000	0.000000	0.000000
12	45.4711	0.41987	0.0000	0.0000	0.0000	-	0.0000	-0.018 m=0.0 -0.419870	0.000000	0.000000	0.000000	-0.018000	0.000000	0.000000	0.000000	0.000000
13	45.4711	0.41987	0.0000	0.0000	0.0000	-	0.0000	-0.0195 m=0.0 -0.419870	0.000000	0.000000	0.000000	-0.019500	0.000000	0.000000	0.000000	0.000000
14	45.4711	0.41987	0.0000	0.0000	0.0000	-	0.0000	-0.021 m=0.0 -0.419870	0.000000	0.000000	0.000000	-0.021000	0.000000	0.000000	0.000000	0.000000
15	45.4711	0.41987	0.0000	0.0000	0.0000	-	0.0000	-0.0225 m=0.0 0.419870	0.000000	0.000000	0.000000	-0.022500	0.000000	0.000000	0.000000	0.000000
16	45.4711	0.41987	0.0000	0.0000	0.0000	-	0.0000	-0.024 m=0.0 -0.419870	0.000000	0.000000	0.000000	-0.024000	0.000000	0.000000	0.000000	0.000000

(Definitions per Mercury6)

Figure G1. Excel generation of test particles.

The coordinates are calculated as outlined in Appendix D, with some variables automatically calculated iteratively as discussed there.

The headers in the first line of each test particle can pick up any of its parameters or other fields as an identifier.

The shaded area is then simply cut and pasted as text into the required input file.

References

Aarseth, SJ 2003, *Gravitational N-body Simulations: Tools and Algorithms*, Cambridge University Press.

Abt, HA 2005, 'Observed Orbital Eccentricities', *The Astrophysical Journal*, vol. 629, no. 1, p. 507.

Akeson, RL, Chen, X, Ciardi, D, Crane, M, Good, J, Harbut, M, Jackson, E, Kane, SR, Laity, AC, Leifer, S, Lynn, M, McElroy, DL, Papin, M, Plavchan, P, Ramirez, SV, Rey, R, Braun, Kv, Wittman, M, Abajian, M, Ali, B, Beichman, C, Beekley, A, Berriman, GB, Berukoff, S, Bryden, G, Chan, B, Groom, S, Lau, C, Payne, AN, Regelson, M, Saucedo, M, Schmitz, M, Stauffer, J, Wyatt, P & Zhang, A 2013, 'The NASA Exoplanet Archive: Data and Tools for Exoplanet Research', *arXiv:1307.2944*.

Alexander, R 2012, 'The Dispersal of Protoplanetary Disks around Binary Stars', *The Astrophysical Journal Letters*, vol. 757, p. L29.

Alexandre, CMC, Gwenaël, B & Jacques, L 2012, 'Pumping the Eccentricity of Exoplanets by Tidal Effect', *The Astrophysical Journal Letters*, vol. 744, no. 2, p. L23.

Bate, MR, Bonnell, IA, Clarke, CJ, Lubow, SH, Ogilvie, GI, Pringle, JE & Tout, CA 2000, 'Observational implications of precessing protostellar discs and jets', *Monthly Notices of the Royal Astronomical Society*, vol. 317, pp. 773-81.

Beuermann, K, Dreizler, S, Hessman, F & Deller, J 2012, 'The quest for companions to post-common envelope binaries: III. A reexamination of HW Virginis', *Astronomy & Astrophysics*, vol. 543.

Beust, H 2003, 'Symplectic integration of hierarchical stellar systems', *Astronomy and Astrophysics*, vol. 400, no. 3, pp. 1129-44.

Bodenheimer, P 1978, 'Evolution of rotating interstellar clouds. III-On the formation of multiple star systems', *The Astrophysical Journal*, vol. 224, pp. 488-96.

Bonavita, M & Desidera, S 2007, 'The frequency of planets in multiple systems', *A&A*, vol. 468, no. 2, pp. 721-9.

Bonnell, IA & Bate, MR 1994, 'Massive Circumbinary Discs and the Formation of Multiple Systems', *Monthly Notices of the Royal Astronomical Society*, vol. 269, pp. L45-L8.

Borkovits, T, Derekas, A, Kiss, LL, Király, A, Forgács-Dajka, E, Bíró, IB, Bedding, TR, Bryson, ST, Huber, D & Szabó, R 2013, 'Dynamical masses, absolute radii and 3D orbits of the triply eclipsing star HD 181068 from Kepler photometry', *Monthly Notices of the Royal Astronomical Society*, vol. 428, no. 2, pp. 1656-72.

Carroll, BW & Ostlie, DA 2007, *An Introduction to Modern Astrophysics*, 2nd edn, 1 vols., Pearson Addison-Wesley, San Francisco.

Carter, JA, Fabrycky, DC, Ragozzine, D, Holman, MJ, Quinn, SN, Latham, DW, Buchhave, LA, Van Cleve, J, Cochran, WD & Cote, MT 2011, 'KOI-126: A triply

eclipsing hierarchical triple with two low-mass stars', *Science*, vol. 331, no. 6017, pp. 562-5.

Chambers, JE 1999, 'A hybrid symplectic integrator that permits close encounters between massive bodies', *Monthly Notices of the Royal Astronomical Society*, vol. 304, no. 4, pp. 793-9.

Chambers, JE, Quintana, EV, Duncan, MJ & Lissauer, JJ 2002, 'Symplectic Integrator Algorithms for Modeling Planetary Accretion in Binary Star Systems', *The Astronomical Journal*, vol. 123, no. 5, p. 2884.

de Souza Torres, K & Anderson, D 2008, 'Symplectic Integrator Mercury: Bug Report'.

Derekas, A, Kiss, LL, Borkovits, T, Huber, D, Lehmann, H, Southworth, J, Bedding, TR, Balam, D, Hartmann, M & Hrudkova, M 2011, 'HD 181068: A Red Giant in a Triply Eclipsing Compact Hierarchical Triple System', *Science*, vol. 332, no. 6026, pp. 216-8.

Desidera, S & Barbieri, M 2007, 'Properties of planets in binary systems. The role of binary separation', *Astronomy and Astrophysics*, vol. 462, pp. 345-53.

Desidera, S, Carolo, E, Gratton, R, Fiorenzano, AFM, Endl, M, Mesa, D, Barbieri, M, Bonavita, M, Cecconi, M, Claudi, RU, Cosentino, R, Marzari, F & Scuderi, S 2011, 'A giant planet in the triple system HD132563', *arXiv:1107.0918*.

Dommanget, J & Nys, O 2002, 'CCDM (Catalog of Components of Double & Multiple stars) (Dommanget+ 2002)', *VizieR Online Data Catalog*, vol. 1274, p. 0.

Donnison, J & Mikulskis, D 1995, 'The effect of eccentricity on three-body orbital stability criteria and its importance for triple star systems', *Monthly Notices of the Royal Astronomical Society*, vol. 272, pp. 1-10.

Doolin, S & Blundell, KM 2011, 'The dynamics and stability of circumbinary orbits', *Monthly Notices of the Royal Astronomical Society*, vol. 418, no. 4, pp. 2656-68.

Duncan, MJ, Levison, HF & Lee, MH 1998, 'A Multiple Time Step Symplectic Algorithm for Integrating Close Encounters', *The Astronomical Journal*, vol. 116, no. 4, p. 2067.

Dvorak, R 2008, *Extrasolar Planets*, Wiley-VCH.

Eggenberger, A, Udry, S & Mayor, M 2004, 'Statistical properties of exoplanets. III. Planet properties and stellar multiplicity', *Astronomy and Astrophysics*, vol. 417, pp. 353-60.

Eggl, S, Pilat-Lohinger, E, Funk, B, Georgakarakos, N & Haghighipour, N 2013, 'Circumstellar habitable zones of binary-star systems in the solar neighbourhood', *Monthly Notices of the Royal Astronomical Society*, vol. 428, no. 4, pp. 3104-13.

Eggleton, PP & Tokovinin, AA 2008, 'A catalogue of multiplicity among bright stellar systems', *Monthly Notices of the Royal Astronomical Society*, vol. 389, no. 2, pp. 869-79.

Elser, S, Grimm, SL & Stadel, JG 2013, 'Super Earths and Dynamical Stability of Planetary Systems: First Parallel GPU Simulations Using GENGA', *arXiv:1305.4070*.

Fabrycky, D 2010, Detection and Dynamics of Transiting Exoplanets. Observatoire de Haute-Provence, France.

Farago, F & Laskar, J 2010, 'High-inclination orbits in the secular quadrupolar three-body problem', *Monthly Notices of the Royal Astronomical Society*, vol. 401, no. 2, pp. 1189-98.

Fekel Jr, F 1981, 'The properties of close multiple stars', *The Astrophysical Journal*, vol. 246, pp. 879-98.

Haghighipour, N 2008, '9 Formation, Dynamical Evolution, and Habitability of Planets in Binary Star Systems', *Exoplanets: Detection, Formation, Properties, Habitability*, p. 223.

Hessman, F, Dhillon, V, Winget, D, Schreiber, M, Horne, K, Marsh, T, Guenther, E, Schwope, A & Heber, U 2010, 'On the naming convention used for multiple star systems and extrasolar planets', *arXiv preprint arXiv:1012.0707*.

Holman, MJ & Wiegert, PA 1999, 'Long-term stability of planets in binary systems', *The Astronomical Journal*, vol. 117, no. 1, p. 621.

Horner, J, Hinse, T, Wittenmyer, R, Marshall, J & Tinney, C 2012, 'A dynamical analysis of the proposed circumbinary HW Virginis planetary system', *Monthly Notices of the Royal Astronomical Society*, vol. 427, no. 4, pp. 2812-23.

Jones, B, Sleep, P & Chambers, J 2001, 'The stability of the orbits of terrestrial planets in the habitable zones of known exoplanetary systems', *Astronomy and Astrophysics*, vol. 366, no. 1, pp. 254-62.

Julia, F & Jean-Luc, M 2012, 'Predicting Planets in Kepler Multi-planet Systems', *The Astrophysical Journal*, vol. 751, no. 1, p. 23.

Kane, SR & Hinkel, NR 2012, 'On the Habitable Zones of Circumbinary Planetary Systems', *arXiv:1211.2812*.

Kane, SR & Hinkel, NR 2013, 'On the Habitable Zones of Circumbinary Planetary Systems', *The Astrophysical Journal*, vol. 762, no. 1, p. 7.

Kasting, JF, Whitmire, DP & Reynolds, RT 1993, 'Habitable Zones around Main Sequence Stars', *Icarus*, vol. 101, no. 1, pp. 108-28.

Kopparapu, RK, Ramirez, R, Kasting, JF, Eymet, V, Robinson, TD, Mahadevan, S, Terrien, RC, Domagal-Goldman, S, Meadows, V & Deshpande, R 2013, 'Habitable Zones around Main-sequence Stars: New Estimates', *The Astrophysical Journal*, vol. 765, no. 2, p. 131.

Kozai, Y 1962, 'Secular perturbations of asteroids with high inclination and eccentricity', *The Astronomical Journal*, vol. 67, p. 591.

Lee, JW, Kim, S-L, Kim, C-H, Koch, RH, Lee, C-U, Kim, H-I & Park, J-H 2009, 'The sdB+ M eclipsing system HW Virginis and its circumbinary planets', *The Astronomical Journal*, vol. 137, no. 2, p. 3181.

Leung, GC & Lee, MH 2013, 'An Analytic Theory for the Orbits of Circumbinary Planets', *The Astrophysical Journal*, vol. 763, no. 2, p. 107.

Levison, HF & Duncan, MJ 1994, 'The long-term dynamical behavior of short-period comets', *Icarus*, vol. 108, no. 1, pp. 18-36.

Levison, HF & Duncan, MJ 2013, 'Swift: A solar system integration software package', *Astrophysics Source Code Library*, vol. 1, p. 03001.

Malmberg, D, Davies, MB & Chambers, JE 2007, 'The instability of planetary systems in binaries: How the Kozai mechanism leads to strong planet–planet interactions', *Monthly Notices of the Royal Astronomical Society: Letters*, vol. 377, no. 1, pp. L1-L4.

Mardling, RA & Aarseth, SJ 2001, 'Tidal interactions in star cluster simulations', *Monthly Notices of the Royal Astronomical Society*, vol. 321, no. 3, pp. 398-420.

Moeckel, N & Veras, D 2012, 'Exoplanets bouncing between binary stars', *Monthly Notices of the Royal Astronomical Society*, vol. 422, no. 1, pp. 831-40.

Moore, A & Quillen, AC 2011, 'QYMSYM: A GPU-accelerated hybrid symplectic integrator that permits close encounters', *New Astronomy*, vol. 16, no. 7, pp. 445-55.

Perryman, M 2011, *The Exoplanet Handbook*, Cambridge University Press.

Pourbaix, D, Boffin, HMJ, Chini, R & Dembsky, T 2013, 'The multiplicity of φ Phe revisited', *arXiv:1304.7756*.

Quintana, EV, Lissauer, JJ, Chambers, JE & Duncan, MJ 2002, 'Terrestrial planet formation in the α Centauri system', *The Astrophysical Journal*, vol. 576, no. 2, p. 982.

Rappaport, S, Deck, K, Levine, A, Borkovits, T, Carter, J, Mellah, IE, Ojeda, RS & Kalomeni, B 2013, 'Triple-Star Candidates Among the Kepler Binaries', *arXiv:1302.0563*.

Rein, H 2012, 'A proposal for community driven and decentralized astronomical databases and the Open Exoplanet Catalogue', *arXiv:1211.7121*.

Roell, T, Seifahrt, A, Neuhäuser, R & Mugrauer, M 2012, 'Extrasolar planets in stellar multiple systems', *arXiv:1204.4833*.

Schneider, J, Dedieu, C, Sidaner, PL, Savalle, R & Zolotukhin, I 2011, 'Defining and cataloging exoplanets: the exoplanet.eu database', *arXiv preprint arXiv:1106.0586*.

Stagg, C 1984, 'Almost-square orbits in the restricted problem of three bodies', *Celestial mechanics*, vol. 32, no. 4, pp. 365-70.

Steffen, J, Quinn, S, Borucki, W, Brugamyer, E, Bryson, S, Buchhave, L, Cochran, W, Endl, M, Fabrycky, D & Ford, E 2011, 'The architecture of the hierarchical triple star

KOI 928 from eclipse timing variations seen in Kepler photometry', *Monthly Notices of the Royal Astronomical Society: Letters*, vol. 417, no. 1, pp. L31-L5.

Šuvakov, M & Dmitrašinovic, V 2013, 'Three Classes of Newtonian Three-Body Planar Periodic Orbits', *Physical Review Letters*, vol. 110, no. 11, p. 114301.

Terrell, D, Munari, U & Siviero, A 2007, 'Observational studies of early-type binary stars: VV Orionis', *Monthly Notices of the Royal Astronomical Society*, vol. 374, no. 2, pp. 530-4.

Tokovinin, A 1993, 'Relative orientation of angular momenta in multiple star systems', *Astronomy Letters*, vol. 19, pp. 383-8.

Tokovinin, A 2000, 'Statistics of multiple stars: some clues to formation mechanisms', in IAU Symposium: *proceedings of theIAU Symposium* pp. 84-92.

Tokovinin, A 2001, 'Statistics of multiple stars: some clues to formation mechanisms', in The Formation of Binary Stars: *proceedings of theThe Formation of Binary Stars* pp. 84-92.

Tokovinin, A 2004, 'Statistics of multiple stars', in Revista Mex. Astron. Astrofis.(Ser. Conf.): *proceedings of theRevista Mex. Astron. Astrofis.(Ser. Conf.)* p. 7.

Van Hamme, W & Wilson, R 2007, 'Third-body parameters from whole light and velocity curves', *The Astrophysical Journal*, vol. 661, no. 2, p. 1129.

Verrier, P & Evans, N 2006, 'Planets and Asteroids in the γ Cephei System', *Monthly Notices of the Royal Astronomical Society*, vol. 368, no. 4, pp. 1599-608.

Verrier, P & Evans, N 2007, 'Planetary stability zones in hierarchical triple star systems', *Monthly Notices of the Royal Astronomical Society*, vol. 382, no. 4, pp. 1432-46.

Verrier, P & Evans, N 2009, 'High-inclination planets and asteroids in multistellar systems', *Monthly Notices of the Royal Astronomical Society*, vol. 394, no. 4, pp. 1721-6.

Wheatley, PJ, Mukai, K & De Martino, D 2003, 'X-ray observations of 4 Draconis: symbiotic binary or cataclysmic triple?', *Monthly Notices of the Royal Astronomical Society*, vol. 346, no. 3, pp. 855-60.

Wisdom, J & Holman, M 1991, 'Symplectic maps for the n-body problem', *The Astronomical Journal*, vol. 102, pp. 1528-38.

Wittenmyer, RA, Horner, JA, Marshall, JP, Butters, OW & Tinney, CG 2011, 'Revisiting the proposed planetary system orbiting the eclipsing polar HU Aquarii', *arXiv:1110.2542*.

Wright, JT, Fakhouri, O, Marcy, GW, Han, E, Feng, Y, Johnson, JA, Howard, AW, Fischer, DA, Valenti, JA & Anderson, J 2011, 'The exoplanet orbit database', *Publications of the Astronomical Society of the Pacific*, vol. 123, no. 902, pp. 412-22.